



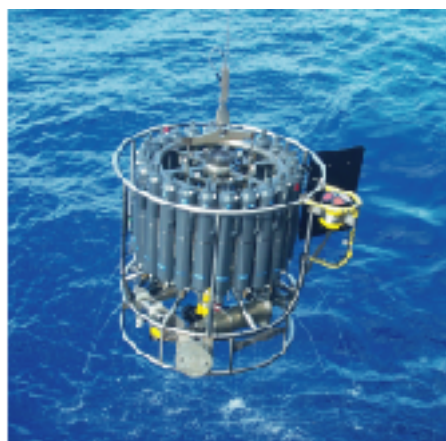
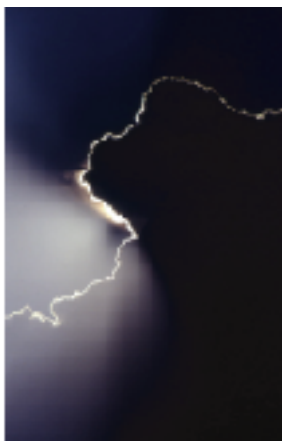
Max-Planck-Institut für Meteorologie  
*Max Planck Institute for Meteorology*



MAX-PLANCK-GESELLSCHAFT

# Mechanisms and Predictability of North Atlantic - European Climate

Holger Pohlmann



Berichte zur Erdsystemforschung

$\frac{6}{2004}$

*Reports on Earth System Science*

## Hinweis

Die Berichte zur Erdsystemforschung werden vom Max-Planck-Institut für Meteorologie in Hamburg in unregelmäßiger Abfolge herausgegeben.

Sie enthalten wissenschaftliche und technische Beiträge, inklusive Dissertationen.

Die Beiträge geben nicht notwendigerweise die Auffassung des Instituts wieder.

Die "Berichte zur Erdsystemforschung" führen die vorherigen Reihen "Reports" und "Examensarbeiten" weiter.



## Notice

*The Reports on Earth System Science are published by the Max Planck Institute for Meteorology in Hamburg. They appear in irregular intervals.*

*They contain scientific and technical contributions, including Ph. D. theses.*

*The Reports do not necessarily reflect the opinion of the Institute.*

*The "Reports on Earth System Science" continue the former "Reports" und "Examensarbeiten" of the Max Planck Institute.*

## Anschrift / Address

Max-Planck-Institut für Meteorologie  
Bundesstrasse 53  
20146 Hamburg  
Deutschland

Tel.: +49-(0)40-4 11 73-0  
Fax: +49-(0)40-4 11 73-298  
Web: [www.mpimet.mpg.de](http://www.mpimet.mpg.de)

## Layout:

Bettina Diallo, PR & Grafik

Titelfotos:

vorne:

Christian Klepp - Jochem Marotzke - Christian Klepp

hinten:

Katsumasa Tanaka - Christian Klepp - Clotilde Dubois

Mechanismen und Vorhersagbarkeit des  
nordatlantisch - europäischen Klimas

*Mechanisms and Predictability of  
North Atlantic - European Climate*

Dissertation zur Erlangung des Doktorgrades der Naturwissenschaften  
im Fachbereich Geowissenschaften der Universität Hamburg  
vorgelegt von

Holger Pohlmann  
aus Nienburg/Weser

Hamburg 2005

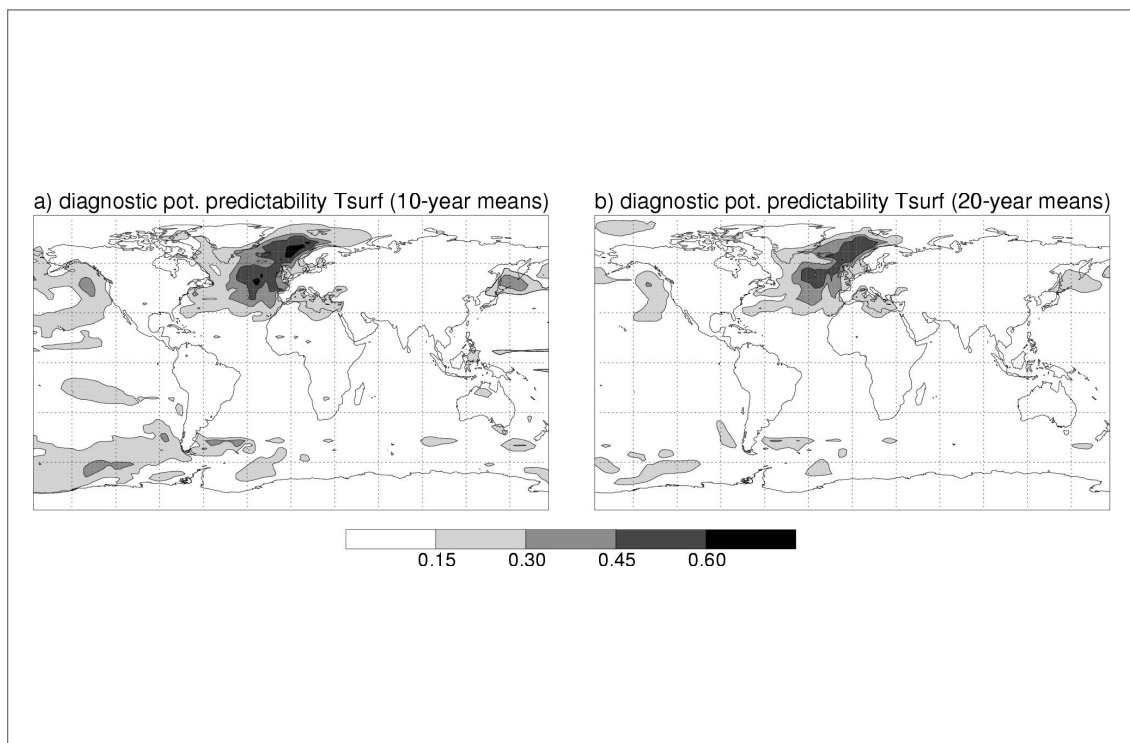
Holger Pohlmann  
Max-Planck-Institut für Meteorologie  
Bundesstrasse 53  
20146 Hamburg  
Germany

Als Dissertation angenommen  
vom Fachbereich Geowissenschaften der Universität Hamburg

auf Grund der Gutachten von  
Herrn Prof. Dr. Detlef Stammer und  
Herrn Prof. Dr. Mojib Latif  
Hamburg, den 11. Januar 2005  
Professor Dr. Helmut Schleicher  
Dekan des Fachbereiches Geowissenschaften

# Mechanisms and Predictability of North Atlantic - European Climate

---



**Holger Pohlmann**

Hamburg 2005



# Contents

<b>ABSTRACT.....</b>	<b>5</b>
<b>1. INTRODUCTION.....</b>	<b>7</b>
1.1 MOTIVATION.....	7
1.1.1 Difference between weather forecasts and climate prediction .....	7
1.1.2 Mechanisms of North Atlantic – European climate.....	8
1.2 SCIENTIFIC OBJECTIVES.....	9
1.3 CONTENTS OF THE PH.D. THESIS.....	11
<b>2. ATLANTIC VERSUS INDO-PACIFIC INFLUENCE ON ATLANTIC- EUROPEAN CLIMATE .....</b>	<b>13</b>
2.1 INTRODUCTION .....	13
2.2 EXPERIMENTS AND METHODOLOGY .....	14
2.3 RESULTS .....	15
2.3.1 Atlantic versus Indo-Pacific influence.....	15
2.3.2 Response in the Atlantic-European region .....	16
2.4 SUMMARY AND CONCLUSIONS .....	18
<b>3. INFLUENCE OF THE OCEANS ON NORTH ATLANTIC CLIMATE VARIABILITY: A COMPARISON OF RESULTS FROM 4 ATMOSPHERIC GCMS.....</b>	<b>21</b>
3.1 INTRODUCTION .....	21
3.2 MODELS AND DATA.....	22
3.3 DATA ANALYSIS.....	23
3.3.1 Preprocessing .....	23
3.3.2 Optimal detection .....	24
3.3.3 Regression analysis .....	25
3.4 RESULTS .....	25
3.4.1 Climatologies .....	25
3.4.2 Unfiltered data .....	25
3.4.3 Linear trend .....	28
3.4.4 Detrended data .....	30
3.5 CONCLUSIONS .....	33
<b>4. NORTH ATLANTIC FORCING OF CLIMATE AND ITS UNCERTAINTY FROM A MULTI-MODEL EXPERIMENT .....</b>	<b>37</b>
4.1 INTRODUCTION .....	37
4.2 MODELS AND METHODOLOGY .....	40

4.2.1 Models .....	40
4.2.2 Simulations of each model .....	41
4.2.3 Construction of SST anomalies .....	41
4.2.4 Extra simulations of the HadAM3 model .....	42
4.3 INDIVIDUAL MODEL RESPONSES .....	43
4.4 MULTI-MODEL MEAN RESPONSE, ITS ORIGIN AND SIGNIFICANCE .....	44
4.4.1 Methodologies .....	44
4.4.2 Tropical response .....	45
4.4.3 Extratropical response.....	47
4.5 COMPARISON WITH OBSERVATIONAL RESPONSE .....	49
4.6 INTER-MODEL RESPONSE DIFFERENCES .....	50
4.6.1 Quantification of differences .....	50
4.6.2 Physical interpretation of inter-model differences.....	51
4.7 RESPONSE TO ATLANTIC FORCING, AND ITS UNCERTAINTY .....	52
4.8 LINEARITY OF THE RESPONSE.....	52
4.9 THE IMPORTANT TIMESCALES FOR THE RESPONSE.....	53
4.10 DISCUSSION AND CONCLUSIONS.....	54
<b>5. ESTIMATING THE DECADEAL PREDICTABILITY OF A COUPLED AOGCM</b> .....	<b>61</b>
5.1 INTRODUCTION .....	61
5.2 MODEL AND EXPERIMENTS .....	63
5.3 METHODS .....	63
5.3.1 Diagnostic potential predictability.....	63
5.3.2 Prognostic potential predictability .....	64
5.4. RESULTS .....	66
5.4.1 Climate variability .....	66
5.4.2 Diagnostic potential predictability.....	67
5.4.2 Diagnostic potential predictability.....	68
5.4.3 Oceanic prognostic potential predictability .....	68
5.4.4 Atmospheric prognostic potential predictability.....	71
5.5 SUMMARY AND DISCUSSION.....	72
<b>6. INFLUENCE OF THE MULTIDECADAL ATLANTIC MERIDIONAL OVERTURNING CIRCULATION VARIABILITY ON EUROPEAN CLIMATE</b>	<b>77</b>
6.1 INTRODUCTION .....	77
6.2 MODEL AND EXPERIMENTS .....	78
6.3 RESULTS .....	78
6.4 SUMMARY AND DISCUSSION.....	81
<b>7. INTERANNUAL TO DECADEAL CLIMATE PREDICTABILITY: A MULTI- PERFECT-MODEL-ENSEMBLE STUDY</b> .....	<b>85</b>
7.1 INTRODUCTION .....	85
7.2 THE ENSEMBLE EXPERIMENTS.....	86

7.3 POTENTIAL PREDICTABILITY OF MOC VARIATIONS .....	88
7.4 POTENTIAL PREDICTABILITY OF SURFACE CLIMATE VARIATIONS .....	91
7.5 DISCUSSION .....	93
<b>8. SUMMARY AND OUTLOOK.....</b>	<b>97</b>
8.1 SUMMARY OF RESULTS .....	97
8.2 OUTLOOK.....	98
<b>A. METHODOLOGIES.....</b>	<b>101</b>
A.1 ANALYSIS OF VARIANCES.....	101
A.2 OPTIMAL DETECTION ANALYSIS .....	102



## Abstract

This study investigates the mechanisms of North Atlantic-European climate using atmosphere general circulation models (AGCMs). Experiments with the AGCM ECHAM4, in which the sea surface temperature (SST) forcing is restricted to either the Atlantic or the Indo-Pacific oceans, show that both oceanic regions have an influence on North Atlantic-European climate in winter. In the experiment with SST forcing restricted to the Indo-Pacific oceans the atmospheric response projects on the North Atlantic Oscillation (NAO), while in the experiment with SST forcing restricted to the Atlantic Ocean the atmospheric response projects on the East-Atlantic Pattern. A multi-model intercomparison study shows that the region with the dominant influence on North Atlantic-European winter climate varies between different AGCMs. The dominant forcing of the atmospheric variability in the North Atlantic-European region in ECHAM4 is from the tropical eastern Pacific. However, in three other AGCMs the dominant forcing of this mode is from the tropical North Atlantic region. The importance of North Atlantic SST for North Atlantic-European climate is shown in another multi-model intercomparison study. The idealized North Atlantic SST anomaly pattern for this experiment has the structure of a tripole, which is believed to have the strongest impact on North Atlantic climate. Agreements between the responses in the different AGCMs are found concerning the NAO, Eurasian temperatures, rainfall over America and Africa, and the Asian monsoon. The results suggest that the extratropical North Atlantic region response is associated with remote Caribbean and tropical Atlantic SST anomalies, and with local forcing. All of these results support the conclusion that the ocean has a significant influence on North Atlantic-European climate.

In addition to the mechanisms, this study investigates the predictability of North Atlantic-European climate. A control integration and ensemble experiments with the coupled atmosphere-ocean general circulation model (AOGCM) ECHAM5/MPI-OM are analyzed to investigate the decadal climate predictability. The ensemble experiments are realized with slightly perturbed atmospheric but the same oceanic initial conditions. The results show that the North Atlantic thermohaline circulation (THC) and SST are potentially predictable on multidecadal timescales. Over the ocean the predictability of surface air temperature (SAT) is very similar to that of SST, and this signal proceeds into the lower troposphere. Over land there is little evidence of decadal predictability of SAT with classical predictability methods. However, the estimation of the potential predictability over the European continent with probabilistic methods, commonly used in seasonal and medium-range forecasting, exhibits some limited success on decadal timescales. A multi-model comparison study with five AOGCMs confirms the potential predictability of North Atlantic THC and SST, albeit with skill levels dependent on the AOGCM. In general, models with greater decadal THC variability have higher levels of potential predictability.

## Zusammenfassung

In dieser Studie werden die Mechanismen des nordatlantisch-europäischen Klimas mit Hilfe von Zirkulationsmodellen der Atmosphäre (AGCM) untersucht. Experimente mit dem AGCM ECHAM4, bei dem die Variabilität des Antriebs mit Meeresoberflächentemperaturen (SST) entweder auf den Atlantik oder den Indo-Pazifik begrenzt ist, zeigen, dass beide Ozeanregionen einen Einfluss auf das atlantisch-europäische Winterklima haben. In dem Experiment, bei dem die SST Variabilität des Antriebs auf den Indo-Pazifik begrenzt ist, ist der atmosphärische Respons dem Muster der Nordatlantischen Oszillation (NAO) ähnlich. Hingegen ist im anderen Experiment, bei dem die SST Variabilität des Antriebs auf den Atlantik begrenzt ist, der Respons dem Ostatlantik-Muster (EAP) ähnlich. Eine Vergleichsstudie mehrerer Modelle zeigt, dass die Region des dominanten Einflusses auf das nordatlantisch-europäische Klima zwischen verschiedenen AGCM unterschiedlich ist. Bei Experimenten mit dem AGCM ECHAM4 dominiert der Einfluss der SST aus der Region des tropischen östlichen Pazifiks. In drei anderen AGCM Experimenten dominiert jedoch der Einfluss der SST aus der Region des tropischen Nordatlantiks. In einer weiteren Multimodell-Vergleichsstudie wird die Bedeutung der SST aus der Region des Nordatlantiks für das nordatlantisch-europäische Klima gezeigt. Das in diesem AGCM Experiment verwendete idealisierte SST Anomalienmuster hat die Struktur eines Tripols von dem angenommen wird, dass er den stärksten Einfluss auf das nordatlantische Klima hat. Die Simulationen mit den verschiedenen AGCM zeigen Übereinstimmungen, die die NAO, Temperaturen in Eurasien, Regen über Amerika und Afrika und den asiatischen Monsun betreffen. Die Ergebnisse lassen vermuten, dass die außertropische nordatlantische Region aus der Karibik und dem tropischen Atlantik sowie lokal beeinflusst wird. All diese Ergebnisse unterstützen die Schlussfolgerung, dass der Ozean einen signifikanten Einfluss auf das nordatlantisch-europäische Klima hat.

In dieser Studie wird darüberhinaus die Vorhersagbarkeit des nordatlantisch-europäischen Klimas auf dekadischen Zeitskalen untersucht. Ein Kontrollexperiment und Ensembleexperimente mit dem gekoppelten Atmosphäre-Ozean Zirkulationsmodell (AOGCM) ECHAM5/MPI-OM wurden analysiert, um die dekadische Klimavorhersagbarkeit zu untersuchen. Die Ensembleexperimente wurden mit geänderten atmosphärischen bei jedoch unveränderten ozeanischen Anfangsbedingungen realisiert. Die Ergebnisse zeigen, dass die nordatlantische thermohaline Zirkulation (THC) und SST auf multidekadischen Zeitskalen potenziell vorhersagbar sind. Über dem Ozean ist die Vorhersagbarkeit von Lufttemperaturen sehr ähnlich zu der von SST und dieses Signal setzt sich auch in die untere Troposphäre fort. Über Land besteht nur geringfügige dekadische Vorhersagbarkeit mit den klassischen Vorhersagbarkeitsmethoden. Die Anwendung von Wahrscheinlichkeitsmethoden für die Bestimmung der potenziellen Vorhersagbarkeit, die gewöhnlich in saisonalen und mittelfristigen Klimavorhersagen Anwendung finden, zeigt jedoch einen eingeschränkten Erfolg auf dekadischen Zeitskalen. Eine Vergleichsstudie mit fünf verschiedenen AOGCM bestätigt die potenzielle Vorhersagbarkeit der nordatlantischen THC und SST, allerdings mit unterschiedlicher Güte. Im allgemeinen haben Modelle mit starker THC-Variabilität eine bessere potenzielle Vorhersagbarkeit.

## CHAPTER 1

### Introduction

#### 1.1 Motivation

##### 1.1.1 Difference between weather forecasts and climate prediction

In the 1960's Edward Lorenz tried to model the weather. While carrying out an experiment, Lorenz made an accidental discovery. He had completed a run, and wanted to recreate the pattern. Using a printout, Lorenz entered some variables into the computer and expected the simulation to proceed the same as it had before. To his surprise, the pattern began to diverge from the previous run, and after a few weeks of simulated time, the pattern was completely different. This discovery provided the basis for chaos theory. The concept is now known as the Butterfly Effect: Small deviations in the initial conditions (a butterfly flapping its wings) affect the weather prediction for regions thousands of miles away some days later.

Edward Lorenz was looking for a way to model the action of the chaotic behaviour of a fluid. Hence, he developed a mathematical model for convection. Convection starts in a laboratory when a fluid is heated from below or cooled from above. When the temperature difference reaches a threshold, a regular circulation starts. With increasing temperature difference other forms of regular circulation develop until the system becomes chaotic. In this state the system jumps unpredictably between different circulation forms. The temporal evolution of the result from the mathematical model, projected into phase space, displays the Lorenz attractor. The discovery of Lorenz explains the limitations of weather prediction.

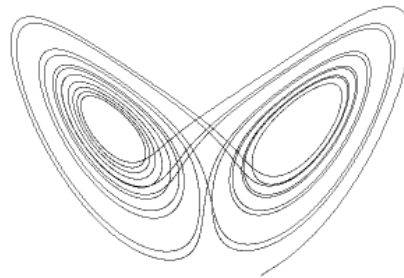


**Figure 1.1** *An example of a Lorenz attractor in the phase space.*

But how could climate predictions be possible when weather forecasts are limited to 10 to 14 days in advance? The definition of climate can help to overcome this contradiction. Climate in a narrow sense is usually defined as the statistical description of weather elements over a period of time. Climate is describing the macroscopic weather

characteristics like the mean or the variance, not the microscopic single weather phenomenon. Climate science is asking for the probability of events in a specified period.

In certain circumstances macroscopic weather characteristics (climate) are predictable although the forecast of microscopic characteristics (weather) are not. As with weather forecasting, climate prediction depends on initial and boundary conditions. For weather forecasting the initial conditions are important and the boundary conditions are treated often as constant. The prediction of climate depends additionally on boundary conditions. An example is the realization of climate predictions with atmospheric general circulation models (AGCMs) forced by sea surface temperatures (SSTs). The climate prediction is almost independent from the initial state of the AGCM due to averaging several ensemble simulations. Another example of important boundary conditions is the prediction of climate change, which depends mainly on the future evolution of greenhouse gases. But the initial conditions are not unimportant for climate predictions. An example is the prediction of the El Niño/Southern Ocean (ENSO) phenomenon on seasonal timescales with coupled atmosphere-ocean general circulation models (AOGCMs).

### **1.1.2 Mechanisms of North Atlantic – European climate**

The mechanisms of climate variability depend on the different timescales. So, which timescales are important for climate predictability? This study aims to estimate the limits of climate predictability using coupled AOGCMs with constant boundary forcing. In particular, to understand the predictability associated with the pronounced decadal and multidecadal internal oceanic variability, described by many modelling studies, climate variability on shorter timescales are also important for the generation of long-term climate variability: The integration of high-frequency atmospheric climate fluctuations by the ocean results in low-frequency climate variability. Climate variability on longer timescales associated with external forcing, like the increase of greenhouse gases or variability in solar radiation, are of course also important for decadal to multidecadal climate variability, but they are not the focus of this study.

For the investigation of the predictability of North Atlantic – European climate an understanding of the physical mechanisms is important. The North Atlantic Oscillation (NAO) is the most important climate signal in the Atlantic-European sector on interannual time-scales. It has undergone major low frequency fluctuations during the last century, with high values predominating at the beginning and end of the century and low values in the 1950s-1970s. These fluctuations were associated with large anomalies in storminess, temperature, and rainfall, with major socio-economic impacts on Europe. However, the NAO explains on interannual timescales approximately 40% of the variability, so the understanding of other climate modes, like the East-Atlantic Pattern, could also be of benefit. The current understanding of the causes of these climate fluctuations is limited. Interactions between the oceans and the atmosphere are known to be a major cause of climate fluctuations on seasonal timescales (e.g., ENSO) and may also be the dominant cause of climate variability on longer timescales.

## 1.2 Scientific objectives

The first part of this thesis explores the role of the oceans for North Atlantic-European climate. The influence of SST on the NAO is controversial. A large amount of the variance of the NAO is due to the internal, nonlinear variability of the atmosphere. Experiments with AGCMs forced by a climatological annual cycle of boundary conditions without any interannual variability simulate an NAO with a realistic spatial pattern and spectrum. However, ensemble simulations with AGCMs forced by observed interannually varying SST and sea ice (SI) conditions are able to reproduce a remarkable amount of the observed NAO variability. Here, experiments with AGCMs are performed to understand the mechanisms of North Atlantic-European climate. The oceanic influence on the atmospheric circulation is important in respect to the predictive capability of climate. The following question is guiding the investigation:

- I. Has the ocean an influence on North Atlantic-European climate and - if this is the case - which part of the world's ocean is most important?

The oceanic influence on the atmospheric circulation in the North Atlantic-European region in ensemble simulations with the AGCM ECHAM4 is presented in **Chapter 2**. Experiments with SST/SI forcing restricted to either the Atlantic or the Indo-Pacific and climatological SST/SI forcing elsewhere are performed to separate the role of the Atlantic from that of the Indo-Pacific Oceans in Atlantic-European climate. The atmospheric response in these experiments is studied with the analysis of variances (ANOVA) and the optimal detection analysis (ODA), which are described in the **Appendix**.

The ODA is also applied to another set of ECHAM4 ensemble integrations with globally prescribed SST/SI forcing. Additional to the leading modes of boundary forced variability the climatological mean and linear trends are investigated. The results are compared with that of three other AGCMs (HadAM3, ARPEGE, and ECHAM5) as part of a multi-model intercomparison study, which is presented in **Chapter 3**.

The influence of the Atlantic Ocean on climate is further investigated in an idealized experiment with ECHAM4. A control experiment with climatological SST/SI forcing is performed. Two sensitivity experiments are made with SST/SI anomalies added to and subtracted from the climatological SST/SI in the North Atlantic. The response of the atmospheric circulation and the influence on the climate are investigated. The results of the experiments with ECHAM4 are compared with those of four other AGCMs (HadAM3, ARPEGE, ECHAM5, and CAM2) as part of another multi-model intercomparison study, which is presented in **Chapter 4**.

Table 1.1 gives an overview of the AGCM experiments, which are presented in the first part of this thesis. The ECHAM4 experiments presented in Chapters 2 and 4 are performed and all ECHAM4 experiments (Chapters 2, 3 and 4) are analyzed within this Ph.D. thesis. In two multi-model intercomparison studies (Chapters 3 and 4) the ECHAM4 results are compared with the results of other AGCMs.

Chapter	Model type	Exp. type	Model	Ens. size	Exp. name	Integr. period (yrs)
2	AGCM	AMIP	ECHAM4	6	GOGA	24 (1971-1994)
			ECHAM4	6	AOGA	24 (1971-1994)
			ECHAM4	6	I+POGA	24 (1971-1994)
3	AGCM	AMIP	ECHAM4	6		44 (1951-1994)
			ECHAM5	4		49 (1949-1997)
			ARPEGE	8		50 (1949-1998)
			HadAM3	6		129 (1871-1999)
4	AGCM	Idealized	ECHAM4		C, A+, A-	21, 21, 21
			ECHAM5		C, A+, A-	21, 21, 21
			ARPEGE3		C, A+, A-	21, 21, 21
			HadAM3		C, A+, A-	21, 21, 21
			CAM2		C, A+, A-	21, 21, 21

**Table 1.1** A summary of the AGCM experiments used in this study. The experiment type AMIP is forced by observed SST/SI of the given period. In the experiments AOGA and I+POGA the forcing is restricted to the Atlantic and Indo-Pacific oceans, respectively, while a climatological annual cycle is used elsewhere. The idealized experiments are forced with a climatological annual cycle of SST/SI (C) and an SST/SI anomaly pattern added to (A+) and subtracted from (A-) these values.

The second part of this study investigates the predictability of North Atlantic-European climate. On seasonal timescales great progress has been attained with the ability to predict the ENSO phenomenon. On decadal to multidecadal timescales the large-scale oceanic circulation is assumed to provide a potential for climate prediction. Especially, variations in the THC may be predictable a few decades ahead, as shown by a number of model studies. The predictability attributed to this climate variability is investigated in this study using coupled AOGCM experiments. The main question considered here is:

## II. To which extent is North Atlantic-European climate predictable?

The coupling of the AGCM ECHAM5 and the ocean general circulation model MPI-OM without the use of flux adjustments provides a new tool for the estimation of climate predictability. The analyses of the results from the preliminary and final versions of this AOGCM, which are performed during this work, are used in the coupled model working group at the Max Planck Institute for Meteorology for the investigation and improvements of the AOGCM ECHAM5/MPI-OM.

A 500-year long control integration and ensemble predictability experiments with the AOGCM ECHAM5/MPI-OM are analyzed to estimate the decadal climate predictability. The ensemble predictability experiments are realized with slightly perturbed atmospheric but the same oceanic initial conditions. The results of the diagnostic and prognostic potential predictability approaches are presented in **Chapter 5**.

The same experiments with ECHAM5/MPI-OM are used in another study to investigate the influence of the North Atlantic meridional overturning circulation on European climate in a probabilistic manner. The decadal climate predictability is investigated in

this study with a probabilistic technique, which is more commonly used in medium-range and seasonal forecasting. The results are presented in **Chapter 6**.

The results of the predictability analyses with ECHAM5/MPI-OM, which are presented in Chapters 5 and 6, are compared to the results of four other AOGCMs (HadCM3, ARPEGE/ORCALIM, BCM, and INGV) to investigate the interannual to decadal climate predictability and its uncertainties. The results of this multi-model intercomparison are presented in **Chapter 7**.

Table 1.2 gives an overview of the AOGCM experiments, which are presented in the second part of this thesis. The experiments with the AOGCM ECHAM5/MPI-OM are analyzed in Chapters 5 and 6. These results are compared in Chapter 7 with the results of other AOGCMs in a multi-model intercomparison study.

Chapter	Model type	Model	Number of ens. exp.	Number of ens. members in each exp.	Length of ensemble runs (yrs)	Length of control run (yrs)
5	AOGCM	ECHAM5/MPI-OM	3	6	20	500
6	AOGCM	ECHAM5/MPI-OM	3	6	20	500
7	AOGCM	ECHAM5/MPI-OM	3	6	20	500
		INGV	2	2	20	100
		ARPEGE/ORCALIM	2	6	25	200
		HadCM3	3	8	20	2000
		BCM	2	3	20	300

**Table 1.2** *A summary of the coupled AOGCM experiments used in this study.*

Additional to the conclusions given at the end of each paper the results are summarized in **Chapter 8** in order to answer the two leading questions, which are presented in this Section and guiding this Ph.D. thesis. An outlook concludes this Ph.D. thesis presenting the author's mind on possibilities and limitations for further investigations of mechanisms and predictability of North Atlantic-European climate.

### 1.3 Contents of the Ph.D. thesis

This Ph.D. thesis consists of six papers, which are listed in Table 1.3. All of these papers are in the review process or have been reviewed. The publications presented in Chapters 4 and 5 are already published. In the first part (Chapters 2, 3 and 4) the mechanisms of North Atlantic-European climate are investigated with AGCMs, while in the second part of this thesis (Chapters 5, 6 and 7) the predictability of North Atlantic-European climate is studied with AOGCMs. Three multi-model comparison papers (Chapters 3, 4 and 7) are presented.

Chapter	Authors	Year	Title	Journal	Volume, Page range
2	H. Pohlmann M. Latif	2004	Atlantic versus Indo-Pacific influence on Atlantic-European climate	Geophys. Res. Lett.	in press
3	D. Hodson R. T. Sutton H. Pohlmann M. Rodwell M. Stendel L. Terray	2004	Influence of the oceans on North Atlantic climate variability: A comparison of results from 4 atmospheric GCMs	Climate Dyn.	submitted
4	M. J. Rodwell M. Drévillon C. Frankignoul J. W. Hurrell H. Pohlmann M. Stendel R. T. Sutton	2004	North Atlantic forcing of climate and its uncertainty from a multi-model experiment	Quart. J. Roy. Meteor. Society	130, 2013-2032
5	H. Pohlmann M. Botzet M. Latif A. Roesch M. Wild P. Tschuck	2004	Estimating the decadal predictability of a coupled AOGCM	J. Climate	17, 4463-4472
6	H. Pohlmann F. Sienz M. Latif	2004	Influence of the multidecadal Atlantic meridional overturning circulation variability on European climate	J. Climate	submitted
7	M. Collins M. Botzet A. Carril H. Drange A. Jouzeau M. Latif O. H. Otterå H. Pohlmann A. Sorteberg R. Sutton L. Terray	2004	Interannual to decadal climate predictability: A multi-perfect-model-ensemble study	J. Climate	submitted

**Table 1.3** *A summary of the papers, which are presented in Chapters 2 to 7.*

## **Atlantic versus Indo-Pacific influence on Atlantic-European climate**

(H. Pohlmann, and M. Latif)

### **Abstract**

The influence of the Atlantic and Indo-Pacific oceans on Atlantic-European climate is investigated by analyzing ensemble integrations with the atmospheric general circulation model ECHAM4 forced by anomalous sea surface temperature and sea ice conditions restricted to the Atlantic (AOGA) and Indo-Pacific (I+POGA) oceans. The forcing from both the Indo-Pacific and Atlantic oceans are important for the generation of the sea level pressure (SLP) variability in the Atlantic region in the boreal winter season. Over the North Atlantic the SLP response in the I+POGA experiment projects on the North Atlantic Oscillation, while it projects on the East Atlantic Pattern in the AOGA experiment. In both experiments (I+POGA and AOGA) a quadrupole-type 500hPa height anomaly pattern is simulated which emerges from the tropical Pacific and Atlantic oceans, respectively. In boreal summer the influence of the Atlantic ocean dominates the SLP response in the Atlantic region. The tropical North Atlantic is a key region in forcing the SLP response over the Caribbean Sea in this season.

### **2.1 Introduction**

The Atlantic-European climate variability is dominated by the North Atlantic Oscillation (NAO). The NAO is a sea-saw in sea level pressure (SLP) with centers over the Azores and Iceland. The influence of the NAO on the North Atlantic is widely accepted (e.g. Visbeck et al. 1998). The projection of the NAO onto North Atlantic sea surface temperature (SST) is a tripole pattern on interannual timescales (e.g. Marshall et al. 2001). The correlation is highest when the tripole SST index lags the NAO by about one month indicating an atmospheric influence on the ocean (Deser and Timlin 1997, Czaja and Frankignoul 2002). However, the influence of the ocean on the extratropical atmospheric circulation is not completely understood. A large amount of the variance of the NAO is due to the internal, nonlinear variability of the atmosphere. Experiments with atmosphere general circulation models (AGCMs) forced by a climatological annual cycle of boundary conditions without any interannual variability simulate an NAO with a realistic spatial pattern and spectrum (e.g. Saravanan 1998). However, AGCM ensemble simulations forced by observed interannually varying SST and sea ice (SI) conditions are able to reproduce a remarkable amount of the observed NAO variability (Rodwell et al. 1999, Mehta et al. 2000, Latif et al. 2000, Hoerling et al. 2001). These simulations are commonly referred to as Global Ocean Global Atmosphere (GOGA), meaning that observed SST/SI conditions are prescribed globally. To understand the mechanisms of

the NAO and to decide whether the NAO is part of a coupled air-sea phenomenon, it is important to know which part of the world's ocean has an impact on the NAO.

Sutton and Hodson (2003) showed with an optimal detection analysis (Venzke et al. 1999) applied to GOGA-experiments that the mechanisms of Atlantic-European climate could be different on different timescales. On multidecadal timescales they find an oceanic influence on the NAO encompassing nearly the whole North Atlantic. This mode shows a strong relationship to the North Atlantic thermohaline circulation in coupled atmosphere-ocean general circulation models (AOGCMs) (e.g. Latif et al. 2004). Hoerling et al. (2001) perform AGCM simulations forced by observed SST/SI conditions restricted to the tropical oceans (Tropical Ocean Global Atmosphere – TOGA). They link the NAO trend over the second half of the 20<sup>th</sup> century to a progressive warming of the tropics. Specifically, they exclude the tropical Atlantic as the origin of the NAO trend. The results of idealized SST response AGCM experiments, however, are contradictory. Either, the Indian ocean (Bader and Latif 2003), the eastern tropical Pacific (Schneider et al. 2003), or the North Atlantic (Rodwell et al. 2004) are indicated to contribute to the NAO trend. On shorter (interannual) timescales Sutton and Hodson (2003) find that the climate of the Atlantic-European region is influenced by the Pacific El Niño/Southern Oscillation (ENSO) phenomenon and also by the Atlantic, especially the tropical North Atlantic. Furthermore, the relative importance of these influences is different during different periods, i.e. the oceanic influence on the NAO is non-stationary (Raible et al. 2001, Sutton and Hodson 2003). An AGCM comparison shows a dominant influence of tropical North Atlantic SST on the NAO in three of four models during the period 1951 – 1994 (Hodson et al. 2004). However, the dominant influence on the NAO shifts to the tropical Pacific for two of the models in the extended periods 1947 – 1998 (Terray and Cassou 2002) and 1951 – 1999 (Sutton and Hodson 2003), respectively. The strong El Niño event in 1997/1998 may cause this alteration. Moreover, Terray and Cassou (2002) demonstrate an influence of North Atlantic SST on the NAO with an Atlantic Ocean Global Atmosphere (AOGA) experiment even for the extended period. The AGCM ECHAM4 is used in this study for sensitivity experiments in which the SST forcing is restricted to certain ocean basins to elucidate the Atlantic versus Indo-Pacific influence on Atlantic-European climate.

## **2.2 Experiments and methodology**

Three sensitivity experiments with the AGCM ECHAM4 (Roeckner et al. 1996) are performed: AOGA, I+POGA and GOGA. The AOGA experiment with observed SST/SI forcing restricted to the Atlantic and climatological SST/SI forcing elsewhere is used to determine the role of the Atlantic Ocean for Atlantic-European climate. A counter experiment, I+POGA, with observed SST/SI forcing restricted to the Indo-Pacific and climatological SST/SI forcing elsewhere is used to investigate the influence of the other oceans on Atlantic-European climate. In both experiments, AOGA and I+POGA, the SST/SI forcing is restricted to latitudes north of 30°S. The control experiment, GOGA, with observed SST/SI forcing prescribed globally is performed to test the linearity of the response. For each experiment six ensemble members are performed for the period 1971

– 1994 at T42-L19 resolution. The forcing is taken from the GISST2.2 dataset (Rayner et al. 1996).

The SLP response of these experiments is investigated with the analysis of variances (ANOVA) and the optimal detection analysis (ODA). The ANOVA yields the ratio of the ocean-forced variance to the total variance of a climate variable. These variances are estimated from an ensemble of integrations. The reader is referred to Rowell (1998) for a detailed description of the ANOVA. The second method, the ODA, is a signal-to-noise maximizing EOF algorithm. It yields an estimate of the leading modes of boundary forced variability within an ensemble of integrations. We apply this algorithm to investigate the leading modes (spatial pattern with associated time series) of SST-forced variability in the Atlantic-European region. The reader is referred to Venzke et al. (1999) for a detailed description of the ODA. (See also the **Appendix** for a description of the ANOVA and the ODA).

## 2.3 Results

### 2.3.1 Atlantic versus Indo-Pacific influence

The results of the ANOVA of SLP variability are shown in Figure 2.1. Highest ANOVA values are present in the tropical and subtropical regions in consistence with other (GOGA) studies (Rowell 1998). Over the tropical/subtropical Atlantic ocean the

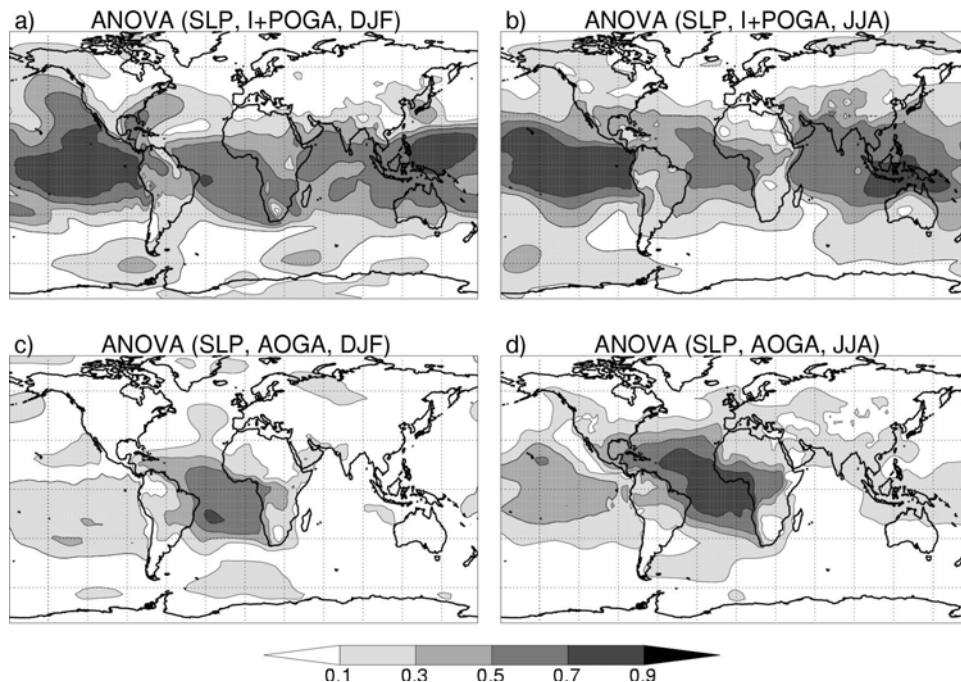


**Figure 2.1** ANOVA values of SLP variability of the I+POGA (upper row) and the AOGA (lower row) experiments for the boreal winter (DJF) (left column) and summer (JJA) (right column) seasons. ANOVA values exceeding 0.1 are significant at the 95% level according to an *F*-test.

ANOVA values of the I+POGA and AOGA experiments are of similar magnitude in the boreal winter season, which suggests that SST from the Indo-Pacific as well as from the Atlantic may generate the SLP variability. In boreal summer, however, the ANOVA values over the tropical/subtropical Atlantic ocean are higher for the AOGA experiment than for the I+POGA experiment, which suggests that the influence from the Atlantic ocean dominates the SLP response in this region.

### 2.3.2 Response in the Atlantic-European region

Figure 2.2a shows the leading mode of the ODA of the SLP variability restricted to the Atlantic-European region for the I+POGA experiment in boreal winter. The data were

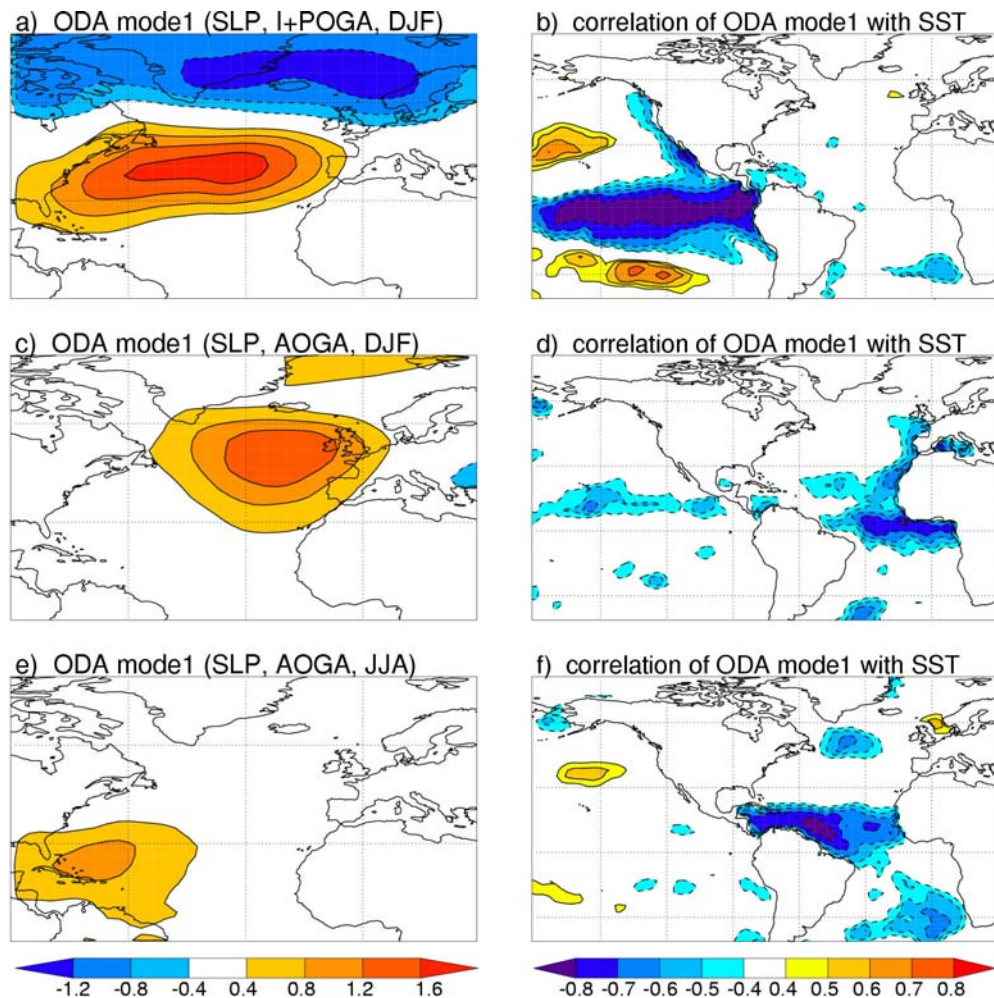


**Figure 2.2** Leading ODA mode of SLP variability [hPa] over the North Atlantic region (left column) and correlation values between the corresponding time series and SST (right column) for the I+POGA experiment in boreal winter (DJF) (upper row), the AOGA experiment in boreal winter (DJF) (middle row) and the AOGA experiment in boreal summer (JJA) (lower row). Correlation values exceeding 0.4 are significant at the 95% level according to a *t*-test.

detrended prior to the analysis. The SLP response pattern projects on the observed NAO structure. Figure 2.2b shows the correlations between the time series associated with this mode and the SST field. The correlation pattern features the significant ENSO influence in the I+POGA experiment. The correlation of this mode with the model NAO index, defined as the leading EOF mode of the ensemble mean SLP in the Atlantic – European region amounts to 0.74 and with SST averaged over the Niño3 region to -0.93. However, the correlation of the time series of the leading ODA mode with the observed NAO index is not significant. Some evidence for an ENSO influence on Atlantic – European climate exists also from observational studies (Fraedrich et al. 1992) and an AGCM experiment (Merkel and Latif 2002), but the explained variance is low. The leading mode of the ODA is a monopole in the AOGA experiment in the boreal winter season (Figure 2.2c) which projects on the East Atlantic Pattern (EAP). The corresponding SST correlation pattern is shown in Figure 2.2d. In this experiment the leading mode of the ODA projects on tropical eastern Atlantic SST, with strongest (anti-) correlations in the equatorial region. The leading mode of the ODA is also a monopole in the AOGA experiment in the boreal summer season (Figure 2.2e), which is located over the Caribbean Sea. The corresponding SST correlation pattern (Figure 2.2f) points to the tropical North Atlantic as a key region in forcing this SLP mode. No significant connection to the North Atlantic in summer was found in the leading ODA mode of the I+POGA experiment.

Figure 2.3a shows the composites of the 500hPa geopotential height (Z500) field of the I+POGA experiment for boreal winter averaged over the years with a high (1972, 1974, 1989) minus low (1973, 1983, 1992) leading ODA mode. The composites pattern of the I+POGA experiment projects on the observed PNA quadrupole with an eastward extension into the North Atlantic. Figure 2.3b shows the composites of the Z500 field of the AOGA experiment for boreal winter averaged over the years with a high (1972, 1977, 1981) minus low (1982, 1988, 1990) leading ODA mode. The pattern is also a quadrupole with centers over the extratropical North Atlantic and the Middle East, and centers of opposite sign over the subtropical North Atlantic and Northeast Europe.

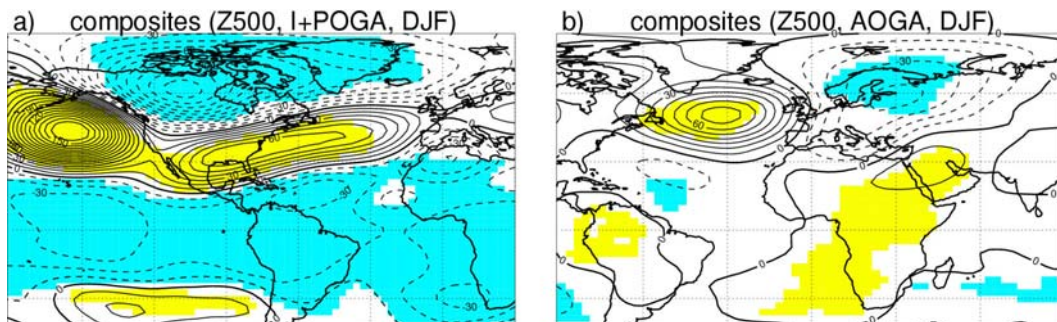


**Figure 2.3** *Difference of the Z500 field [gpm] between high and low phases of the leading ODA mode of the (a) I+POGA and (b) AOGA experiments for the boreal winter (DJF) season. The shaded yellow and blue regions indicate significance on the 95% level according to a t-test.*

The trend of the ensemble and winter mean Z500 field of the GOGA experiment is the most realistic of all experiments and displays a dipole structure in the Atlantic-European region. The dipole projects onto the NAO pattern, with a decrease over the Arctic and an increase over the subtropical Atlantic and southern Europe (not shown). Over the North Atlantic, the linear combination of the Z500 fields from the I+POGA and AOGA experiments results in a stronger and therefore more realistic dipole than in the experiments with the restricted SST/SI forcing alone (not shown). This result suggests a relevance of both SST/SI from the Atlantic and Indo-Pacific oceans for the NAO trend. However, the Z500 trend is unrealistic (positive) especially in the region of the Aleutian Low in both the GOGA and AOGA experiments and in the sum of the AOGA and I+POGA experiments.

## **2.4 Summary and conclusions**

The forcing from both the Indo-Pacific and Atlantic oceans are important for the generation of the SLP variability in the Atlantic region in the boreal winter season. The leading ODA mode of the wintertime SLP variability of the I+POGA experiment, which projects on the NAO, is anticorrelated with ENSO. The teleconnection between these two climate phenomena involves the PNA, with an eastward extension into the North Atlantic. A strong sensitivity of the NAO to tropical Pacific SST is also present in the coupled AOGCM ECHAM4/OPYC (Roeckner et al., 1996b). Therefore, the strong sensitivity to tropical Pacific SST in the I+POGA experiment does not seem to be caused by a lack of feedbacks from the ocean to the atmosphere. The teleconnection between ENSO and the NAO in the I+POGA experiment in the boreal winter season can be explained by an El Niño-related weakening of the North Atlantic mean meridional pressure gradient and a southward shift of the North Atlantic stormtrack (Merkel and Latif 2002). In the absence of varying Indo-Pacific SST, a quadrupole Z500 anomaly response pattern emerges in boreal winter in the AOGA experiment. This pattern is spatially shifted to the PNA and extends over the North Atlantic – Eurasian – African region. In boreal summer, however, the influence of the Atlantic ocean dominates the SLP response over the North Atlantic. SST variability in the tropical North Atlantic drives the SLP response over the Caribbean Sea in this season.

## **Acknowledgments**

We thank Jürgen Bader, Daniel Hodson, Noel Keenlyside, Ute Merkel and Erich Roeckner for the discussion of our results and comments on this paper. This work was supported by the European Union project PREDICATE, and the German Ministry for Education and Research (BMBF) project DEKLIM.

## **References**

Bader, J., and M. Latif, 2003: The impact of decadal-scale Indian Ocean sea surface temperature anomalies on Sahelian rainfall and the North Atlantic Oscillation. *Geophys. Res. Lett.*, 22, 2169, doi:10.1029/2003GL018426.

Czaja, A., and C. Frankignoul, 2002: Observed impact of Atlantic SST anomalies on the North Atlantic Oscillation. *J. Climate*, 15, 606-623.

Deser, C., and M. S. Timlin, 1997: Atmosphere-ocean interaction on weekly timescales in the North Atlantic and Pacific. *J. Climate*, 10, 393-408.

Fraedrich, K., 1994: An ENSO impact on Europe? A review. *Tellus*, 46A, 541-552.

Hodson, D. L. R., R. T. Sutton, H. Pohlmann, M. Rodwell, M. Stendel, and L. Terray, 2004: Influence of the oceans on North Atlantic climate variability: A comparison of results from 4 atmospheric GCMs. (**Chapter 3**). *Climate Dyn.*, submitted.

Hoerling, M., J. Hurrell, and T. Xu, 2001: Tropical origins for recent North Atlantic climate change. *Science*, 292, 90-92.

Latif, M., K. Arpe, and E. Roeckner, 2000: Oceanic control of decadal North Atlantic sea level pressure variability in winter. *Geophys. Res. Lett.*, 27, 727-730.

Latif, M., E. Roeckner, M. Botzet, M. Esch, H. Haak, S. Hagemann, J. Jungclaus, S. Legutke, S. Marsland, U. Mikolajewicz, and J. Mitchell, 2004: Reconstructing, monitoring, and predicting multidecadal-scale changes in the North Atlantic thermohaline circulation with sea surface temperature. *J. Climate*, 17, 1605-1614.

Marshall, J., Y. Kushnir, D. Battisti, P. Chang, A. Czaja, R. Dickson, J. Hurrell, M. McCartney, R. Saravanan, and M. Visbeck, 2001: North Atlantic climate variability: Phenomena, impacts and mechanisms. *Int. J. Climatol.*, 21, 1863-1898.

Mehta, V., M. Suarez, J. Manganello, and T. Delworth, 2000: Oceanic influence on the North Atlantic Oscillation and associated Northern Hemisphere climate variations: 1959-1993. *Geophys. Res. Lett.*, 27, 121-124.

Merkel, U., and M. Latif, 2002: A high resolution AGCM study of the El Niño impact on the North Atlantic/European sector. *Geophys. Res. Lett.*, 29, doi:10.1029/2001GL013726.

Raible, C. C., U. Luksch, K. Fraedrich, and R. Voss, 2001: North Atlantic decadal regimes in a coupled GCM simulation. *Climate Dyn.*, 18, 321-330.

Rayner, N. A., E. B. Horton, D. E. Parker, C. K. Folland, and R. B. Hackett, 1996: Version 2.2 of the global sea-ice and sea surface temperature data set, 1903-1994. CRTN 74, Hadley Centre, Met Office, Bracknell, UK.

Roeckner, E., K. Arpe, L. Bengtsson, M. Christoph, M. Claussen, L. Dümenil, M. Esch, M. Giorgetta, U. Schlese, and U. Schulzweida, 1996a: The atmospheric general circulation model ECHAM-4: Model description and simulation of present-day climate. MPI Report 218, Max Planck Institute for Meteorology, Hamburg, Germany.

Roeckner, E., J. M. Oberhuber, A. Bacher, M. Christoph, and I. Kirchner, 1996b: ENSO variability and atmospheric response in a global coupled atmosphere-ocean GCM. *Climate Dyn.*, 12, 737-754.

Rodwell, M., D. Rowell, and C. Folland, 1999: Oceanic forcing of the wintertime North Atlantic Oscillation and European climate. *Nature*, 398, 320-323.

Rodwell, M. J., M. Drevillon, C. Frankignou, J. W. Hurrell, H. Pohlmann, M. Stendel, and R. T. Sutton, 2004: North Atlantic forcing of climate and its uncertainty from a multi-model experiment. **(Chapter 4)**. *Q. J. Roy. Meteor. Soc.*, 130, 2013-2032.

Rowell, D. P., 1998: Assessing potential seasonal predictability with an ensemble of multidecadal GCM simulations. *J. Climate*, 11, 109-120.

Saravanan, R., 1998: Atmospheric low-frequency variability and its relationship to midlatitude SST variability: Studies using the NCAR Climate System Model. *J. Climate*, 11, 1386-1404.

Schneider, E. K., L. Bengtsson, and Z.-Z. Hu, 2003: Forcing of Northern Hemisphere climate trends. *J. Atmos. Sci.*, 60, 1504-1521.

Sutton, R. T., and D. L. R. Hodson, 2003: Influence of the ocean on North Atlantic climate variability 1871-1999, *J. Climate*, 16, 3296-3313.

Terray, L., and C. Cassou, 2002: Tropical Atlantic sea surface temperature forcing of quasi-decadal climate variability over the North Atlantic-European region. *J. Climate*, 15, 3170-3187.

Venzke, R., M. Allen, R. Sutton, and D. Rowell, 1999: The atmospheric response over the North Atlantic to decadal changes in sea surface temperature. *J. Climate*, 12, 2562-2584.

Visbeck, M., H. Cullen, G. Krahnmann, and N. Naik, 1998: An ocean model's response to North Atlantic Oscillation like wind forcing. *Geophys. Res. Lett.*, 25, 4521-4524.

## **Influence of the oceans on North Atlantic climate variability: A comparison of results from 4 atmospheric GCMs**

(D. Hodson, R. T. Sutton, H. Pohlmann, M. Rodwell, M. Stendel, and L. Terray)

### **Abstract**

The influence of changing ocean conditions on the variability of climate in the North Atlantic region has been studied by analysing, and comparing, ensemble simulations with four different atmospheric GCMs: HadAM3, ARPEGE, ECHAM4 and ECHAM5. Results from all four models support the conclusion that variability in sea surface temperatures (SST) had a significant influence on the climate of the North Atlantic region during the period studied (1951-1994). In three of the models the dominant winter mode of SST-forced variability is an NAO-like dipole pattern, and regression analysis points to the tropical North Atlantic (TNA) as a key region of forcing. Also, three of the models (but not the fourth) simulate a positive trend in the NAO during the period 1951-94, as was observed. All the models simulate a significant response to ENSO over the Atlantic basin. The response over the tropical Atlantic is very consistent between the models, and also observations, but there are significant differences in the response over the North Atlantic. Lastly, we find significant differences in the sensitivity of the models to interannual variability of SST in TNA region. The HadAM3 model shows the highest sensitivity; by contrast, the ECHAM4 model is much more sensitive to tropical Pacific SST than to tropical Atlantic SST.

### **3.1 Introduction**

Variability in climate can arise from processes internal to the atmosphere or from external influences. The external influences include changes in the surface conditions of the oceans, ice sheets and land surface, as well factors that are external to the entire Earth system, such as changes in solar output. Amongst these multiple influences, the role of the oceans is of particular interest because the evolution of (large-scale) ocean conditions is predictable months or even years ahead (e.g., Pohlmann et al. 2004). It follows that if we can understand the way in which changing ocean conditions impact climate, we may be able to provide useful climate predictions.

The influence of changing ocean conditions on the climate of the North Atlantic region is a subject that has received considerable recent attention (e.g. Rodwell et al. 1999, Mehta et al. 2000, Czaja and Frankignoul 2002). A particular focus has been the ocean influence on the North Atlantic Oscillation (NAO), which is the dominant mode of wintertime climate variability in the North Atlantic region (Hurrell 1995). Several studies have shown evidence of a significant ocean influence on the NAO, although there is some disagreement about which regions of the ocean play the most important role. Rodwell et al. (1999) suggested that the Atlantic Ocean was most important, whereas Hoerling et al.

(2001) suggested that the rising trend in the NAO index that was observed in the latter part of the twentieth century was primarily a response to changing conditions in the tropical Pacific and Indian Oceans.

In our previous study (Sutton and Hodson 2003, hereafter SH03) we investigated the ocean influence on North Atlantic climate variability, including the NAO, by analysing an ensemble of six simulations with the Hadley Centre atmospheric GCM HadAM3. Each of the simulations was forced with sea surface temperature (SST) data reconstructed for the period 1871-1999. The simulations were analysed using an optimal detection algorithm (Venzke et al. 1999) to separate the influence of the ocean from the influence of internal atmospheric variability. The results showed that: 1) on multidecadal timescales the ocean influence is dominated by a single mode that is associated primarily with changes in the North Atlantic SST, has a strong projection on the NAO in wintertime, and may be a response to fluctuations in the thermohaline circulation; 2) on interannual timescales the climate of the North Atlantic region is influenced by the Pacific ENSO phenomenon but also by SST anomalies in the Atlantic, especially the tropical North Atlantic (TNA region). In addition, SH03 showed that the relative importance of the Pacific and Atlantic influences varied during the time period 1871-1999, i.e. the ocean influence was nonstationary.

The results of SH03 gave valuable insights into the role of the ocean in North Atlantic climate variability, but an important question is whether the results are reproducible. Do experiments with other models support the same conclusions? This is the key question we address in the present paper. We make use of results generated as part of the European Union funded PREDICATE project. Within this project ensemble simulations were performed with four different atmospheric GCMs forced with the same (or very similar) SST data. We use the same tools as SH03 to analyse the results from the different models, focussing on the period 1951-1994, and on wintertime.

The structure of the paper is as follows. Section 2 describes the models and data sets used. Section 3 explains the treatment of the data and the optimal detection methodology. The results, including a separate discussion of multidecadal and interannual timescales, are presented in Section 4, and the conclusions are in Section 5.

### **3.2 Models and data**

The atmosphere models employed for this study were: HadAM3, ARPEGE-climat(v3), ECHAM4 and a preliminary version of ECHAM5. HadAM3 is a version of the UK Hadley Centre atmosphere GCM. This model employs an Arakawa B grid and hybrid vertical coordinates. It has a horizontal resolution of  $2.5^\circ$  latitude  $\times$   $3.75^\circ$  longitude with 19 hybrid levels in the vertical. ARPEGE-climat has been developed at Météo France from the Arpege/IFS operational model developed by Météo France and ECMWF. It is a T63 spectral model with an effective horizontal resolution of  $2.8^\circ$  latitude  $\times$   $2.8^\circ$  longitude and 31 hybrid levels in the vertical. ECHAM4 and ECHAM5 have been developed by the Max Planck Institute for Meteorology in Hamburg from a version of the ECMWF model. They are both T42 spectral models with effective horizontal resolutions

of  $2.8^\circ$  latitude  $\times$   $2.8^\circ$  and with 19 hybrid levels in the vertical. For a detailed description of the models and their behaviour the reader is referred to Pope et al. (2000) (HadAM3), Cassou and Terray (2001) (ARPEGE-climat), Roeckner et al. (1996) (ECHAM4) and Roeckner et al. (2003) (ECHAM5).

Each model was forced with sea surface temperature and sea ice extent data taken from UK Met Office analyses of surface observations. The same version of the data was not used in all cases, but for the period considered the differences between the versions are small, and did not appear to impact our analyses. ECHAM4 was forced with the GISST 2.2 dataset (Rayner et al. 1996), and ARPEGE-climat was forced with a blend of GISST2.3 (from 1947 to 1982) and GISST 3.0 (from 1983 to 1998). HadAM3 and ECHAM5 were both forced with HadISST (Rayner et al. 2003), which is the most recent version of the “GISST” datasets. Additionally, the ECHAM4 simulations included time-varying observed greenhouse gas forcing. Whether this forcing affects our results will be discussed later, but it should be noted that - to the extent that the rising trend in greenhouse gases has influenced SST - all the models will include a component of this externally forced response.

Ensemble simulations were available for each of the four models. The ensemble is used to sample the atmospheric internal variability, and individual ensemble members differ only in the initial atmospheric conditions. Table 3.1 shows the ensemble size and time period of the simulations available for each model. To compare the results from the different models we analyse the maximum period of time that was common to all model integrations - 1951-1994.

In addition to the model data, and observational SST data, a dataset of global sea level pressure observations, GMSLP2.1f (Basnet and Parker 1997), was used to evaluate certain model results. This dataset covers the period 1871-1994.

Model	Ensemble Size	Resolution	SST	Time Period
HadAM3	6	$2.5^\circ \times 3.75^\circ$	HadISST	1871-1999
Arpege-climat(v3)	8	T63 ( $2.8^\circ \times 2.8^\circ$ )	GISST2.3+GISST3.0	1949-1998
Echam4	6	T42 ( $2.8^\circ \times 2.8^\circ$ )	GISST2.2	1951-1994
Echam5	4	T42 ( $2.8^\circ \times 2.8^\circ$ )	HadISST	1949-1997

**Table 3.1** Comparison of model experiments. “GISST2.3+GISST 3.0” means ARPEGE-climat was forced with a blend of GISST2.3 (from 1947 to 1982) and GISST 3.0 (from 1983 to 1998).

### 3.3 Data analysis

#### 3.3.1 Preprocessing

As in SH03 we analyse Mean Sea Level Pressure (MSLP) data and restrict our attention to the North Atlantic region  $0-80^\circ\text{N}$ ,  $90^\circ\text{W}-30^\circ\text{E}$ . For this study we consider only wintertime (December-February; djf). DJF anomalies were constructed by, first, averaging monthly mean data over the three winter months and then subtracting, at each grid point, the time mean value. The initial analysis was performed on this data.

The results of SH03 indicated distinct variability on multidecadal and interannual timescales. These timescales were separated by application of a low pass, time domain, filter. An issue with the use of such filters is end effects. Such effects are more serious for shorter timeseries. Because in this study we are considering a time period of only 44 years (rather than 129 years considered by SH03) we used a simpler approach to separate the low frequency and higher frequency variability. Specifically, we considered the low frequency signal to be that part of the total variability that is extracted by regressing on a linear trend. The residual variance we treat as high frequency variability. As we shall see, this approach yields results which can be usefully compared with the results of SH03.

### 3.3.2 Optimal detection

Optimal detection provides a methodology to determine the common, boundary forced, variability within the ensemble of integrations. Because it involves no explicit use of the SST data optimal detection provides an objective way to identify those aspects of the ocean variability to which the atmosphere is most sensitive. The specific algorithm we use is described in detail by Venzke et al. (1999), and more briefly by SH03. (See also the **Appendix** for a description of this algorithm). The algorithm yields an estimate of the leading modes (spatial patterns with associated time series) of SST-forced variability. We will not discuss the full details of the methodology here but will note two important details. First, an important stage in the analysis involves projection of the ensemble mean model data onto the leading modes of internal variability (or “noise”). A choice must be made about how many noise Empirical Orthogonal Functions (EOFs, e.g., Wilks 1995) to retain. Secondly, a choice must also be made concerning the number of optimal filters to retain when constructing the dominant modes of SST-forced variability. Optimal filters are patterns that optimally discriminate between the SST-forced signal and the noise. The choice of how many to retain is guided by examining the signal-to-noise ratio for each optimal filter, together with the fraction of the ensemble mean variance each represents. The number of optimal filters to retain is decided by examining how well separated, both in terms of signal-to-noise ratio and ensemble mean variance fraction, are the leading optimal filters from the remainder.

In this study we chose to retain 30 (from 44) noise EOFs, the same number as SH03. Our results are robust to changes in this choice for all the models except ECHAM4. In the case of ECHAM4, by changing the noise cut off it was possible to swap the order of the two leading modes of SST forced variability. This result highlights the fact that, in ECHAM4, the two leading modes are not well separated from each other.

Also following SH03 we used the first two optimal filters to construct the dominant forced modes. In the case of unfiltered data, for HadAM3 and ARPEGE-climat the first two optimal filters were well separated from the remainder both in terms of their signal-to-noise ratio and the ensemble mean variance they explained. For ECHAM4 and ECHAM5 the separation of the first two optimal filters was less clear, but we chose two retain two filters to facilitate comparison of the different models. In the case of the detrended data (describing the high frequency variability), the first two optimal filters were well separated from the remainder in HadAM3 and ECHAM5. In the ARPEGE-

climat and ECHAM4 models a single optimal filter was well separated from the remainder, but we again retained the first two optimal filters so as to treat the data from the different models in a consistent way.

### **3.3.3 Regression analysis**

The optimal detection methodology extracts variability that is common to all the ensemble members without making any explicit use of the SST data. To identify the pattern of SST that is responsible for forcing the atmosphere we regress the SST data that was used to force the model on the timeseries associated with the mode in question. This approach assumes a linear response. Because the regression residuals are not expected to be uncorrelated in time we model them using an AR(1) process in the regression procedure (see Allen and Smith (1994) for further details). Lastly, we also use regression analysis to investigate the atmospheric response to specific aspects of the SST variability.

## **3.4 Results**

### **3.4.1 Climatologies**

To give a point of reference for our later comparisons, Fig 3.1 shows a comparison between the observed (DJF) MSLP climatology over the North Atlantic region and that of the four models. The major features of the observations - the Iceland Low, Azores High, and northeastward track of the strongest MSLP gradients - are well captured by all the models. The position of the Iceland Low is generally well captured, while the position of the Azores High tends to be east of the observed position. In three of the four models (ECHAM4, ECHAM5 and ARPEGE-climat) the difference in pressure between the Iceland Low and Azores High is greater than in the observations, whereas in HadAM3 the difference is less than is observed.

Fig 3.1 also shows, for each model, the leading EOF of internal MSLP variability (estimated using the departures of the individual ensemble members from the ensemble mean). These patterns may be viewed as the model representations of the NAO. The patterns show considerable agreement between the models but some differences in amplitude. The strong gradients that indicate fluctuations in the westerly winds show a more northward tilt in ECHAM5 than in the other models. In the case of the observations the leading mode of interannual variability is shown. Note that SST-forced variability as well as internal variability will contribute to this mode and thus, as expected, the amplitude of variability is greater. The pattern is most similar to that found in the ECHAM5 model.

### **3.4.2 Unfiltered data**

In this section we examine the results of the optimal detection analysis applied to the unfiltered data and draw comparisons between the different models. Figs 3.2(a-d) show the leading mode of forced MSLP variability for winter (djf) in the four models. Panels e-h show the regression of the SST forcing field onto the time series (panels i-l) associated

with the leading mode. These modes explain between 9% and 15% of the total variance in a single ensemble member (see Table 3.2).

	HadAM3	Arpege	Echam4	Echam5
a)	14.8±1.3	13.9±1.3	10.7±0.5	10.7±2.8
b)	9.8±1.4	9.1±1.2	5.9±0.8	4.4±0.2
c)	8.4±1.1	4.6±0.5	9.1±0.6	10.8±2.3
d)	7.6±0.6	9.1±0.3	4.3±0.3	10.2±0.4

**Table 3.2** a) Fraction of the total variance in North Atlantic DJF MSLP of a single ensemble member explained by first unfiltered mode from Fig 3.2 for each of the three models. The values are the mean of the fraction of the variance explained (FVE) for each ensemble member. The uncertainty is the uncertainty in the estimate of this mean. b) as a) but the FVE by a linear trend. c) as a) but for the the first mode of the detrended data. d) as c) but for the second mode.

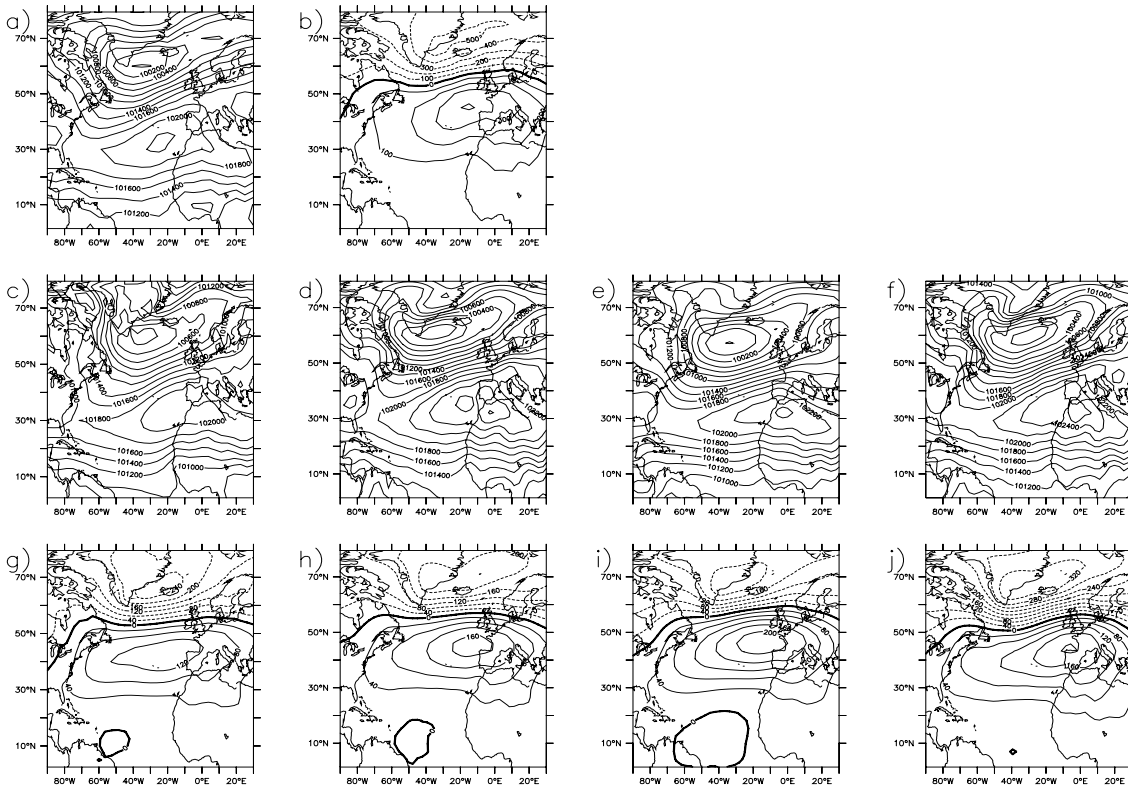


**Figure 3.1** a) Observed Mean Sea Level Pressure (MSLP, Pa) climatology over the N. Atlantic Region (NAR) for DJF (1951-1994). b) First EOF of Observed MSLP over NAR (DJF) (1951-1994). Contours are in Pa per standard deviation of the associated timeseries. Ensemble mean MSLP Climatology (1951-1994) over NAR (DJF) for c) HadAM3 d) ECHAM4 e) ARPEGE-climat f) ECHAM5. First EOF of internal noise (departures from ensemble mean) (1951-1994) for g) HadAM3 h) ECHAM4 i) ARPEGEclimat j) ECHAM5. Contours are in Pa per standard deviation of the associated timeseries.

For three of the four models (HadAM3, ARPEGE-climat and ECHAM5) the spatial pattern of the leading mode features a dipole structure in MSLP reminiscent of the NAO. Comparison with Fig 3.1 shows that the orientation of the dipole tends to be rotated, in a clockwise sense, relative to the leading mode of internal variability. In all three cases the timeseries show a prominent rising trend with interannual-to-decadal fluctuations in addition. The SST regression patterns (Fig 3.2(e,g,h)) indicate that the largest fraction of variance explained occurs in the tropical North Atlantic (TNA) region; this suggests that the TNA is a likely region of forcing for this mode, with negative TNA SST anomalies being associated with a positive NAO. This result is consistent with the findings of SH03 and also other modelling studies (Sutton et al. 2001, Cassou and Terray 2001). In the

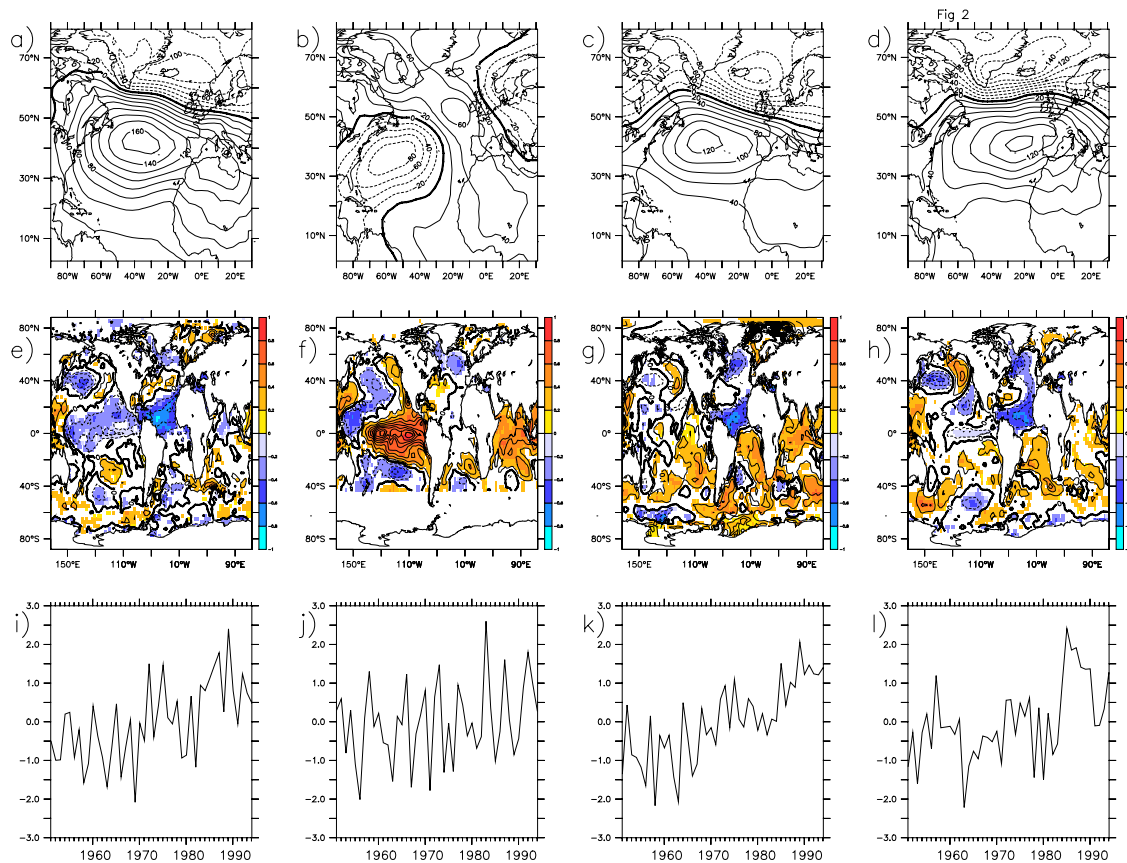


**Figure 3.2** (a-d) The dominant mode of forced variability in MSLP over the North Atlantic region in DJF for a) HadAM3 b) ECHAM4 c) ARPEGE-climat d) ECHAM5. Contour interval is 20 Pa per standard deviation of the associated timeseries. (e-h) SST forcing field regressed onto the time series below for e) HadAM3 f) ECHAM4 g) ARPEGE-climat h) ECHAM5. The contour show the regression coefficient. The contour interval is 0.1K per standard deviation of the time series. The shading shows the fraction of the variance in SST that is explained by the time series. White areas are where the regression is not significant at the  $2.0\sigma$  level. (I-l) Time series (PC) associated with the pattern directly above for i) HadAM3 j) ECHAM4 k) ARPEGE-climat l) ECHAM5.

ARPEGE-climat and ECHAM5 results the TNA SST signal is part of a dipolar pattern of SST anomalies in the tropical Atlantic region, and in the ARPEGE-climat results there is also a significant SST signal in the Indian Ocean. The differences in the SST patterns for the different models highlight the fact that, from these experiments alone, it is difficult to be sure exactly which regions of the ocean are responsible for forcing the NAO-like response. Nevertheless the consistency of the signature in TNA SST is strong evidence for the importance of this region.

The results for ECHAM4 (panels b,f,j) show a dominant mode of forced variability that is clearly different from the other models. The SST pattern suggests that in this model ENSO is the dominant influence. (In the other three models, ENSO is associated with the second mode of SST-forced variability.) Recall from Section 3.3.2, however, that this result is sensitive to the number of noise EOFs retained. If 15 rather than 30 EOFs are retained then the leading mode in ECHAM4 is an NAO-like pattern as seen in the other models, and negative SST anomalies in the TNA region are again associated with a positive NAO. The sensitivity of the ECHAM4 results suggests, however, that the response of this model to TNA SST may be weaker relative to the ENSO influence than is found in the other models.

In SH03 the model data were filtered to separate the ocean's influence on multidecadal variability from the influence on interannual variability. The presence of a significant trend in the time series associated with the leading mode of unfiltered data in three of the four models, motivates a similar timescale separation in this study. As explained in Section 3.3.1, we perform the separation by the simple method of regressing on a linear trend. The results are discussed in succeeding sections.

### **3.4.3 Linear trend**

We regressed the SST data, the ensemble mean MSLP from each model, and the observed MSLP, onto a standardized linear trend with a positive gradient. The results are shown in Fig 3.3. HadAM3, ARPEGE-climat and ECHAM4 (Fig 3.3 a,b,c) all show an NAO-like pattern over the North Atlantic Ocean. The patterns for HadAM3 and ARPEGE-climat are very similar, while in ECHAM4 the MSLP dipole is shifted eastward over Europe. It is possible that the eastward shift in ECHAM4 is a response to the time-dependent greenhouse gas forcing that was included in the integrations of this model (Jung and Hilmer 2001, Ulbrich and Christoph 1999). Without further experiments, however, it is not possible to separate the greenhouse gas influence from the influence of trends in the ocean.

An NAO-like pattern, perhaps most similar to that found in ECHAM4, is also seen in the observations. The results for HadAM3, ARPEGE-climat and ECHAM4 support the suggestion from other studies (Rodwell et al. 1999, Mehta et al. 2000, Latif 2001, Hoerling et al. 2001) that the rising trend in the NAO that was observed in the late twentieth century was, at least in part, a response to changes in the ocean. Interestingly, however, the result for ECHAM5 does not support the same conclusion. There is a significant trend in MSLP over the TNA region but no significant trend at higher latitudes

over the North Atlantic. This result is perhaps surprising given the leading mode of SST forced variability in ECHAM5 (Fig. 3.2d,h,l). The timeseries associated with this mode has a positive trend, and the spatial pattern has a dipolar structure resembling the NAO. Fig 3.3d implies, however, that variability of the NAO-like pattern must be associated primarily with the interannual-to-decadal fluctuations seen in the timeseries of Fig. 3.2l, rather than with the trend component. We have confirmed this inference by regressing the ECHAM5 ensemble mean MSLP data on the detrended timeseries. It appears, therefore, that the sensitivity of ECHAM5 to SST trends differs from the sensitivity of the other models.

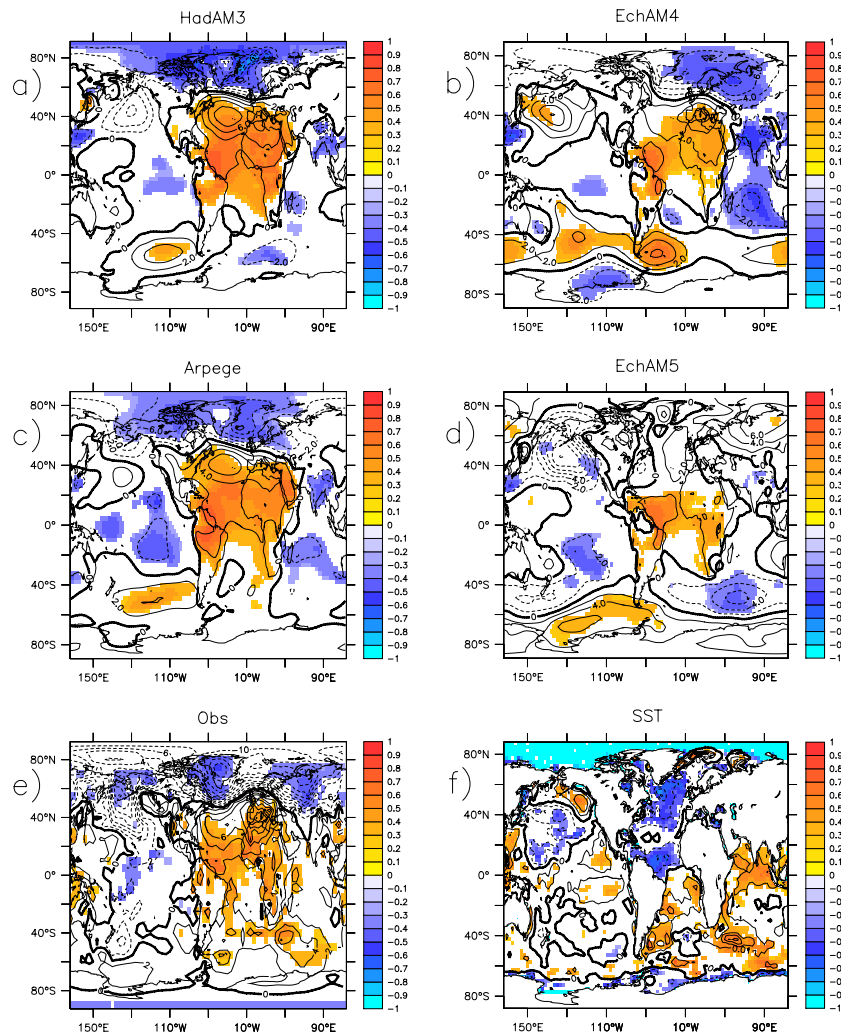


**Figure 3.3** Ensemble mean MSLP (1951-1994) regressed onto a linearly increasing trend for a) HadAM3 b) ECHAM4 c) ARPEGE-climat d) ECHAM5. e) Observed MSLP (1951-1994) regressed onto a linearly increasing trend. f) SST (HadISST) (1951-1994) regressed onto a linearly increasing trend. Contours show the regression coefficient. Contour interval is 2 Pa/year for (a-e) and 0.01K/year for (f). The shading shows the fraction of the variance in MSLP explained by the trend. White areas are where the regression is not significant at the  $2.0\sigma$  level.

The SST pattern in 3.3f indicates a falling trend in SST over most of the North Atlantic and a rising trend over the South Atlantic and the Indian Ocean. The pattern of SST is very similar to that which SH03 linked to multidecadal variability in the NAO (based on the analysis of a longer record of almost 130 years' data). The dipolar pattern in the Atlantic basin suggests a role for fluctuations in the thermohaline circulation. As noted by SH03, however, it is likely that other factors, such as the climate response to increasing levels of greenhouse gases, are also important for understanding the SST trends in the late twentieth century. Given the trends in SST, Hoerling et al. (2001) suggested that the dominant influence on the rising trend in the NAO was from the Indo-Pacific, and that the role of the Atlantic was minor. By contrast, SH03 and our present results shown in Figure 3.3 suggest that trends in the Atlantic are likely to have played had an important role.

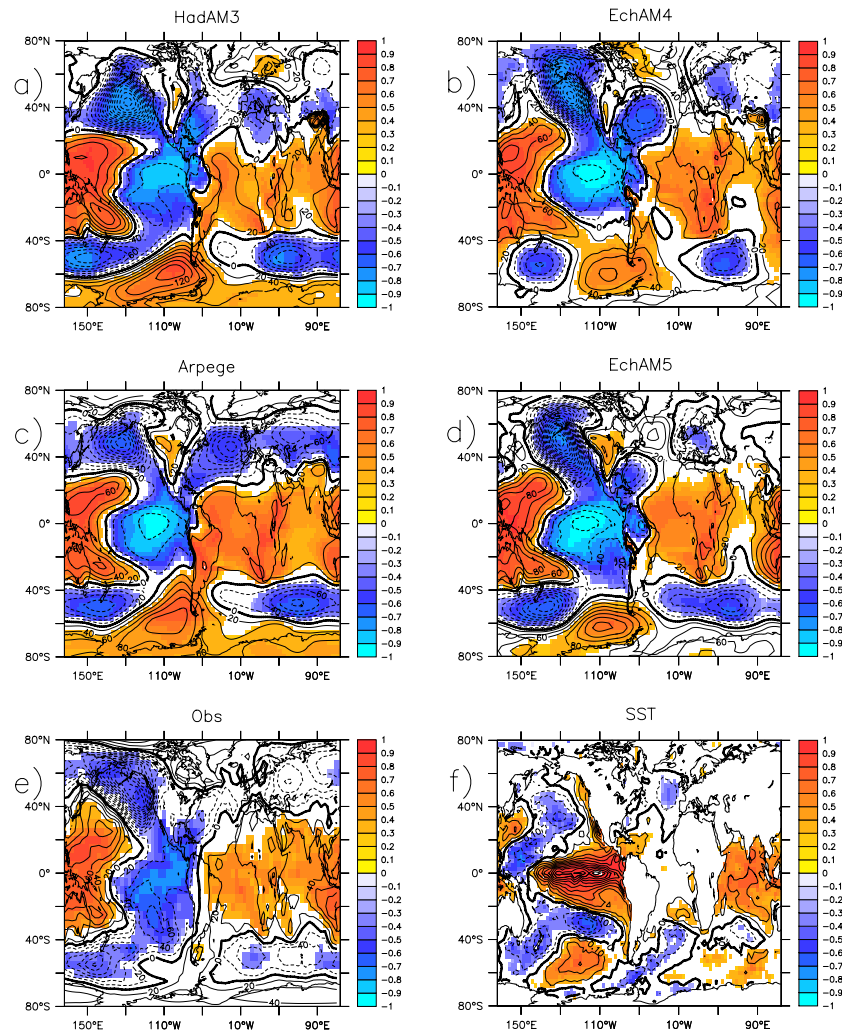
#### 3.4.4 Detrended data

We turn now to analysis of the detrended MSLP variability. We repeated the optimal detection analysis on the detrended DJF data and examined the two leading modes (results not shown). Table 3.2 gives the fraction of the total variance in a single ensemble member that is accounted for by these modes. We found that the influence of ENSO is prominent in all four models. In ECHAM4 the leading mode is associated with ENSO, as was the case for the unfiltered data. In the other three models (HadAM3, ARPEGE-climat and ECHAM5) the SST patterns indicate that the second mode is most closely related to ENSO. For these three models the leading mode again shows a dipolar pattern of MSLP anomalies over the North Atlantic, but the associated SST patterns do not suggest that a single region of the ocean is responsible for the forcing. Significant SST anomalies are found in the tropical Atlantic region but also in the Pacific Ocean and, in the case of HadAM3 and ECHAM5, in the Indian Ocean. Evidently, in this case the optimal detection analysis is not providing a clear separation between the influences of the different ocean basins. The same result was found by SH03 in their analysis of interannual variability. They also showed that regression analysis could shed further light on the Pacific and Atlantic influences. Following SH03 we therefore performed regression analyses using, firstly, an index of detrended Nino3 DJF SST, and secondly an index of detrended DJF SST in the TNA region.

Fig 3.4 shows the results of regression on the detrended Nino3 DJF SST index; individual panels correspond to the detrended ensemble mean MSLP from each of the models, the detrended observed MSLP data and the detrended SST forcing data. The major features of the observed MSLP pattern are seen in all of the models - e.g. the dipolar pattern of the Southern Oscillation over the tropical Pacific, and the enhancement of the Aleutian Low. Closer inspection, however, shows some notable differences between the models. Over the North Pacific the pattern of anomalies simulated by ECHAM4 and ECHAM5 shows the best agreement with the observations. By contrast in HadAM3 and ARPEGE climat the anomalous Aleutian Low extends too far southwestward, reaching as far as Japan. Over the Atlantic basin the observations indicate a response that is clearly significant only over the tropics and subtropics. All the models capture the positive MSLP anomalies observed over the tropical Atlantic and the negative MSLP anomalies observed over the

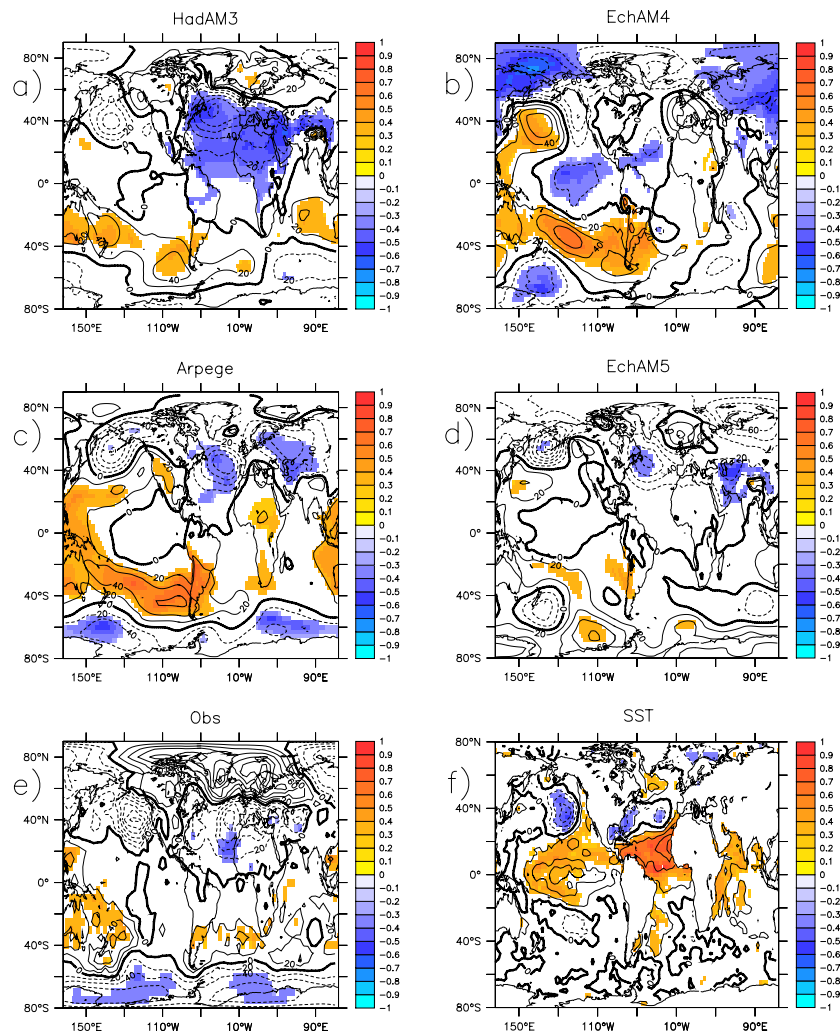
Caribbean. Over the North Atlantic there are some significant differences between the models. ECHAM4 and ECHAM5 simulate a similar pattern that features a band of positive anomalies that reaches from Greenland to North Africa. This feature is not seen in ARPEGE-climat, which simulates negative MSLP anomalies over the whole N. Atlantic, or in HadAM3. These notable differences between the responses of the different models to ENSO variability provide a caution against reliance on any single model.

Fig 3.5 shows the results of regression on the detrended DJF TNA SST index. The strongest signal is found in the HadAM3 model which again shows an NAO-like pattern,



**Figure 3.4** Detrended ensemble mean MSLP (1951-1994) regressed onto detrended Nino3 index (210E:270E,5S:5N) for each model; a) HadAM3 b) ECHAM4 c) ARPEGE-climat d) ECHAM5. e) Detrended observed MSLP regressed onto detrended Nino3 index. f) Detrended SST regressed onto detrended Nino3 index. The contours and shading are as in Fig 3.2.

with a negative projection on the NAO associated with positive TNA SST anomalies. However, only the negative SLP anomalies over the tropical and midlatitude North Atlantic (also extending eastward over North Africa and Southern Europe) are clearly significant. The other three models do show weak negative SLP anomalies (associated with positive TNA SST anomalies) over the tropical or mid-latitude North Atlantic but these anomalies are weak and only marginally significant. The ECHAM4 model shows a pattern of response that is very similar to that seen in Fig 3.4 associated with ENSO. Inspection of panel f in Fig 3.5 shows that there is in fact a weak positive correlation between SST anomalies in the TNA region and SST anomalies in the central tropical Pacific, and it appears that the latter are the dominant influence in ECHAM4. The MSLP pattern for ARPEGE-climat also has some similarities to the ENSO response seen in that model, suggesting a similar dominance of Pacific SST influence over Atlantic SST influence.



**Figure 3.5** As Fig 3.4 but for a detrended index of Tropical North Atlantic SST (7.5W:75W,0:20N).

Panel e in Fig 3.5 shows the results of regressing the detrended observed MSLP data on the detrended TNA DJF SST index. This panel cannot be directly compared with the model results since it represents a single realisation rather than an ensemble mean, and because in the real world the ocean can respond to atmospheric fluctuations as well as forcing them. This said, the regression suggests marginally significant negative MSLP anomalies over the tropical and mid-latitude North Atlantic as is seen in each of the models, and a negative projection on the NAO as is seen in HadAM3. SH03, based on a longer observational record (129 years), found that there is a significant - albeit weak - association between interannual variability of TNA SST and interannual variability in an NAO-like pattern of MSLP.

Although it is not possible to draw firm conclusions about which model may be most realistic Figure 3.5, and the earlier results, suggest that the models differ considerably in their sensitivity to variability in TNA SST. HadAM3 is clearly the most sensitive, while - by way of contrast - ECHAM4 appears to be much more sensitive to tropical Pacific SST than to tropical Atlantic SST.

### 3.5 Conclusions

We have investigated the influence of the oceans on North Atlantic climate variability by analyzing ensemble integrations with four atmospheric GCMs, focussing on the period 1951-94. A particular motivation was to explore whether the conclusions reached by Sutton and Hodson (2003) (SH03) were sensitive to the model employed. Our key findings are as follows:

- All the models support the conclusion that variability in sea surface temperatures (SST) had a significant influence on the climate of the North Atlantic region during the period 1951-1994.
- In three of the models (HadAM3, ARPEGE-climat, ECHAM5) the dominant winter time (djf) mode of SST-forced variability in MSLP over the North Atlantic Region is an NAO-like dipole pattern, and regression analysis points to the tropical North Atlantic as a key region of forcing.
- Three of the models (HadAM3, ARPEGE-climat, ECHAM4) simulate a positive trend in the NAO during the period 1951-94, as was observed. The results for these models are consistent with the suggestion of SH03 that this trend was forced, at least in part, by changes in Atlantic SST. ECHAM5, however, simulates no significant trend in the NAO.
- All the models simulate a significant response to ENSO over the Atlantic basin. Over the tropical Atlantic there is a high degree of consistency between the models, and also the observations, but over the extratropical North Atlantic there are notable differences. ECHAM4 and ECHAM5 simulate the most realistic response to ENSO over the North Pacific
- Our results suggest there are significant differences in the sensitivity of the models to interannual variability of SST in tropical North Atlantic (TNA) region. The HadAM3 model shows the highest sensitivity and simulates a response that projects on the NAO (a result for which there is some support from observations).

By contrast, the ECHAM4 model is much more sensitive to tropical Pacific SST than to tropical Atlantic SST.

The fact that there are significant differences between the models in terms of their response to SST variability provides an important caution against relying too heavily on the behaviour of any single model. A key challenge is of course to understand the reasons for the differences, and to further assess the extent to which individual models are behaving in a realistic manner. This is a major task that will require considerable further research. Within the PREDICATE project, there are two studies that should help to achieve progress. Firstly, an additional set of experiments have been conducted in which the same models considered here were forced by idealised Atlantic SST anomalies. Analysis of these simulations is underway (Rodwell et al. 2004), and the simpler form of the SST forcing makes comparison between the models, and understanding the reasons for differences more straightforward. Secondly, a specific study (Stendel et al. 2003) is using a novel technique to investigate how the response within an individual model is sensitive to changes in the mean state of the atmosphere.

SH03 noted that an important limitation of their study was that analysis was mostly limited to identification of the *linear* response to SST variability. The same limitation applies to this study, and investigation of nonlinearities is another important area for future work. In addition, it is important to keep in mind that in the real world sea surface temperature is not an externally prescribed variable. Indeed, experiments in which atmosphere models are forced with prescribed SST can sometimes give a misleading impression of the ocean's influence on the atmosphere (Bretherton and Battisti 2000, Sutton and Mathieu 2002). It follows that insights gained from atmosphere model experiments must ultimately be tested using coupled models.

### **Acknowledgements**

We would like to thank UKMO for the use of the GMSLP dataset. This work was supported by the EU Framework 5 programme under contract EVK2-1999-00020 (PREDICATE). RTS is supported by a Royal Society research fellowship.

### **References**

- Allen, M., and L. Smith, 1994: Investigating the origins and significance of low-frequency modes of climate variability. *Geophys. Res. Lett.*, 21, 883–886.
- Basnet, T., and D. Parker, 1997: Development of the global mean sea level pressure data set gmslp2. Hadley Centre Climate Research Technical Note CRTN.
- Bretherton, C. S., and D. S. Battisti, 2000: An interpretation of the results from atmospheric general circulation models forced by the time history of the observed sea surface temperature distribution. *Geophys. Res. Lett.*, 27, 767–770.

- Cassou, C., and L. Terray, 2001: Oceanic forcing of the wintertime low-frequency atmospheric variability in the North Atlantic European sector: A study with the arpege model. *J. Climate*, 14, 4266–4291.
- Czaja, A., and C. Frankignoul, 2002: Observed impact of Atlantic SST anomalies on the North Atlantic Oscillation. *J. Climate*, 15, 606–623.
- Hoerling, M. P., J. W. Hurrell, and T. Y. Xu, 2001: Tropical origins for recent North Atlantic climate change. *Science*, 292, 90–92.
- Hurrell, J. W., 1995: Decadal trends in the North Atlantic Oscillation: Regional temperatures and precipitation. *Science*, 269, 676–679.
- Jung, T., and M. Hilmer, 2001: The link between the North Atlantic Oscillation and Arctic sea ice export through Fram Strait. *J. Climate*, 14, 3932–3943.
- Latif, M., 2001: Tropical Pacific/Atlantic Ocean interactions at multi-decadal timescales. *Geophys. Res. Lett.*, 28, 539–542.
- Mehta, V., M. Suarez, J. Manganello, and T. Delworth, 2000: Oceanic influence on the North Atlantic Oscillation and associated northern hemisphere climate variations: 1959–1993. *Geophys. Res. Lett.*, 27, 121–124.
- Pohlmann, H., M. Botzet, M. Latif, A. Roesch, M. Wild, and P. Tschuck, 2004: Estimating the decadal predictability of a coupled AOGCM. (**Chapter 5**). *J. Climate*, 17, 4463–4472.
- Pope, V., M. Gallani, P. Rowntree, and R. Stratton, 2000: The impact of new physical parametrizations in the Hadley Centre climate model: HadAM3. *Climate Dyn.*, 16, 123–146.
- Rayner, N. A., E. B. Horton, D. E. Parker, C. K. Folland, and R. B. Hackett, 1996: Version 2.2 of the global sea-ice and sea surface temperature data set, 1903–1994. CRTN 74, Hadley Centre, Met Office, Bracknell, UK.
- Rayner, N. A., D. E. Parker, E. B. Horton, C. K. Folland, L. V. Alexander, D. P. Rowell, E. C. Kent, and A. Kaplan, 2003: Global analyses of sea surface temperature, sea ice, and night marine air temperature since the late nineteenth century. *J. Geophys. Res.*, 108, 4407, doi:10.1029/2002JD002670.
- Rodwell, M. J., D. P. Rowell, and C. K. Folland, 1999: Oceanic forcing of the wintertime North Atlantic Oscillation and European climate. *Nature*, 398, 320–323.
- Rodwell, M. J., M. Drévillon, C. Frankignoul, J. W. Hurrell, H. Pohlmann, M. Stendel, and R. T. Stutton, 2004: North Atlantic forcing of climate and its uncertainty from a multi-model experiment. (**Chapter 4**). *Q. J. Roy. Meteor. Soc.*, 130, 2013–2032.

Roeckner, E., K. Arpe, L. Bengtsson, M. Christoph, M. Claussen, L. Dümenil, M. Esch, M. Giorgetta, U. Schlese, and U. Schulzweida, 1996: The atmospheric general circulation model ECHAM-4: Model description and simulation of present-day climate. MPI Rep. 218, Max-Planck-Institut für Meteorologie, Hamburg, Germany, 90 pp.

Roeckner, E., G. Bäuml, L. Bonaventura, R. Brokopf, M. Esch, M. Giorgetta, S. Hagemann, I. Kirchner, L. Kornblüeh, E. Manzini, A. Rhodin, U. Schlese, U. Schulzweida, and A. Tompkins, 2003: The atmospheric general circulation model ECHAM5: Part 1: Model description. MPI Rep. 349, Max-Planck-Institut für Meteorologie, Hamburg, Germany, 127 pp.

Stendel, M., I. Mogensen, S. Thorsen, and E. Kaas, 2003: Response to extratropical SST anomalies in an empirically modified general circulation model. *Climate Dyn.*, submitted.

Sutton, R. T., and D. L. R. Hodson, 2003: Influence of the ocean on North Atlantic climate variability 1871-1999. *J. Climate*, 16, 3296–3313.

Sutton, R., and P.-P. Mathieu, 2002: Response of the atmosphere-ocean mixed-layer system to anomalous ocean heat-flux convergence. *Q. J. Roy. Meteor. Soc.*, 128, 1259-1275.

Sutton, R., W. Norton, and S. Jewson, 2001: The North Atlantic Oscillation - what role for the ocean? *Atmospheric Science Letters*, 1, 89–100.

Ulbrich, U., and M. Christoph, 1999: A shift of the NAO and increasing storm track activity over Europe due to anthropogenic greenhouse gas forcing. *Climate Dyn.*, 15, 551–559.

Venzke, R., M. Allen, R. Sutton, and D. Rowell, 1999: The atmospheric response over the North Atlantic to decadal changes in sea surface temperature. *J. Climate*, 12, 2562–2584.

Wilks, D., 1995: *Statistical Methods in the Atmospheric Sciences*, Academic Press. 373–398.

## North Atlantic forcing of climate and its uncertainty from a multi-model experiment

(M. J. Rodwell, M. Dréville, C. Frankignoul, J. W. Hurrell, H. Pohlmann, M. Stendel, and R. T. Sutton)

### Abstract

To understand recent climate change in the North Atlantic region and to produce better climate forecasts with uncertainty estimates it is important to determine the atmospheric ‘response’ to Atlantic sea-surface temperature (SST) forcing. There have been conflicting results regarding the strength, character and tropical versus-extratropical origin of this response. For model-based studies, this may indicate differing sensitivities to Atlantic SST, but the comparison is complicated by changes in experimental design. Here, a highly controlled experiment with five atmospheric models is undertaken. The influence of realistic (if reasonably strong) and optimally chosen North Atlantic (equator to 70°N) SST anomalies is isolated. Unexpected global agreement between the models is found (e.g. the North Atlantic Oscillation (NAO), Eurasian temperatures, rainfall over the Americas and Africa, and the Asian monsoon). The extratropical North Atlantic region response appears to be associated with remote Caribbean and tropical Atlantic SST anomalies, and with local forcing. Some features such as the European winter-temperature response would be stronger than atmospheric ‘noise’ if the prescribed SST anomalies persisted for just two years. More generally, Atlantic air–sea interaction appears to be important for climate variability on the 30-year timescale and, thus, to be important in the climate-change context. The multimodel mean response patterns are in reasonable agreement with observational estimates, although the model response magnitudes may be too weak. The similarity between their responses helps to reconcile models. Intermodel differences do still exist and these are discussed and quantified.

### 4.1 Introduction

At intraseasonal to interannual timescales it is well known that it is the transients in the North Atlantic atmosphere that drive much of the variability in sea-surface temperature (SST) (see, for example, Cayan (1992)). Nevertheless it is possible that two-way air–sea interaction could play a significant role in North Atlantic climate variability, particularly at longer timescales (Bjerknes 1964). Here, one aspect of this coupling is considered: that of the atmospheric response to North Atlantic SST forcing and the timescale dependence of the importance of this response for climate variability.

It is widely recognized that tropical North Atlantic SSTs can affect tropical deep convection and upper-tropospheric vorticity forcing which, through the action of barotropic Rossby waves can have a teleconnective impact on the climate of the North Atlantic (Hoskins and Karoly 1981). Rowntree (1976), Okumura *et al.* (2001), Terray and

Cassou (2002) and many others have investigated the extratropical impact of such tropical Atlantic SST. Nevertheless, it is unclear how well current models represent the processes and interactions involved in this response: the generation of tropical SST anomalies (SSTAs), evaporation, convection etc. The role played by extratropical North Atlantic SST in forcing North Atlantic climate is probably less clear as there is little or no model consensus at present (see Kushnir *et al.* (2002) for a summary). The locally forced response can be thought of as the combination of a local baroclinic response to extratropical SST (e.g. Kushnir 1994) and the interaction between this response and the North Atlantic storm-track which produces a barotropic signal (e.g. Palmer and Sun 1985). Peng and Whitaker (1999) and Hall *et al.* (2001) suggested that this interaction is highly sensitive to the position of the storm-track and this may be one reason for the model discrepancies. The relatively low number of realizations and the high level of atmospheric internal variability may also help explain the differences. The combined response to tropical and extratropical SST is even more complicated. For example, Lau and Nath (1996) suggested that mid-latitude ocean–atmosphere coupling could enhance the amplitude and persistence of a tropically forced response.

The ‘analysis of variance’ (ANOVA, see, for example, Davis *et al.* (1997), see also the **Appendix**) of ensembles of ‘AMIP-style’ (Gates 1992) atmospheric general-circulation model (AGCM) simulations forced with observed SST has been used elsewhere to estimate the fraction of total atmospheric variance that can be attributed to SST forcing. ANOVA successfully highlights regions that are generally susceptible to forcing by SST in model simulations and is also useful for model intercomparison. The clear picture that emerges is that a high proportion of tropical atmospheric interannual variability in these models is forced by the prescribed SST. For December–February (DJF) mean-sea-level pressure (MSLP), over 70% of the tropical Atlantic interannual variability can be explained by SST forcing. In the extratropics, the value is much smaller (often less than 20% of total interannual variability). It could be argued that such a small percentage makes it fruitless to investigate the extratropical response to SST forcing. However, in view of the redness of the SSTA spectrum, the percentage should be larger at longer timescales. ANOVA can be extended to the frequency domain to assess the proportion of variance explained by SST forcing at longer timescales (Rowell and Zwiers 1999). The percentage of variance explained at decadal timescales is generally higher than at interannual timescales, but results are less robust across experiments. For example the French ARPEGE3 AGCM shows 40% of the decadal June–August (JJA) MSLP variance near Iceland to be explained by SST forcing (1947–1998) (Laurent Terray, personal communication) while the UK HadAM3 model shows less than 20%. The German ECHAM4 model gives an intermediate value. Using an earlier version of HadAM3, (HadAM1), Rowell and Zwiers (1999) showed that no significant decadal DJF variability was explained by SST forcing over the extratropical North Atlantic for the period 1949–1993 whereas, for the same period, HadAM3 suggests that over 40% of decadal variability as far north as Iceland can be explained by SST forcing. It is unclear how much of these differences can be attributed to model differences, as the relatively short length of the observed SST record puts a limit on achievable significance. Another limitation is that ANOVA does not indicate the relative importance of different oceanic regions (tropical Pacific, tropical Atlantic, extratropical Atlantic etc.) in the overall

forcing. In addition, it is possible that particular patterns of SSTAs will have a disproportionately strong impact in certain regions or on certain ‘modes’ of atmospheric variability, but that this is obscured by the mean statistic given. For example, Rodwell *et al.* (1999) highlighted the response to a tripole pattern in North Atlantic SSTAs. This was seen in idealized experiments with fixed tripole SSTAs and in a regression analysis between the simulated North Atlantic Oscillation (NAO, Walker and Bliss 1932) and prescribed observed SST in a six-member ensemble of atmospheric model experiments. Their quoted correlation between observed and hindcast winter NAO index, 0.41, was confirmed by Mehta *et al.* (2000), but Mehta *et al.*’s results suggested that a six-member ensemble may be too small to get a robust result.

Barsugli and Battisti (1998) developed a one-dimensional energy-balance model of atmosphere–ocean coupling. The model, which is widely credited with capturing some of the essential features of air–sea interaction, appears to throw doubt on the meaningfulness of using AMIP-style AGCM simulations to study atmospheric predictability. For example, Bretherton and Battisti (2000) noted that correlations between observed variations and those of AMIP-style simulations may be exaggerated. This is because the AGCM will adjust to the observed SSTAs that were, in reality, partly forced by unpredictable atmospheric anomalies, and ensemble averaging can inflate the correlations by reducing the simulated atmospheric ‘noise’. These results suggest some inaccuracy in the ‘percentage of decadal variance explained by SST forcing’, if such a quantity is actually meaningful. However, the model of Barsugli and Battisti (1998) is intentionally simple and it does omit potentially important feedback mechanisms such as temperature advection by Ekman currents (e.g. Bjerknes 1964, Palmer and Sun 1985, Rodwell *et al.* 1999) and the effects of lower frequency variations in the ocean circulation. Adding quasi-geostrophic dynamics to the model, Ferreira *et al.* (2001) showed that the coupling to oceanic Rossby waves could lead to weakly unstable modes and a small climate predictability up to six years in advance. Using a more comprehensive coupled ocean–atmosphere general-circulation model (OAGCM), Collins (2002) did find decadal predictability of surface air-temperature anomalies over the North Atlantic. A working assumption in the study by Collins is that the model is perfect. Whether the model does capture well enough features such as the variability of the thermohaline circulation, its relationship with SST and the atmospheric response to SST forcing (represented by the parameter ‘b’ in the model of Barsugli and Battisti 1998) is not straightforward to validate against observations.

One approach to investigate air–sea interaction in the observations and to validate these interactions in OAGCMs is to use a lagged maximal-covariance analysis technique. Using such techniques, Czaja and Frankignoul (1999, 2002), Rodwell and Folland (2002, 2003) and Rodwell (2003) have been able to identify statistically significant estimates of the observational responses to SST forcing, although the shortness of the instrumental record, atmospheric internal variability and autocorrelation, and external forcing factors such as the El-Niño–Southern Oscillation can complicate a simple interpretation. Rodwell and Folland (2003) and Rodwell (2003) applied the same technique to an ensemble of HadAM3 simulations and to a long 1500-year simulation of an OAGCM (HadCM3, which includes HadAM3 as its atmospheric component). Results suggest that

the atmospheric model does respond to SST forcing with the correct (500 hPa geopotential height) patterns, but too weakly.

Here, the aim is to address some of the questions raised above concerning the response to SST forcing, while avoiding the issues concerning predictability. A multimodel experiment is conducted where prime consideration is given to producing robust, physically justifiable and statistically significant results. Specifically, the aim is to (1) produce a best multi-model estimate of the atmospheric response to ‘optimally chosen’ seasonally fixed SSTAs, (2) investigate the physics and origin of the response, (3) look for strong and coherent local anomalies (that may not have been highlighted by the more generalized ANOVA technique), (4) compare the response with observationally based estimates for validation purposes, (5) estimate the importance of the response in climate variability over a range of timescales and (6) examine inter-model differences.

	Model	Origin	Type	Resolution		Reference
				Horizontal	Vertical	
H3	HadAM3	UK	Grid-point	2.5° lat × 3.75° long	19 levels	Pope et al. (2000)
A3	ARPEGE3	France	Spectral	T63 (2.8° × 2.8°)	31 levels	Déqué et al. (1994)
E4	ECHAM4	Germany	Spectral	T42 (2.8° × 2.8°)	19 levels	Roeckner et al. (1996)
E5	ECHAM5	Germany	Spectral	T42 (2.8° × 2.8°)	19 levels	Roeckner et al. (2003)
C2	CAM2	USA	Spectral	T42 (2.8° × 2.8°)	26 levels	

**Table 4.1** Details of atmospheric models used in this study. Physics terms are calculated on a T42 Gaussian grid in ARPEGE3. ECHAM5 simulations were run at the Danish Meteorological Institute.

In section 4.2, the models are summarized and experimental details, including the methodology used to optimize the SSTAs, are described. The individual model responses are compared in section 4.3. Section 4.4 gives the multi-model mean response, compares it with atmospheric internal variability and discusses the likely SSTs (tropical versus extratropical) responsible for the response. Section 4.5 compares the mean model response with observational estimates. Section 4.6 discusses inter-model differences. Section 4.7 summarizes the response, its uncertainty and significance. Section 4.8 demonstrates linearity in the multi-model response. Assuming linearity, the timescales over which North Atlantic air–sea interaction is important for natural climate variability are estimated in section 4.9. Further discussion and the conclusions are given in section 4.10.

## 4.2 Models and methodology

### 4.2.1 Models

The five different atmospheric models investigated are detailed in Table 4.1. All the models have previously been well tested and show reasonable climates. There are mean biases from observational reanalysis estimates, although these are thought to have only a secondary effect on the sensitivities of interest here. Typical maximal values include a +4 hPa summer MSLP bias in model A3 over the central North Atlantic and a similar bias in the winter Azores high in E4. H3 shows a 30% deficit in North Atlantic winter blocking

frequency (Pope *et al.* 2000). For each model, the NAO is well represented by the first empirical orthogonal eigenfunction (EOF1) of North Atlantic region winter MSLP. For example, the DJF EOF1 in an ensemble of six *H3* simulations forced with observed SST between 1946 and 1998 explains 42%, 31%, 36%, 45%, 39% and 42% of the total variance, respectively. The corresponding observational value is 43%. The observed strong anticorrelation between the Azores high and the Icelandic low in DJF ( $r \approx -0.69$ ) is well captured in the models tested (*H3*, *E4*, *E5*). For example, four ensemble members of *E5* give values of  $-0.63$ ,  $-0.65$ ,  $-0.70$  and  $-0.55$ , respectively. The same three models also well capture the relationships between the NAO and European precipitation and surface temperatures (Walker and Bliss 1932, Hurrell 1995, Rodwell *et al.* 1999). There is no reason to believe that the other two models behave significantly differently in these respects.

#### 4.2.2 Simulations of each model

For each model, a 21-year control simulation *C* was forced with the 1948–1998 climatological mean annual cycle in SST and sea ice (and the same pre-industrial CO<sub>2</sub> and trace gases). Simulations *A+* and *A-* were made with SSTAs (see below) added to, and subtracted from, the climatological SSTs in the North Atlantic. All integrations were started at the beginning of February. The first ten months were disregarded. Analysis was made on the 20 years of seasonal-mean data for each standard season (DJF, MAM, JJA and SON where, as usual, letters correspond to the first letter of each month). Rodwell and Ingram (2000) showed, for an earlier version of the Met Office model (HadAM2b), that 20 years of data are adequate to identify field-significant responses in the North Atlantic region.

#### 4.2.3 Construction of SST anomalies

The aim is to define SSTA patterns that are realistic in structure and magnitude and, if possible, ‘optimal’ in the sense that they are thought to have the strongest impact on the North Atlantic climate. To do this, SSTAs are based on the observational lagged maximum covariance analysis (MCA) of Rodwell (2003) applied to monthly-mean SST and the subsequent seasonal-mean 500 hPa geopotential height (*Z500*). The procedure, which can be skipped by the reader if desired, is detailed in the next paragraph.

Monthly-mean SST data, ( $SST_{m,y}$ ) where *m* is the month and *y* is the year, are taken from the HadISST1 dataset (Rayner *et al.* 2003) in the box (90°W–15°E, 0–70°N) for 1948 to 1998. Three-month-mean *Z500* data, ( $Z500_{m,y}$ ) where *m* is the central month of the ‘season’, are taken from the National Centers for Environmental Prediction (NCEP) reanalyses (Kalnay *et al.* 1996) in the box (90°W–45°E, 10°N–80°N) for the same period. For each month *m* the *lagged* MCA is applied to ( $SST_{m-2,y}$ ,  $Z500_{m,y}$ )  $y \in \{1948, \dots, 1998\}$  to obtain the first pair of anomaly covariance patterns ( $SSTA_{m-2}$ ,  $Z500A_m$ ). As with Czaja and Frankignoul (1999), statistical significance is based on a Monte Carlo test of the squared covariance. Eight out of the 12 three-month running seasons are found to be significant at the 10% level. For the significant patterns, the use of a lag suggests that an ocean-forced response is obtained and additional tests (Rodwell and Folland 2002) tend

to confirm this interpretation. The SST anomaly  $SSTA_{m-2}$  is thought to affect the atmosphere by persisting through the months  $m - 1$ ,  $m$ ,  $m + 1$  and forcing the Z500 field quasi-instantaneously (at a monthly temporal resolution). Rodwell and Folland (2002) show  $SSTA$ -pattern autocorrelations of 0.8–0.9 between November and the months of DJF.  $SSTA_{m-2}$  could have been used as the optimal forcing  $SSTA$  for month  $m$  but, since not all  $SSTA_{m-2}$  patterns are statistically significant, a simplification using just the significant MCA patterns was sought. It was found from pattern correlations that there is a reasonably clear separation between the SST patterns corresponding to  $m \in \{S, O, N, D, J, F\}$  (with three patterns statistically significant) and  $m \in \{M, A, M, J, J, A\}$  (with five patterns significant). Hence an Autumn/Winter pattern,  $SSTA_{SONDJF}$ , and a Spring/Summer pattern,  $SSTA_{MAMJJA}$ , were defined as the means of the three and five statistically-significant MCA patterns, respectively. For each month  $m$  the original SST data,  $(SST_{m,y})_{y \in \{1948, \dots, 1998\}}$ , is projected onto either  $SSTA_{SONDJF}$  if  $m \in \{S, O, N, D, J, F\}$ , or  $SSTA_{MAMJJA}$  if  $m \in \{M, A, M, J, J, A\}$ , to obtain a time coefficient. A scaling factor  $SCALE_m$  is defined as 2.5 times the standard deviation of the time coefficient. For each  $m \in \{S, O, N, D, J, F\}$ , the ‘optimal’ SST forcing anomaly is defined as  $A_m = SCALE_m \times SSTA_{SONDJF}$ . Similarly, for each  $m \in \{M, A, M, J, J, A\}$ , the optimal  $SSTA$  forcing anomaly is defined as  $A_m = SCALE_m \times SSTA_{MAMJJA}$ .  $A_m$  is assumed to occur at the central date of the month. For the model forcing, it is added to (for  $A+$ ), or subtracted from (for  $A-$ ), the climatological monthly-mean SST, and linear time-interpolation is made between the centres of consecutive months. The transition between the February and March patterns (and the August and September patterns) is not thought to have a detrimental impact on the total atmospheric circulation, as the total circulation at any instant is likely to be dominated by atmospheric internal variability.

There are several advantages for using the above procedure: the SSTAs have realistic patterns, they may lead to a stronger atmospheric response than randomly chosen patterns, they do not favour any particular model (as they are based on observations) and, importantly, by using them it may be possible to compare the model responses with the best estimates of the real response (assumed to be the Z500 patterns arising from the same lagged MCA). The difference in seasonal-mean SST ( $A+ - A-$ ) is shown in the surface temperature (TEMP) fields in Fig. 4.2. Although reasonably large, such SSTAs do exist in the raw seasonal-mean data.

#### 4.2.4 Extra simulations of the HadAM3 model

The HadAM3 simulations,  $A+$  and  $A-$ , were repeated with different initial conditions to ensure better statistical significance when this model is considered alone. A parallel pair of HadAM3 simulations (termed  $H_{CK}$ ) was made with a change to a single model parameter (the Charnock parameter) to check for sensitivity in the results. A further additional pair of simulations of HadAM3 (termed  $H_{TR}$ ) was made with just the tropical SSTAs applied (the SSTAs south of the green line in the top panels of Fig. 4.2 (TEMP)).  $H_{CK}$  and  $H_{TR}$  were also repeated with different initial conditions to improve significance.

### 4.3 Individual model responses

Figure 4.1 shows the mean seasonal-mean MSLP difference ( $A+ - A-$ ) for each model. This difference is an estimate of each model's response to North Atlantic SSTs. Statistical significance at the 10% level using a two-sided  $t$ -test is indicated by shading. The percentage of the total area shown that is significant is quoted in the bottom right corner of each panel. Using the binomial distribution test of Livezey and Chen (1983) all panels are found to be field significant at the 10% level, assuming 55 spatial degrees of freedom for the global MSLP (Livezey and Chen suggested 30–60 degrees of freedom for the northern hemispheric Z500). All but two panels are significant at the 5% level assuming just 14 spatial degrees of freedom. A major result, which was unexpected based on a knowledge of the discrepancies highlighted in the introduction, is that the difference fields of the models appear quite similar, both locally in the North Atlantic region and also globally. JJA shows the best field significance, with negative anomalies over the tropical and subtropical Atlantic and over North and South America, and generally

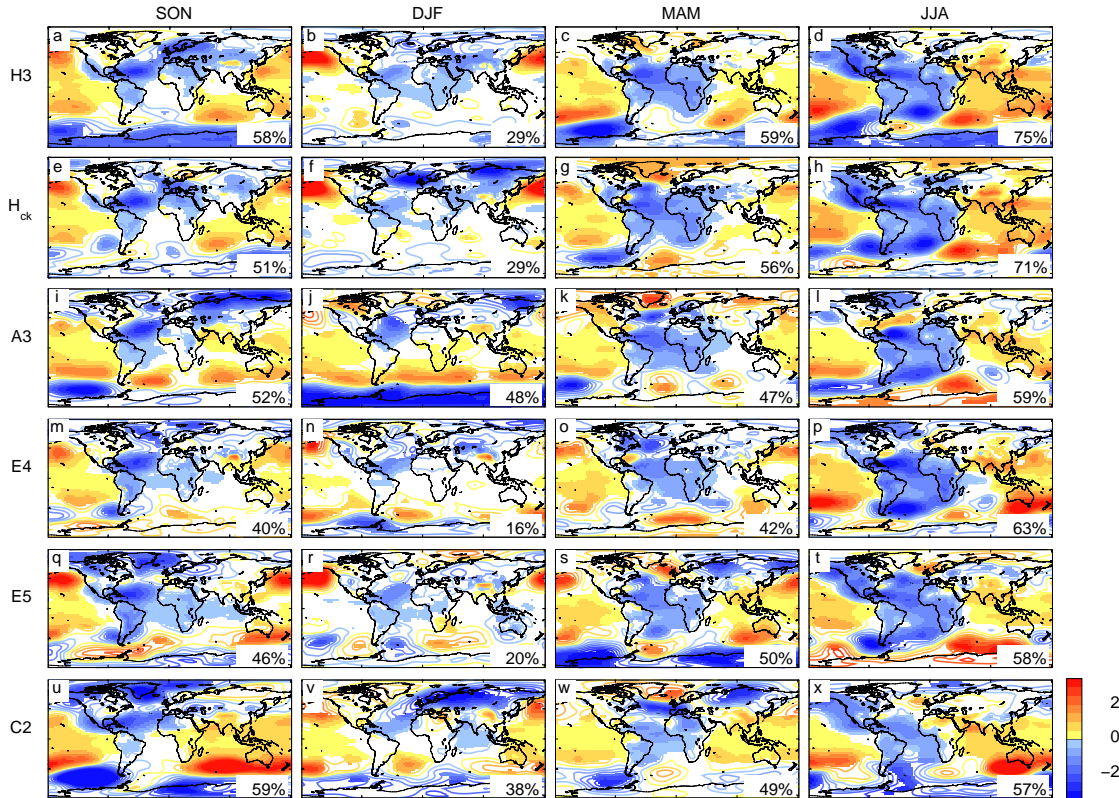


**Figure 4.1** The 20-year-mean (40-year for H3 and H<sub>CK</sub>) mean-sea-level pressure (MSLP) responses (hPa) of six atmospheric models in each season to imposed sea-surface temperature anomalies (SSTAs) in the North Atlantic. Note that SSTAs, ( $A+ - A-$ ), are shown in the top panels of Fig. 4.2. Signals that are significant at the 10% level using a two-sided  $t$ -test are filled in colour, other values are contoured. The percentage given in the bottom right-hand corner of each panel is the percentage of the area shown that is significant at the 10% level (and, therefore, indicates the degree of field significance). See the text for a definition of the models.

positive anomalies elsewhere. A striking feature for MAM, Fig. 4.1 (third column), is that all models (with the exception of *E4*) show a negative NAO dipole response in the North Atlantic region, with high pressures to the north and low pressures to the south. The Azores-minus-Iceland MSLP (i.e. the NAO-index anomaly) is negative for all models including *E4*. Values are  $-0.22$ ,  $-2.39$ ,  $-0.88$ ,  $-0.30$ ,  $-2.65$ , and  $-3.37$  hPa for *H3*, *HCK*, *A3*, *E4*, *E5*, and *C2*, respectively (mean= $-1.64$  hPa, standard deviation = 1.34 hPa). In DJF, all models show consistent positive anomalies in the Aleutian low and, although not individually significant, all models show pressure anomalies of around  $-1$  hPa over the whole of Eurasia. There is also a consistent pattern of MSLP anomalies over the North Atlantic, and even Greenland, during SON. Although the striking feature is the similarity in global and North Atlantic responses, there are also differences between models. The extent to which these differences reflect true model differences rather than being associated with chaotic atmospheric internal variability is discussed later.

#### 4.4 Multi-model mean response, its origin and significance

##### 4.4.1 Methodologies

The similarity between models makes it legitimate to construct a multi-model mean and to refer to the mean anomalies as the ‘response’ to SST forcing. An issue highlighted in the introduction concerns the timescale-dependence of the importance for climate variability of forcing by SST. To determine what timescales, if there are any, at which the response is important for natural climate variability, the response is compared with the magnitude of temporally filtered atmospheric internal variability. Before introducing the model results, the simple method of determining these timescales is discussed.

For each model,  $i$  (1 to 6), and year,  $j$  (1 to 20), the difference between the two simulations,  $d_{ij} = A^{+ij} - A^{-ij}$ , can be partitioned into an SST-forced response and random chaotic variability which is generated internally by the atmosphere. For a particular season, the response for model  $i$  can be estimated by the mean,  $d_i = \frac{1}{20} \sum_{j=1}^{20} d_{ij}$ , and the internal variability by the residual time-series  $(d_{ij} - d_i)_{j=1}^{20}$ . The response is likely to be smaller than the standard deviation of the residual time-series at most grid points. However, if timescales shorter than, say,  $n$  years are filtered from the residual timeseries, then the signal to noise ratio will increase. The relevant question is at what filtering timescale,  $n$ , does the response to the fixed SSTAs used become comparable with the internal variability? Here the timescale is estimated by looking for equality between the magnitudes of the response and the filtered internal variability:

$$\frac{V(d_{ij} - d_i)}{2n} = d^2 \quad (4.1)$$

where the left-hand side estimates the variance of the filtered internal variability and the right-hand side is the square of the estimated (multi-model) response,  $d = \frac{1}{6} \sum_{i=1}^6 d_i$ .

Note that  $V(d_{ij} - d_i) = \frac{1}{120} \sum_{i,j} (d_{ij} - d_i)^2$  is the sample variance of the concatenation of the residual time-series of all models. The factor  $1/n$  in (1) reflects the reduction in variance associated with taking the mean of  $n$ -years, and the factor  $1/2$  arises from the fact that the difference of two simulations,  $A+$  and  $A-$  has been taken. The assumption has been made that the concatenation of residual time-series at each grid point represents white noise. This latter assumption could be compromised by (for example) possible reddening effects due to interactions with the land surface. However, the variance of internal variability, as a function of filtering timescale, has also been estimated in another way (not assuming white noise) by using non-overlapping consecutive  $n$ -year time intervals (where  $n$  is a factor of 20). Similar timescales are found. Note also that internal variability is found to have a negligible impact on the multi-model mean.

Where short timescales (e.g. 1–2 years) are highlighted by this method, these indicate regions where the response would play a major role in observed climate anomalies (assuming the multi-model is perfect and the observed SSTAs agree in pattern and magnitude with those applied). Of particular interest here are regions that are not already highlighted by the analysis of variance applied to AMIP-style simulations. These are regions where the general influence of SSTAs may be small, but where a strong impact is achieved from the particular SSTAs used here. The location of these regions will clearly be sensitive to the choice of SSTAs used (this ‘caveat’ is the ‘trade-off’ in these experiments for greater statistical significance).

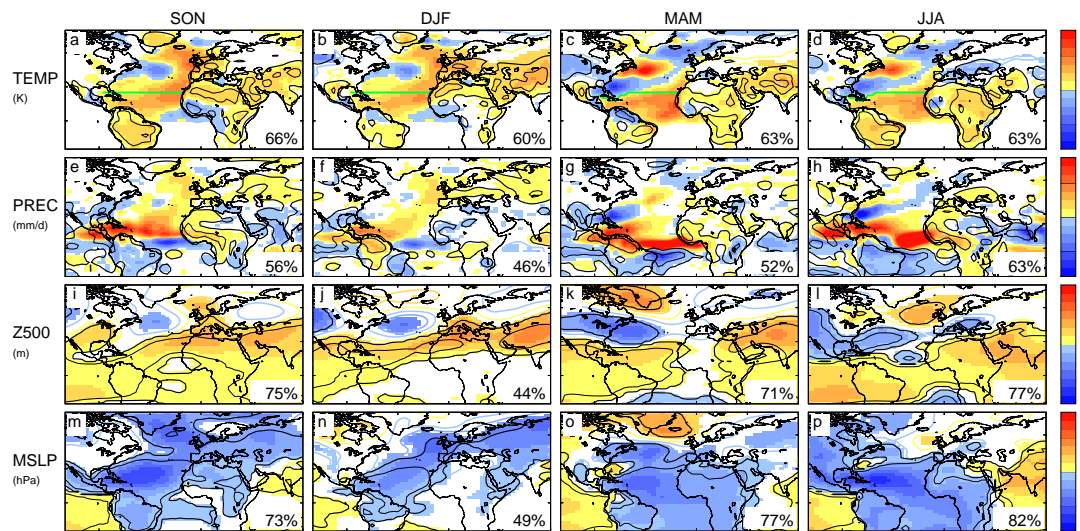
Where timescales longer than about two years are indicated, these timescales are likely to be *underestimated*. This is because the SSTA magnitudes used are probably too large to be realistic beyond one- to two-year averages and, therefore, the response is too strong for a simple comparison with filtered internal variability on these timescales. To include a timescale-dependence of the forcing strength, a linear scaling parameter can be applied to the response. Justification for using a linear scaling and how it is defined is discussed later.

Figure 4.2 shows, coloured, the multi-model mean difference  $d = (A+ - A-)$  for surface temperature, precipitation, Z500 and MSLP. All responses are clearly field significant (5% field significance is attained when 44% of the area is point-wise significant, assuming nine degrees of freedom for the regional Z500). Below, we only highlight features in the multi-model mean that are *stronger than decadal filtered internal variability* (inside the thick black contour) and *common to all models*.

#### 4.4.2 Tropical response

In all seasons there is a tropical-Atlantic baroclinic response (positive Z500 anomalies overlying negative MSLP; Fig. 4.2, rows 3 and 4) and this is clearly related to locally forced changes in precipitation, a northward shift of the intertropical convergence zone (ITCZ) (Nobre and Shukla 1996) and an associated strengthening of the subtropical jet. The weaker DJF precipitation response may be because the tropical SSTAs are weakest in DJF and do not engage strongly with the ITCZ, which is near its March southern

extreme (Nobre and Shukla 1996). The positive ITCZ precipitation anomalies over the Sahel in JJA (Fig. 4.2(h)) (Folland *et al.* 1986) and the Amazon in MAM (Fig. 4.2(g)) (Nobre and Shukla 1996) are stronger than biennially filtered internal variability (inside the thin black contour) and lead to evaporative cooling and cold surface temperatures (Figs. 4.2(d) and (c), respectively). These regions are also generally highlighted in an analysis of variance as having high ‘potential predictability’. Throughout the rest of the tropics, throughout the year, the response is more equivalent-barotropic (Z500 and MSLP anomalies with the same sign—see, for example, Figs. 4.2(l) and (p)), with reduced ITCZ precipitation apparently subordinate to the large-scale forcing. The striking one-standard-deviation reduction in the Indian summer monsoon rainfall (Fig. 4.2(h)) is the strongest manifestation of this, suggesting causality for the ‘observed’ palæo relationship with North Atlantic SST (Gupta *et al.* 2003).



**Figure 4.2** Seasonal-mean results from the multi-model mean of six models forced with the same North Atlantic sea-surface temperature (SST) anomalies. The rows correspond to surface temperature (TEMP), total precipitation (PREC), 500 hPa geopotential height (Z500) and mean-sea-level pressure (MSLP), respectively. The SST anomalies, ( $A+ - A-$ ), used in the North Atlantic region can be seen in the top panels. The duplicate  $H3$  and  $H_{CK}$  simulations are not used. Signals that are significant at the 10% level using a two-sided  $t$ -test are filled in colour, other values are contoured (contours indicate values at the centre of each colour range). The quoted percentages in the bottom right-hand corner of each panel refer to the percentage of the area shown (land area for TEMP) for which the anomaly is statistically significant at the 10% level (and, therefore, indicate the degree of field significance). Black contours indicate the timescale  $n = V(d_{ij} - d_i)/2d^2$  (thick: ten years, thin: two years) at which the multi-model mean response is an important component of climate variability. The timescale is not applicable for TEMP over the sea. For clarity, the timescale for PREC is not plotted over the SST forcing region where it is nearly always less than two years, and it is smoothed for TEMP and PREC using a triangular truncation at T31. When the timescale dependence of the forcing strength is considered, the thick black contour is associated with a 30-year timescale. See the text for more details.

### 4.4.3 Extratropical response

For MAM and JJA, wave-like responses are seen in the Z500 field over the extratropical North Atlantic region (Figs. 4.2(k) and (l)) and these are equivalent-barotropic in structure (compare Figs. 4.2(k) and (l) with Figs. 4.2(o) and (p)). These responses are reminiscent of ray-tracing results based on the linear barotropic response to subtropical upper-tropospheric vorticity forcing (Hoskins and Karoly 1981). For MAM, the (zonal wave-number 1) response (Fig. 4.2(k)) is stronger than decadal filtered internal variability, even over Greenland and, as seen previously, it projects onto the NAO at the surface (Fig. 4.2(o)). For JJA (Fig. 4.2(l)), an anticyclonic centre to the west of the UK appears to mark the southward turning point for this (higher zonal wave-number) response. A further cyclonic centre, possibly associated with the same wave-like response, is seen over southern Europe and the Mediterranean in JJA. Row 1 of Fig. 4.3 shows the 40-year Z500 results for  $H_3$ . Although the first 20 years of  $H_3$  are included in the multi-model mean, the similarity between  $H_3$  (Fig. 4.3, row 1) and the multi-model mean (Fig. 4.2, row 3) suggests that further experiments with HadAM3 can help clarify the roles of the tropical and extratropical SSTAs in the multi-model mean. (Clearly, one doesn't need to appeal to this similarity to assess the origin of the response in HadAM3 alone.) Row 2 of Fig. 4.3 shows parallel results for the tropical SSTA experiment,  $H_{TR}$ . For MAM, and to a lesser extent JJA, the similarity between  $H_3$  and  $H_{TR}$  (and the multi-model mean) does indeed indicate a tropical origin for these waves (the off-equatorial Caribbean may be particularly important—Hoskins and Sardeshmukh (1987)). Where significant,  $(H_3 - H_{TR})$  would highlight the influence of extratropical SSTAs alone, or features that require both tropical and extratropical SSTAs to be present. Statistical significance is likely to be more difficult to obtain for  $(H_3 - H_{TR})$ , if only because a difference between two such fields contains twice the internal variability. Nevertheless, there are statistically significant differences. For example, surface latent-heat fluxes and precipitation differences (not shown) clearly highlight the role of extratropical SSTAs to the east of Florida and in the Gulf of Mexico. For MAM, these appear to force a similar wave-like pattern (perhaps by inducing a similar Rossby-wave source (Sardeshmukh and

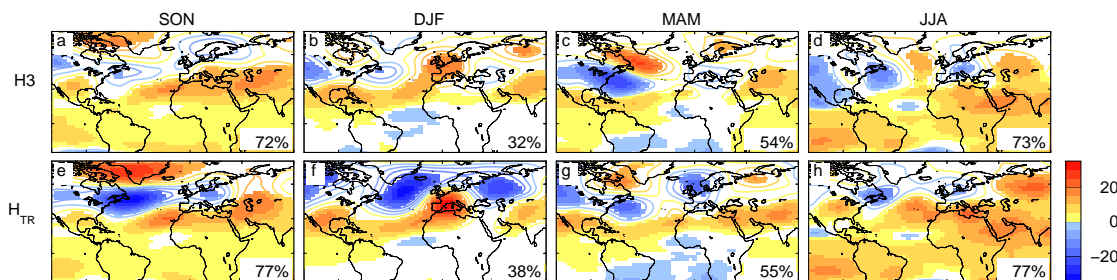


**Figure 4.3** The 40-year mean 500 hPa geopotential-height (Z500) responses (m) in HadAM3 when forced with the full North Atlantic sea-surface-temperature (SST) anomaly patterns,  $H_3$ , (top row) and when forced with just the tropical part of the SSTA patterns,  $H_{TR}$  (bottom row). Signals that are significant at the 10% level using a two-sided  $t$ -test are filled in colour, other values are contoured. The percentage given in each panel is the percentage of the area shown which is significant at the 10% level (and, therefore, indicates the degree of field significance).

Hoskins 1988) over the Caribbean) although there are some phase differences. For JJA, the extratropical SSTAs may actually set the position of the high to the west of the UK (compare Figs. 4.3(d) and (h)) and be necessary, if not necessarily sufficient, for the remote coolness of the southern European low.

The extratropical multi-model Z500 responses for SON and DJF, Figs. 4.2(i) and (j), (which are forced by similar SSTAs) are similar to each other, suggesting that the response is particularly robust.  $H_{TR}$  (Figs. 4.3(e) and (f)) suggests that much of the HadAM3 Z500 response is forced by tropical and Caribbean SSTAs. To achieve a similar magnitude of response in DJF and SON, one can speculate that compensation may occur in the DJF Rossby-wave source with stronger mean absolute-vorticity gradients in the winter North American jet stream compensating for weaker tropical precipitation (compare Figs. 4.2(e) and (f)) and upper-tropospheric divergent-flow anomalies. In addition to the likely tropical forcing of a barotropic component of the extratropical response, Figs. 4.2(i) and (m) and Figs. 4.2(j) and (n) suggest that the multi-model extratropical response is quite baroclinic in nature (Kushnir 1994, Kushnir and Held 1996). Local SSTAs are seen in Figs. 4.2(e) and (f) to force important changes in precipitation (Kushnir and Held 1996, Rodwell et al. 1999, Frankignoul and Kestenare 2002) and atmospheric latent heating (Peterson et al. 2002) as far north as 60°N. The SON and DJF European temperature anomalies of +1 K (Figs. 4.2(a) and (b)) are stronger than biennially filtered internal variability (indicated by the thin black contour) and would, therefore, be discernible if similar SSTAs were sustained for just two years. This response is a clear example of a strong forced signal that is not highlighted by the analysis of variance of AMIP-style simulations. HadAM3 suggests that extratropical SSTAs are important for this response. The increased precipitation seen downstream over central and northern Asia in these seasons (Figs. 4.2(e) and (f)) may be a combined advective effect of tropically enhanced westerlies (Figs. 4.3(e) and (f)) and extratropically increased moisture supply. An interesting feature of the  $H3$  and  $H_{TR}$  results is that the statistically significant response to extratropical SSTAs in HadAM3 appears to damp the tropically forced response in SON and DJF (compare Figs. 4.3(a) and (e) with Figs. 4.3(b) and (f)). The extratropically forced Z500 response does appear to have a physical basis although the apparent damping may be coincidental and model dependent. For this reason it is discussed in the inter-model differences section 6.

Over the southern USA and Mexico, precipitation is reduced in all seasons but JJA (Fig. 4.2, row 2). The experiments with HadAM3 offer an interesting explanation of the origin of this response.  $H_{TR}$  suggests that the tropical SSTAs force a reduction in precipitation and an increase in land-surface temperature throughout the year (not shown), but that the cold extratropical SSTAs in  $(H3 - H_{TR})$  off Florida and over the Gulf of Mexico tend to counteract this effect in JJA, possibly by enhancing the land-sea temperature contrast during the North American monsoon. The multi-model precipitation signal over the southern USA and Mexico is stronger in places than biennially filtered internal variability for SON, MAM and JJA, but the region is not highlighted by a general analysis of variance. The MSLP anomalies seen over much of the USA in JJA (Fig. 4.2(p)) are also stronger than biennially filtered internal variability. Analysis of variance of the ECHAM3.5 AGCM does highlight this region as more strongly influenced by the SST

(see, for example, Kushnir *et al.* (2002)), and HadAM3 shows particularly strong decadal potential predictability in this region (based on an analysis of variance, not shown). The interesting result here is that the Atlantic is implicated in the forcing (in addition to the generally accepted view that the tropical Pacific plays an important role (Kushnir *et al.* 2002)).

#### 4.5 Comparison with observational response

Figure 4.4 shows the Z500 patterns that arise in the MCA (Rodwell 2003) which was used to produce the SSTAs. (The shaded area is limited to that used in the MCA). While keeping in mind the uncertainties associated with these patterns (Rodwell and Folland 2002), it is worth comparing them with the model results. Area-weighted pattern correlations are made between the MCA Z500 pattern and the statistically significant parts of the multi-model mean response. These pattern correlations are quoted in Fig. 4.4 and indicate that the multi-model mean, where point-wise significant, generally agrees quite well (but not perfectly) with these MCA patterns in SON, MAM and JJA. Scaling Livezey and Chen's (1983) mid-estimate of 45 degrees of freedom for hemispheric Z500 to the area of significant multi-model mean response in the MCA region would suggest eight, eight and nine degrees of freedom for SON, MAM and JJA, respectively. Assuming these degrees of freedom, the pattern correlations are significantly different from zero at the 4%, 7% and 10% levels, respectively based on a one-sided *t*-test. The *significant* extratropical wave-like pattern in MAM in the multimodel mean (Fig. 4.2(k)), and also in *H3* and *H<sub>CK</sub>* alone (Figs. 4.3(c) and (g)), agrees well with that in the MCA (Fig. 4.4(c)). There is also extratropical wave-like agreement for JJA (compare Fig. 4.2(l) and Fig. 4.4(d)) albeit with some phase or positional differences (*H3* alone, Fig. 3(d), shows the best extratropical agreement with Fig. 4.4(d)). For SON, the best agreement between the multi-model mean (Fig. 4.2(i)) and MCA (Fig. 4.4(a)) appears to occur in the subtropics, with poorer agreement in the extratropics (although *H3* and *H<sub>CK</sub>*, Figs. 4.3(a) and (e), show reasonable extratropical agreement with Fig. 4.4(a)). The correspondence between model responses and MCA clearly breaks down for DJF (compare Fig. 4.2(j) and Fig. 4.4(b)), with little agreement, even in the subtropics. This may possibly be associated with increased storminess in the extratropical winter observations that could 'confuse' the MCA. There is better subtropical agreement between the multimodel DJF

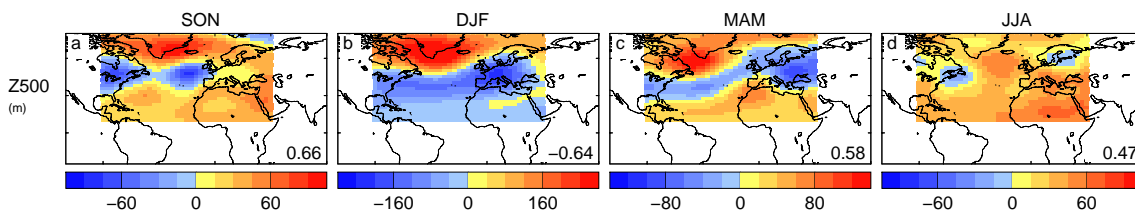


**Figure 4.4** The 500 hPa geopotential-height (Z500) anomaly patterns that arise in the maximal covariance analysis used to produce the forcing sea-surface-temperature anomalies. The patterns are scaled by five ( $2 \times 2.5$ ) times the standard deviation of their principal components so that they can be roughly compared with the multi-model mean. Area-weighted pattern correlations with the statistically significant parts of the multi-model mean are quoted.

response and that detected in the observations for NDJ using a slightly different MCA technique (Czaja and Frankignoul 2002). Further discussion of stormtrack-related differences is given in section 6.

Overall, considering the uncertainties and possible sources of discrepancy, these results do tend to validate the MCA technique *and* suggest that the model response patterns, at least in terms of Z500, are approximately correct. The increased magnitude in the MCA results may partly reflect the optimization inherent in the MCA technique although it may also suggest that the multi-model response to SST forcing is too weak. The latter explanation is consistent with the conclusions of Rodwell and Folland (2003).

## 4.6 Inter-model response differences

### 4.6.1 Quantification of differences

Until now, the main concentration has been on the similarity between the model responses. Clearly, however, there are differences. Here, these differences are quantified and an attempt is made to partition the differences into a true difference between the statistically expected responses of the models and a part associated with sampling uncertainty. Figure 4.5 shows (coloured) inter-model standard deviations for TEMP and MSLP which are plotted, for ease of comparison, with the same sign as the multi-model mean. These standard deviations are generally weaker than the multi-model response (compare with Fig. 4.2). Hence, although there are differences between the individual model MSLP responses in Fig. 4.1, these differences do not obscure the mean response.

Each model mean anomaly can be considered to be the sum of the model's response to SSTA forcing and the average of 20 years of internal variability. It is found that internal variability *does* contribute significantly to the inter-model standard deviation. The black contour in Fig. 4.5 shows where (20-year filtered) atmospheric internal variability would be expected to account for 50% of the inter-model variance, i.e. where:

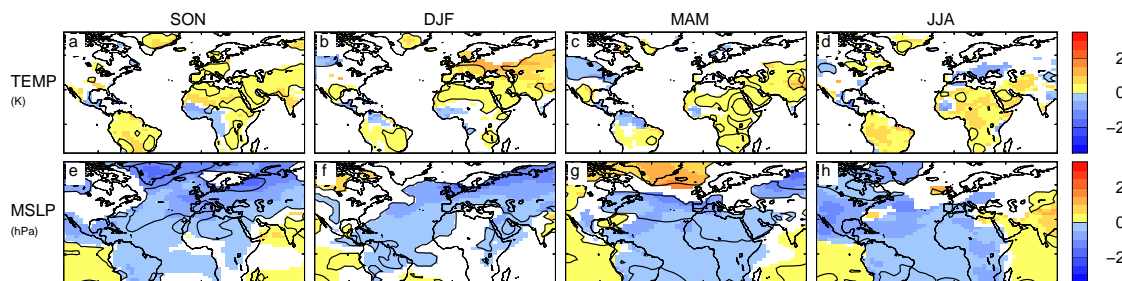


**Figure 4.5** The standard deviation of inter-model variability, coloured and plotted with the same sign as the multi-model mean, and only where the multi-model mean is statistically significant. The rows correspond to surface temperature (TEMP) and mean-sea-level pressure (MSLP). The black contour indicates where residual atmospheric internal variability is estimated to account for 50% of inter-model variance. See the text for more details.

$$\frac{1}{20}V(d_{ij} - d_i) = \frac{1}{2}V(d_i - d) \quad (2)$$

with definitions as before. The left-hand side represents the 20-year filtered internal variance and the right-hand side represents half the inter-model variance. By examining the area enclosed by the black contour in Fig. 4.5 it is clear that, with the exception of JJA, much of the inter-model variance is actually associated with residual internal variability. Hence the model responses obtained from longer simulations would be even more similar than they are here. The uncertainty in the MAM NAO response (Fig. 4.5(g)) is seen to be partly associated with residual internal variability.

#### 4.6.2 Physical interpretation of inter-model differences

For SON and DJF,  $(H3 - H_{TR})$  (not shown) indicates a strong North Atlantic equivalent-barotropic high centred above, and downstream of, the cool SSTAs off Newfoundland. Anomalies in surface latent-heat fluxes, precipitation *and* MSLP are clearly associated with the imposed extratropical SSTAs (over the eastern as well as western North Atlantic). The anomalous circulation is similar to the observational results of Kushnir and Held (1996) and the idealized modelling result of Rodwell *et al.* (1999) and would act, as in the paper by Hoskins and Karoly (1981), to satisfy surface thermodynamic balance. The response leads to an apparent (possibly coincidental) damping of the tropically forced extratropical response in HadAM3 (as noted earlier). The response to such extratropical SSTAs is likely to be sensitive to model storm-track characteristics (Peng and Whitaker 1999, Peng *et al.* 2002, Kushnir *et al.* 2002). The more robust linear baroclinic response of the multi-model mean is, perhaps, indicative of inter-model storm-track differences, and this may be another factor in the poorer extratropical correspondence between multi-model mean and observations in SON and DJF.

A3 shows Caribbean precipitation differences much more strongly linked to local evaporation than the other models in JJA and this may help explain its somewhat different (not necessarily wrong) extratropical response (Fig. 4.1(l)). Such tropical differences highlight the fact that even the relatively well understood tropical forcing of the extratropical circulation is not well represented in current models. This clear model difference, together with the general reduction in internal variability in JJA, helps explain why inter-model differences are more strongly highlighted in Figs. 4.5(d) and (h) (i.e. not enclosed in a black contour).

$H_{CK}$  had its Charnock parameter, which affects surface fluxes of heat and momentum (Janssen and Viterbo 1996), increased by a factor 2.5 compared with  $H3$ . The anticipation was that this might increase sensitivity to SSTAs, particularly in regions of high wind speed. Consistent with this anticipation,  $H_{CK}$  (Fig. 4.1, row 2) does appear to show a general strengthening of the extratropical response over  $H3$  (Fig. 4.1, row 1), particularly in DJF and MAM. In addition, south of 30°N where surface wind speeds are generally smaller,  $(H_{CK} - H3)$  Z500 and MSLP are almost invariably not statistically significant. For MAM there is a statistically significant (and physically consistent) enhancement of the SST-forced surface latent-heat-flux (LHF) pattern and the NAO MSLP dipole when

the Charnock parameter is increased. The previously quoted NAO index anomalies for  $H3$  and  $H_{CK}$  were  $-0.22$  and  $-2.39$ , respectively. However, field significance for  $(H_{CK} - H3)$  in MAM, even over just the extratropical box ( $120^\circ\text{W}-90^\circ\text{E}$ ,  $30^\circ\text{N}-80^\circ\text{N}$ ), is poor (11% of the area is statistically significant for MSLP), and so there must be some doubt at present over how much of this change in the NAO index can really be attributed to the change in the Charnock parameter. The season which generally shows the best  $(H_{CK} - H3)$  field significance over all the parameters tested is DJF (the largest percentage area of point-wise significance is 25% for Z500). This is consistent with the fact that surface wind speeds are generally largest in winter. However, there is a (statistically significant) *reduction* in the SST-forced LHF in DJF as the Charnock parameter is increased. This means that the apparent extratropical enhancement seen between Figs. 4.1(b) and (f) does not have a simple explanation. SON and JJA do not show statistically significant changes in SST-forced LHF associated with a change in the Charnock parameter.

#### 4.7 Response to Atlantic forcing, and its uncertainty

We can, now, make a meaningful estimate of the response to the chosen SST forcing, of the uncertainty in the magnitude of the response and of the fraction of this uncertainty that is due to model error. For example, the mean northern European ( $0^\circ\text{E}-20^\circ\text{E}$ ,  $45^\circ\text{N}-52^\circ\text{N}$ ) land surface-temperature anomaly in DJF is  $+1.00$  K (Fig. 4.2(b)). The inter-model standard deviation is  $0.58$  K (Fig. 4.5(b)) with 69% of the inter-model variance explained by residual atmospheric internal variability. The remaining 31% can be attributed to model differences. For the UK,  $\text{TEMP} \approx 0.90(\pm 0.37)$  K, which is comparable in magnitude (and sign) with that predicted to occur by 2050 under low CO<sub>2</sub> emission scenarios (Hulme *et al.* 2002). Note that the peak magnitudes of the SSTAs ( $A+ - A-$ ) used here do occur in reality (e.g. as recently as JJA 2003) and are predicted to occur in a more sustained fashion under medium to high CO<sub>2</sub> emission scenarios (Cubasch *et al.* 2001).

#### 4.8 Linearity of the response

The multi-model nonlinear (anti-symmetric) component (Peng *et al.* 2002) to the Z500 anomalies,  $(A+ - C) + (A- - C)$ , Fig. 4.6, is smaller than the *collocated* significant linear component,  $(A+ - A-)$ , Fig. 4.2, row 3, and is not field significant. Pure statistics may partly explain this result, although it seems reasonable to infer that, to a first approximation, the multi-model response is primarily linear. Such linearity has been

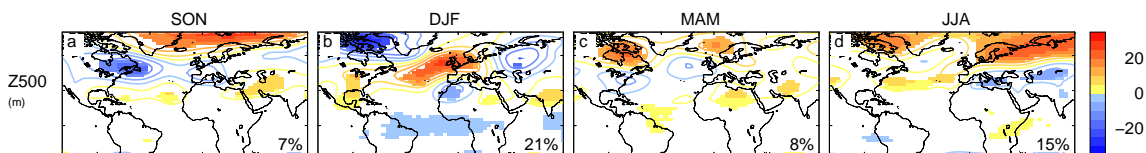


**Figure 4.6** The multi-model mean nonlinear 500 hPa geopotential-height (Z500) anomalies,  $(A+ - C) + (A- - C)$ . Signals that are significant at the 10% level using a two-sided *t*-test are filled in colour, other values are contoured. The percentage given in each panel is the percentage of the area shown which is significant at the 10% level (and, therefore, indicates the degree of field significance).

suggested previously based on observations for the tropics (Nobre and Shukla 1996) and extratropics (Kushnir 1994).

#### 4.9 The important timescales for the response

For natural variability, the typical magnitude of SSTAs is a function of the timescale over which they occur. SSTAs of the magnitude used here ( $A^+ - A^-$ ) may well exist naturally for a single season or possibly even for the same season in two consecutive years, by chance or associated with the ‘re-emergence mechanism’, for example. The re-emergence mechanism involves the insulation of winter/spring-forced deep mixed-layer thermal anomalies by a summertime shallow stable layer and their reemergence at the surface in the following late autumn and winter by mixing processes (see, for example, Alexander and Deser (1995)). Hence, the biennial timescales highlighted above indicate regions where the effect of SST forcing really could be important on biennial timescales (based on the SSTA patterns used here). This forcing is likely to be associated mainly with mixed-layer temperature anomalies. SSTAs of the magnitude of ( $A^+ - A^-$ ) would *not* be expected to last for as long as a decade. Hence the response  $d$ , as defined in section 4(a), is also likely to be unrealistically large for long timescales. This implies, for timescales longer than about two years, an underestimation in (1) of the timescale for which the SST-forced response is an important component in climate variability. The aim here is to produce a better estimate for this timescale.

For a more realistic  $n$ -year forcing, for example  $\alpha(n) \times (A^+ - A^-)$ , where  $|\alpha| < 1$ , the approximate linearity established above suggests that the response would be  $\approx \alpha d$ . A better estimate of the timescale may, therefore, be made by solving (1) with  $d^2$  replaced by  $(\alpha d)^2$ . Here,  $\alpha$  is defined as:

$$\alpha(n) = \frac{TRND_{TR}}{TEMP_{TR}} \quad (3)$$

where  $TRND_{TR}(n)$  is the maximal  $n$ -year trend in the observed tropical SST, 1870–present, and  $TEMP_{TR}$  is the applied tropical SST difference, ( $A^+ - A^-$ ).

There is no a priori guarantee that (1) can be solved for  $n$  when  $d^2$  is replaced by  $(\alpha d)^2$ , but trial shows that it can be. The solution for each season gives a timescale for the thick contour in Fig. 4.2 of  $n \approx 30$  years, at which the variance of filtered internal variability matches the squared scaled response. Hence, at a timescale of about 30 years, North Atlantic air–sea interaction may well play an appreciable role in natural climate variability. This timescale is considerably longer than the decorrelation time of the mixed layer and is likely, therefore, to be associated with lower-frequency variations, possibly involving variability of the thermohaline or ‘Gulf Stream’ circulations. Note that nothing is inferred here about predictability.

#### 4.10 Discussion and conclusions

This study has investigated the atmospheric response to North Atlantic (equator to 70°N) sea-surface temperature anomalies. This topic is meaningful if we restrict our interest to the mean quasi-instantaneous atmospheric response.

Because *interannual* atmospheric internal variability is strong compared with the responses of interest, it was considered essential to make the experiments under highly controlled conditions with as few degrees of freedom for the system as possible. This was done by using atmospheric models rather than coupled models, using the same SST and sea-ice climatologies for each model and restricting attention to fixed SSTA patterns. Other controlled conditions include using the same pre-industrial CO<sub>2</sub> and trace gases, although it is unlikely that this would have had a large impact on the results. In order to further improve the chances of achieving statistical significance, ‘optimal’ SSTAs were deduced from a lagged maximal-covariance analysis of observed monthly-mean SST and the following seasonal-mean 500 hPa geopotential height field.

Under these controlled and optimized conditions, the models show rather similar responses. It has been found that the mean response to SSTAs in the models used is generally larger in magnitude than the inter-model standard deviation. Further, the inter-model standard deviation has been shown to be often dominated by atmospheric internal variability so the true inter-model differences are likely to be considerably smaller than the magnitude of the multi-model mean response. The mean response for the particular SSTA patterns chosen includes, for example, a  $-1.6$  hPa effect on the Azores-minus-Iceland North Atlantic Oscillation index,  $+1$  K surface temperature anomalies over Europe and a remote one-standard-deviation decrease in Indian summer monsoon rainfall.

Much of the large-scale response appears to be forced by the tropical SSTAs and communicated via barotropic Rossby waves to the extratropics. Nevertheless, a clear role for extratropical SSTAs in forcing an extratropical response is evident throughout the year. Kushnir *et al.* (2002) highlighted the major discrepancies between (other) models in their *local* extratropical responses. For SON and DJF, a barotropic response associated with extratropical SSTAs is indicated for the one model (HadAM3) investigated here. However, the fact that the extratropical multi-model mean response is rather baroclinic suggests that such barotropic (storm-track related) discrepancies also exist between the current models.

There are reasonable similarities in SON, MAM and JJA between the statistically significant parts of the multi-model response patterns and the estimated observational responses. The magnitudes of the multi-model responses for each season are generally less than those estimated for the observations, and so it seems likely that the models do *not*, at the very least, overestimate the magnitude of the response.

The multi-model results suggest that, for strong SSTA magnitudes such as those that occurred in JJA 2003 for example, air–sea interaction may have a detectable influence on

climate variations on timescales as short as two years. Mixed-layer processes are likely to be important at this timescale. Linear scaling of the response also suggests that air–sea interaction may play a significant role in natural climate variability on a longer timescale of about 30 years. For this timescale, variations in the thermohaline and ‘Gulf Stream’ circulations may be important. One implication of this result is that climate models need to represent accurately variability of these oceanic-circulation features if we are to have confidence in forecasts of climate change. The stronger estimates of the true observational response suggest that, if anything, the 30-year timescale identified here should be considered as an upper bound.

Attention here has focused on the mean response and its magnitude compared with atmospheric internal variability. Clearly SSTAs could also affect the relative importance of different ‘modes’ of variability about the mean climate (Peng and Robinson 2001). This possibility has not been addressed here. To help achieve statistical significance, fixed SSTA patterns have been used for each season. Other SSTA patterns would be likely to give different response patterns (for example the ‘tripole’ SSTA pattern could force an NAO response in DJF, as it does here for MAM). Hence the regions highlighted by the biennial and 10/30-year contours in Fig. 4.2 are also likely to be sensitive to the choice of SSTA patterns. The SSTA patterns most relevant for forcing the atmosphere may vary with timescale. This aspect has not been investigated here although the decadal and multi-decadal nature of the principal components arising from the MCA procedure of Rodwell (2003) suggest that low frequencies do play a major role in the definition of the SSTA patterns used here.

### **Acknowledgements**

This work was completed while MJR was working at the Met Office and during a short sabbatical at the National Center for Atmospheric Research, USA. We thank Christophe Cassou and Adam Philips for help with the CAM2 model and Chris Folland, Jeff Knight, Laurent Terray, the reviewers and associate editor for their help or useful comments. This work was funded by the European Union’s PREDICATE project.

### **References**

- Alexander, M. A., and C. Deser, 1995: A mechanism for the recurrence of wintertime midlatitude SST anomalies. *J. Phys. Oceanogr.*, *25*, 122–137.
- Barsugli, J. J., and D. S. Battisti, 1998: The basic effects of atmosphere–ocean thermal coupling on midlatitude variability. *J. Atmos. Sci.*, *55*, 477–493.
- Bjerknes, J., 1964: Atlantic air–sea interaction. *Adv. Geophys.*, *10*, 1–82.
- Bretherton, C. S., and D. S. Battisti, 2000: An interpretation of the results from atmospheric general circulation models forced by the time history of the observed sea surface temperature distribution. *Geophys. Res. Lett.*, *27*, 767–770.

Cayan, D. R., 1992: Latent and sensible heat-flux anomalies over the northern oceans—Driving the sea-surface temperature. *J. Phys. Oceanogr.*, 22, 859–881.

Collins, M., 2002: Climate predictability on interannual to decadal time scales: The initial value problem. *Climate Dyn.*, 19, 671–692 .

Cubasch, U., G. A. Meehl, G. J. Boer, R. J. Stouffer, M. Dix, A. Noda, C. A. Senior, S. Raper, and K. S. Yap, 2001: ‘Projections of future climate change’. In *Climate change 2001: The scientific basis. Contribution of the working group I to the Third assessment report of the Intergovernmental Panel on Climate Change*. Eds. J. T. Houghton, Y. Ding, D. J. Griggs, M. Noguer, P. J. van der Linden, X. Dai, K. Maskell and C. A. Johnson. Cambridge University Press, Cambridge, UK and New York, USA.

Czaja, A., and C. Frankignoul, 1999: Influence of North Atlantic SST on the atmospheric circulation. *Geophys. Res. Lett.*, 26, 2969–2972.

Czaja, A., and C. Frankignoul, 2002: Observed impact of Atlantic SST anomalies on the North Atlantic Oscillation. *J. Climate*, 15, 606–623.

Davies, J. R., D. P. Rowell, and C. K. Folland, 1997: North Atlantic and European seasonal predictability using an ensemble of multidecadal atmospheric GCM simulations. *Int. J. Climatol.*, 17, 1263–1284 .

Déqué, M., C. Drevet, A. Braun, and D. Cariolle, 1994: The ARPEGE/IFS atmospheric model: A contribution to the French community climate modelling. *Climate Dyn.*, 10, 249–266.

Ferreira, D., C. Frankignoul, and J. Marshall, 2001: Coupled ocean–atmosphere dynamics in a simple midlatitude climate model. *J. Climate*, 14, 3704–3723.

Folland, C. K., T. N. Palmer, and D. E. Parker, 1986: Sahel rainfall and worldwide sea temperatures, 1901–85. *Nature*, 320, 602–607.

Frankignoul, C., and E. Kestenare, 2002: The surface heat flux feedback. Part I: Estimates from observations in the Atlantic and North Pacific. *Climate Dyn.*, 19, 633–647.

Gates, W. L., 1992: AMIP: The Atmospheric Model Intercomparison Project. *Bull. Am. Meteorol. Soc.*, 73, 1962–1970.

Gupta, A. K., D. M. Anderson, and J. T. Overpeck, 2003: Abrupt changes in the Asian southwest monsoon during the Holocene and their links to the North Atlantic Ocean. *Nature*, 421, 354–357.

Hall, N. M. J., J. Derome, and H. Lin, 2001: The extratropical signal generated by midlatitude SST anomaly. Part I: Sensitivity at equilibrium. *J. Climate*, 14, 2035–2053.

Hoskins, B. J., and D. J. Karoly, 1981: The steady linear response of a spherical atmosphere to thermal and orographic forcing. *J. Atmos. Sci.*, 38, 1179–1196.

Hoskins, B. J., and P. D. Sardeshmukh, 1987: A diagnostic study of the dynamics of the northern hemisphere winter of 1985–86. *Q. J. R. Meteorol. Soc.*, 113, 759–778.

Hulme, M., G. J. Jenkins, X. Lu, J. R. Turnpenny, T. D. Mitchell, R. G. Jones, J. Lowe, J. M. Murphy, D. Hassell, P. Boorman, R. McDonald, and S. Hill, 2002: ‘Climate change scenarios for the United Kingdom’ UKCIP02 Scientific Report, Tyndall Centre for Climate Change Research, School of Environmental Sciences, University of East Anglia, Norwich, UK.

Hurrell, J. W., 1995: Decadal trends in the North Atlantic Oscillation: Regional temperatures and precipitation. *Science*, 269, 676–679.

Janssen, P. A. E. M., and P. Viterbo, 1996 Ocean waves and the atmospheric climate. *J. Climate*, 9, 1269–1287.

Kalnay, E., M. Kanamitsu, R. Kistler, W. Collins, D. Deaven, L. Gandin, M. Iredell, S. Saha, G. White, J. Woolen, Y. Zhu, M. Chelliah, W. Ebisuzaki, W. Higgins, J. Janowiak, K. C. Mo, C. Ropelewski, J. Wang, A. Leetmaa, R. Reynolds, R. Jenne, and D. Joseph, 1996: The NCEP/NCAR 40-year reanalysis project. *Bull. Am. Meteorol. Soc.*, 77 437–471.

Kushnir, Y., 1994: Interdecadal variations in North Atlantic sea surface temperatures and associated atmospheric conditions. *J. Climate*, 7, 141–157.

Kushnir, Y., and I. M. Held, 1996: Equilibrium atmospheric response to North Atlantic SST anomalies. *J. Climate*, 9, 1208–1220

Kushnir, Y., W. A. Robinson, I. Bladé, N. M. J. Hall, S. Peng, and R. Sutton, 2002: Atmosphere GCM response to extratropical SST anomalies: Synthesis and evaluation. *J. Climate*, 15, 2233–2256.

Lau, N.-C., and M. J. Nath, 1996: The role of the ‘atmospheric bridge’ in linking tropical Pacific ENSO events to extratropical SST anomalies. *J. Climate*, 9, 2036–2057.

Livezey, R. E., and W. Y. Chen, 1983: Statistical field significance and its determination by Monte Carlo techniques. *Mon. Weather Rev.*, 111, 46–59.

Mehta, V., M. Suarez, J. Manganello, and T. Delworth, 2000: Oceanic influence on the North Atlantic Oscillation and associated northern hemisphere climate variations: 1959–1993. *Geophys. Res. Lett.*, 27, 121–124.

Nobre, P., and J. Shukla, 1996: Variations of sea surface temperature, wind stress, and rainfall over the tropical Atlantic and South America. *J. Climate*, 9, 2464–2479.

Okumura, Y., S.-P. Xie, A. Numaguti, and Y. Tanimoto, 2001: Tropical Atlantic air–sea interaction and its influence on the NAO. *Geophys. Res. Lett.*, 28, 1507–1510.

Palmer, T. N., and Z. Sun, 1985: A modelling and observational study of the relationship between sea surface temperature in the north-west Atlantic and the atmospheric general circulation. *Q. J. R. Meteorol. Soc.*, 111, 947–975.

Peng, S., and J. S. Whitaker, 1999: Mechanisms determining the atmospheric response to midlatitude SST anomalies. *J. Climate*, 12, 1393–1408.

Peng, S., and W. A. Robinson, 2001: Relationships between atmospheric internal variability and the responses to an extratropical SST anomaly. *J. Climate*, 14, 2943–2959.

Peng, S., W. A. Robinson, and S. Li, 2002: North Atlantic SST forcing of the NAO and relationships with intrinsic hemispheric variability. *Geophys. Res. Lett.*, 29, doi: 10.1029.2001GL014043.

Peterson, K. A., R. J. Greatbatch, J. Lu, H. Lin, and J. Derome, 2002: Hindcasting the NAO using diabatic forcing of a simple AGCM. *Geophys. Res. Lett.*, 29, doi: 10.1029/2001GL014502.

Pope, V. D., M. L. Gallani, P. R. Rowntree, and R. A. Stratton, 2000: The impact of new physical parametrizations in the Hadley Centre climate model: HadAM3. *Climate Dyn.*, 16, 123–146.

Rayner, N. A., D. E. Parker, E. B. Horton, C. K. Folland, L. V. Alexander, D. P. Rowell, E. C. Kent, and A. Kaplan, 2003: Global analyses of sea surface temperature, sea-ice, and night marine air temperature since the late nineteenth century. *J. Geophys. Res.*, 108, doi: 10.1029/2002JD002670.

Rodwell, M. J., 2003: ‘On the predictability of North Atlantic climate’. Pp. 173–192 in *The North Atlantic Oscillation*. Eds. J. W. Hurrell, Y. Kushnir, G. Ottersen and M. Visbeck. American Geophysical Union, Washington, DC, USA.

Rodwell, M. J., and C. K. Folland, 2002: Atlantic air–sea interaction and seasonal predictability. *Q. J. R. Meteorol. Soc.*, 128, 1413–1443.

Rodwell, M. J., and C. K. Folland, 2003: Atlantic air–sea interaction and model validation. *Ann. Geophys.*, 46, 47–56.

Rodwell, M. J., and W. J. Ingram, 2000: ‘Notes on optimal run lengths for fixed SST anomaly experiments’. Hadley Centre Internal Note 96, (available from Hadley Centre for Climate Prediction and Research, Met Office, FitzRoy Road, Exeter, Devonshire EX1 3PB, UK).

Rodwell, M. J., D. P. Rowell, and C. K. Folland, 1999: Oceanic forcing of the wintertime North Atlantic Oscillation and European climate. *Nature*, 398, 320–323.

Roeckner, E., K. Arpe, L. Bengtsson, M. Christoph, M. Claussen, L. Dümenil, M. Esch, M. Giorgetta, U. Schlese, and U. Schulzweida, 1996: ‘The atmospheric general circulation model ECHAM-4: Model description and simulation of present-day climate’. Max-Planck-Institut für Meteorologie Report 218 (available from Max-Planck-Institut für Meteorologie, Bundesstr. 53, 20146 Hamburg, Germany).

Roeckner, E., G. Bäuml, L. Bonaventura, R. Brokopf, M. Esch, M. Giorgetta, S. Hagemann, I. Kirchner, L. Kornblüeh, E. Manzini, A. Rhodin, U. Schlese, U. Schulzweida, and A. Tompkins, 2003: ‘The atmospheric general circulation model ECHAM 5: Part 1: Model description’. Max-Planck-Institut für Meteorologie Report 349 (available from Max-Planck-Institut für Meteorologie, Bundesstr. 53, 20146 Hamburg, Germany).

Rowell, D. P., and F. W. Zwiers, 1999: The global distribution of sources of atmospheric decadal variability and mechanisms over the tropical Pacific and southern North America. *Climate Dyn.*, 15 751–772.

Rowntree, P. R., 1976: Response of the atmosphere to a tropical Atlantic ocean temperature anomaly. *Q. J. R. Meteorol. Soc.*, 102, 607–625.

Sardeshmukh, P. D., and B. J. Hoskins, 1988: The generation of global rotational flow by steady idealized tropical divergence. *J. Atmos. Sci.*, 45, 1228–1251.

Terray, L., and C. Cassou, 2002: Tropical Atlantic sea surface temperature forcing of quasi-decadal climate variability over the North Atlantic–European region. *J. Climate*, 15, 3170–3187.

Walker, G. T., and E. W. Bliss, 1932: World Weather V. *Mem. R. Meteorol. Soc.*, 4, 53–84.



## Estimating the decadal predictability of a coupled AOGCM

(H. Pohlmann, M. Botzet, M. Latif, A. Roesch, M. Wild, and P. Tschuck)

### Abstract

On seasonal time scales, ENSO prediction has become feasible in an operational framework in recent years. On decadal to multidecadal time scales, the variability of the oceanic circulation is assumed to provide a potential for climate prediction. To investigate the decadal predictability of the coupled atmosphere–ocean general circulation model (AOGCM) European Centre-Hamburg model version 5/Max Planck Institute Ocean Model (ECHAM5/MPI-OM), a 500-yr-long control integration and “perfect model” predictability experiments are analyzed. The results show that the sea surface temperatures (SSTs) of the North Atlantic, Nordic Seas, and Southern Ocean exhibit predictability on multidecadal time scales. Over the ocean, the predictability of surface air temperature (SAT) is very similar to that of SST. Over land, there is little evidence of decadal predictability of SAT except for some small maritime-influenced regions of Europe. The AOGCM produces predictable signals in lower-tropospheric temperature and precipitation over the North Atlantic, but not in sea level pressure.

### 5.1 Introduction

In the field of climate prediction, great progress has been attained with the ability to predict the El Niño-Southern Oscillation (ENSO) phenomenon (e.g., Latif et al. 1994, 1998). El Niño, the irregular warming of sea surface temperature (SST) in the equatorial east Pacific, coincides with the negative phase of the Southern Oscillation, a seesaw in sea level pressure (SLP) between southeast Asia and the eastern Pacific region. The coupled atmosphere–ocean phenomenon ENSO is the most important climate mode on seasonal to interannual time scales, causing various climate disturbances around the globe. A comprehensive in situ observation system of the equatorial Pacific forms, together with satellite measurements, the basis for ENSO predictions. ENSO predictions are performed routinely by a number of prediction centers using statistical methods and coupled atmosphere–ocean general circulation models (AOGCMs). Recent findings on this topic are published in the *Experimental Long-Lead Forecast Bulletin* (available online at <http://grads.iges.org/ellfb>).

The thermohaline circulation (THC), a component of the global ocean circulation, is driven by differences in the density of seawater, which is controlled by temperature and salinity. In regions of the Labrador and Nordic Seas and in the Southern Ocean around Antarctica, surface water is cooled and sinks into the deep ocean. Surface currents replace the water masses and transport heat poleward (Trenberth and Caron 2001). In the Atlantic, this poleward heat transport contributes to a milder European winter climate than without these currents (Broecker 1991). However, Seager et al. (2002) criticize the

responsibility of these heat transports for European's mild winters and argue that the oceanic heat storage and atmospheric heat transport are important. The discussion of the relative importance of the oceanic heat and salt transports for European climate is ongoing (Rhines and Häkkinen 2003). The THC varies on multidecadal time scales (Dickson et al. 1996, Timmermann et al. 1998, Delworth and Mann 2000). The predictability attributed to this climate variability is investigated in this study using an AOGCM.

Decadal predictability is estimated by diagnostic and prognostic approaches. In the diagnostic approach, the predictability is analyzed by decomposing the variance of a climate variable into a long time scale potentially predictable component and an unpredictable noise component. The diagnostic potential predictability of the Canadian Centre for Climate Modelling and Analysis (CCCma) AOGCM is estimated in the study of Boer (2000) and that of a multimodel ensemble is estimated in the studies of Boer (2001, 2004). Potential predictability is found in the multimodel studies predominantly in the high latitude oceans, with appreciable values on multidecadal time scales especially in the Southern Ocean and the North Atlantic. In the prognostic approach, the predictability is estimated with "perfect model" AOGCM experiments. Starting from identical oceanic and perturbed atmospheric initial conditions, ensemble experiments are performed. The spread within the ensemble is interpreted as an estimate of predictability. The use of identical oceanic initial conditions implies the assumption that the AOGCM could be perfectly initialized with three-dimensional oceanic observational fields. Thus, since this is not possible, this technique gives an upper limit of predictability. Using the Geophysical Fluid Dynamics Laboratory (GFDL) model, Griffies and Bryan (1997a,b) found that in the North Atlantic region the first empirical orthogonal function (EOF) of the dynamical sea surface topography is predictable up to 10–20 yr on average, and SST in the East Greenland Sea is predictable 5–15 yr in advance. Grötzner et al. (1999) used the European Centre-Hamburg model version 3/ Large-Scale Geostrophic (ECHAM3/LSG) model and found that the North Atlantic THC is predictable about one decade in advance, but North Atlantic SST is only predictable about 1 yr in advance. Boer (2000) analyzed simulations with the CCCma model and found predictable surface air temperatures (SATs) on multidecadal time scales mainly in the Southern Ocean. Collins (2002) used the third Hadley Centre Coupled Ocean–Atmosphere GCM (HadCM3) and found that SAT in the North Atlantic region is predictable on decadal time scales. Collins and Sinha (2003) have shown some indication that the multidecadal THC predictability in HadCM3 leads to weak but significant predictability of western European climate. These studies and the recent predictability comparison of Collins et al. (2003) show that the predictability of oceanic and atmospheric components depends strongly on the model formulation. However, the possibilities of decadal climate predictability with AOGCMs are unclear since the number of decadal predictability studies is limited. The AOGCM experiments of this study exhibit relatively high predictabilities and therefore may reveal new chances for climate prediction. The remainder of this paper is organized as follows: The AOGCM and the experiments used in this study are described in section 2. The concepts of diagnostic and prognostic potential predictability are introduced in section 3 and are applied to estimate the climate

predictability of our AOGCM in section 4. Section 5 concludes this paper with a summary and discussion of the results.

## **5.2 Model and experiments**

The model used in this study is the global coupled ECHAM5/Max Planck Institute Ocean Model (MPIOM). The atmospheric component, ECHAM5 (version 5.0; Roeckner et al. 2003), is run at T42 resolution, which corresponds to a horizontal resolution of about  $2.8^\circ \times 2.8^\circ$ . The oceanic component, MPI-OM (Marsland et al. 2003), is based on a C grid version of the Hamburg Ocean Primitive Equation (HOPE) ocean model. It is run on a curvilinear grid with equatorial refinement. A dynamic/thermodynamic sea ice model (see also Marsland et al. 2003) and a hydrological discharge model (Hagemann and Dümenil Gates 2001) are included in this model. The atmospheric and oceanic components are coupled with the Ocean Atmosphere Sea Ice Soil (OASIS) coupler (Terray et al. 1998). The model does not employ flux adjustment or any other corrections.

A 500-yr-long control integration of ECHAM5/MPIOM, in which the concentrations of the greenhouse gases are fixed to the values of the 1990s, is used to estimate the low-frequency climate variability. The first 50 yr of the control integration are not considered in order to allow for the spinup of the coupled system. The North Atlantic THC of this integration exhibits strong multidecadal variations (Latif et al. 2004). From the control integration, three different years (90, 125, and 170), corresponding to intermediate, strong, and weak North Atlantic THC conditions, are selected and used as initial conditions for three ensemble experiments. Each ensemble consists of six experiments realized with slightly perturbed atmospheric, but the same oceanic, initial conditions. The experiments cover a 20-yr-long integration period. These ensemble experiments are referred to as predictability experiments.

## **5.3 Methods**

This study is idealized, since no observational data for the initialization of the experiments or the verification of the results are used. Instead, the upper predictability limit of ECHAM5/MPI-OM is estimated by applying the methods of “prognostic potential predictability” (PPP) and “diagnostic potential predictability” (DPP). For the prognostic predictability approach we perform perfect model ensemble experiments with the AOGCM ECHAM5/MPI-OM, while the 500-yr-long control integration with this AOGCM is analyzed in the diagnostic predictability approach.

### **5.3.1 Diagnostic potential predictability**

The method of analysis of variances (Madden 1976, Rowell 1998, see also the **Appendix** for a description of this analysis) is applied to investigate the variability of our control integration. To distinguish this method from the prognostic approach introduced in the next section, we call it diagnostic potential predictability. DPP attempts to quantify the fraction of long-term variability that may be distinguished from the internally generated natural variability, which is not predictable on long time scales and so may be considered

as noise. For this concept the variance of some mean quantity is investigated to determine whether it is greater than can be accounted for by sampling error given the noise in the system. The variances of a certain climate variable from the control integration (of length  $l = nm$ ) are estimated from the  $m$ -year means ( $\sigma_v^2$ ) and the average of the deviations of the annual means from them ( $\sigma_\varepsilon^2$ ). In a first step, we test the null hypothesis that the data are independent random variables, which possess no long time-scale potential predictability. Following Boer (2004), the null hypothesis is rejected using an F test (e.g., von Storch and Zwiers 1999) if

$$\frac{(m-1)\sigma_v^2}{\sigma_\varepsilon^2} > F_{n-1, n(m-1)}. \quad (5.1)$$

As noted in Rowell (1998), the one-sided test, which is not affected by serial correlation in the data, has to be used. In a second step, DPP is calculated. As Boer (2004) shows, it can be derived in two ways resulting in two different estimates for DPP. We use the more conservative estimate here:

$$DPP = \frac{\sigma_v^2 - \frac{1}{m}\sigma^2}{\sigma^2}, \quad (5.2)$$

where  $\sigma^2 = \sigma_v^2 + \sigma_\varepsilon^2$  is the total variance. The longer time-scale variance is discounted in this equation to account for the fact that short-term noise contributes to the calculated long time-scale variance.

### 5.3.2 Prognostic potential predictability

The ensemble spread (ensemble variance) of a climate variable  $X$  from the ensemble experiments in relation to its variance in the control integration ( $\sigma^2$ ) gives a measure for the PPP. Here, PPP (as a function of the prediction period  $t$ ) is defined as the average over all ensemble experiments:

$$PPP(t) = 1 - \frac{1}{N(M-1)} \frac{\sum_{j=1}^N \sum_{i=1}^M (X_{ij}(t) - \bar{X}_j(t))^2}{\sigma^2}, \quad (5.3)$$

where  $X_{ij}$  is the  $i$ th member of the  $j$ th ensemble,  $\bar{X}_j$  is the  $j$ th ensemble mean, and  $N$  ( $M$ ) is the number of ensembles (ensemble members). In this study, each of the three experiments ( $N = 3$ ) consists of six ensemble members and the control integration ( $M = 7$ ), which is regarded as an additional ensemble member. PPP amounts to a value of 1 for perfect predictability and a value of 0 for an ensemble spread equal to the variance of the control integration. The significance of PPP is estimated, determining if the ensemble

variance is different to the variance of the control integration. The F test is used for this decision; that is, if

$$PPP(t) > 1 - \frac{1}{F_{N(M-1),k-1}}, \quad (5.4)$$

where the degrees of freedom of the control integration ( $k$ ) are reduced with the concept of the decorrelation time for a first-order autoregressive (AR-1) process [Eq. (17.11) in von Storch and Zwiers (1999)].

The results are compared with the statistical climate prediction concept of “damped persistence.” This statistical forecast method takes into account the climatological mean and the damping coefficient estimated from the history of the system. It is based on the concept of Hasselmann’s (1976) stochastic climate model. In this model, the system is divided into a fast (atmosphere) and a slow (ocean) component. In the mathematical formulation of the slow processes, atmospheric variability (weather) is treated as “noise”, which is integrated by the ocean resulting in low-frequency variability. The differential equation describing this AR-1 process is given by

$$\frac{dX(t)}{dt} = -\alpha X(t) + Z(t), \quad (5.5)$$

where  $\alpha$  is the damping coefficient and  $Z(t)$  is a random variable with Gaussian characteristics. The average of several realizations of Eq. (5.5), that is, the noise-free solution, is

$$\bar{X}(t) = X_{c\lim} + X_0 e^{-\alpha t}. \quad (5.6)$$

This equation describes the averaged damping from an initial anomaly  $X_0$  toward the climatological mean  $X_{c\lim}$ . The prognostic potential predictability of a hypothetical ensemble generated by stochastic processes is given by [see Eq. (8) of Griffies and Bryan (1997b)]

$$PPP(t) = e^{-2\alpha t}. \quad (5.7)$$

When the damping coefficient is small, the prognostic potential predictability is high, and a prediction with this statistical method is reasonable.

## 5.4. Results

### 5.4.1 Climate variability

Analyzing the ECHAM5/MPI-OM control integration, Latif et al. (2004) found a close relationship between variations of the North Atlantic THC, defined as the maximum of the meridional overturning circulation (MOC) at 30°N (i.e., the maximum in the North Atlantic in the control integration), and SST averaged over the region 40°–60°N, 50°–10°W. Figure 5.1a shows the linear correlation between decadal means of the North Atlantic THC (maximum MOC at 30°N) and SST over the Northern Hemisphere. Temporal dependence of the data is taken into consideration for statistical tests of the significance of the correlation values reducing the degrees of freedom with the concept of the decorrelation time for an AR-1 process [Eq. (17.11) in von Storch and Zwiers (1999)]. Strongest (positive) correlations exist in the central North Atlantic region. Therefore the same North Atlantic SST index as in Latif et al. (2004) is used to investigate the relation to the atmospheric variables SAT and SLP. Figure 5.1b shows the correlation values between decadal means of the North Atlantic SST index and SAT. Significant positive correlation values exist nearly over the whole North Atlantic, extending also over Europe and Asia. Figure 5.1c shows the correlation values between decadal means of the North Atlantic SST index and SLP. The correlation pattern is a monopole with significant (negative) correlation values over the east Atlantic and Europe. Based on this analysis, we define an east Atlantic–European SLP index as the average over the region 40°–60°N, 30°W–30°E. The model simulates a realistic North Atlantic Oscillation (NAO), shown in Fig. 5.1d as the correlation of the NAO index with SLP in the winter season (January–February–March: JFM). The NAO index is defined as the principal component of the leading EOF of SLP in the North Atlantic–European region (15°–80°N, 90°W–40°E) for the winter season (JFM). The spatial dipole structure of the NAO is different from the monopole structure of the THC projection on the SLP field.

Spectral analyses of climate indices are shown for the North Atlantic THC (Fig. 5.1e), the North Atlantic SST (Fig. 5.1f), the east Atlantic–European SLP (Fig. 5.1g) and the NAO (Fig. 5.1h). The spectra are computed from detrended time series using a “Bartlett” window and two chunks. The spectra of the North Atlantic THC and SST indices are red, and those of the east Atlantic–European SLP and NAO indices are white. The North Atlantic THC spectrum shows a dominant peak at 70 yr and another peak at 100 yr, exceeding the 99% significance level. Peaks of the North Atlantic SST spectrum do not exceed the 99% significance level. The east Atlantic–European SLP spectrum exhibits a peak at 10 yr. Peaks of the NAO spectrum do not exceed the 99% significance level. Particularly, there is little amplitude of variability in the NAO on the time scales associated with the THC variability. This is different from the spectra of the ECHAM3/LSG model (Grötzner et al. 1999), which shows spectral peaks at the time scale associated with the THC both in oceanic and atmospheric quantities of the North Atlantic region.

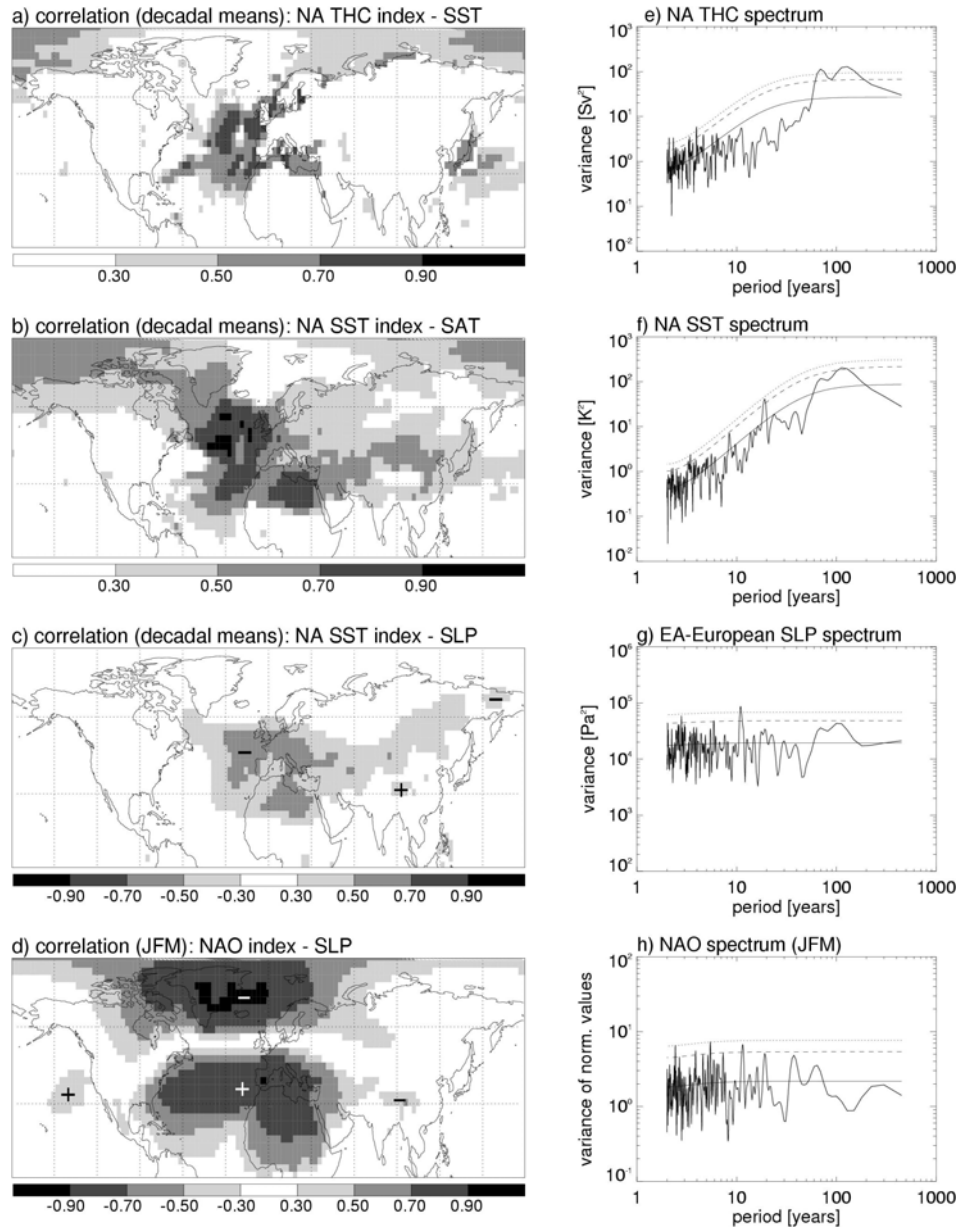


**Figure 5.1** Analyses of the climate variability in the control integration. Correlation maps between (a) the North Atlantic THC index and SST, (b) the North Atlantic SST index and SAT, (c) the North Atlantic SST index and SLP, and (d) the NAO index and SLP. (a)–(c) are based on decadal means. The shaded values are significant on the 95% significance level according to a *t* test. (d) is based on winter (JFM) means. Only positive values are plotted in (a) and (b), and in (c) and (d) the sign of the correlation is marked. Also shown are the spectra of time series for the (e) North Atlantic THC, (f) North Atlantic SST, (g) east Atlantic–European SLP, and (h) NAO. (e)–(g) are based on annual means and (h) is based on winter (JFM) means. Additionally shown in (e)–(h) are the spectra of fitted AR-1 processes (solid), and the 95% (dashed) and 99% (dotted) significance levels according to these processes.

### 5.4.2 Diagnostic potential predictability

Figure 5.2a shows the diagnostic potential predictability for decadal means of surface temperatures (i.e., SST over the oceans and land surface temperature elsewhere) of the control integration. Highest decadal DPP values exist in the North Atlantic and Nordic Seas. Other regions with high decadal DPP are present in the Southern Ocean, in the extratropical North Pacific and also in the subtropical Pacific. Our result of decadal DPP for surface temperatures shows a remarkable similarity to that of a super ensemble of nine climate models (Boer 2004). However, compared to the results of the superensemble mean, the diagnostic potential predictability of our analysis is stronger in the North Atlantic, Nordic Seas, and Pacific and weaker in the Southern Ocean, especially east of the Greenwich meridian to the date line. Figure 5.2b shows the diagnostic potential predictability for 20-yr means of surface temperatures. These DPP values are generally less significant than those based on 10-yr means, although considerable values remain in the North Atlantic and Nordic Seas.

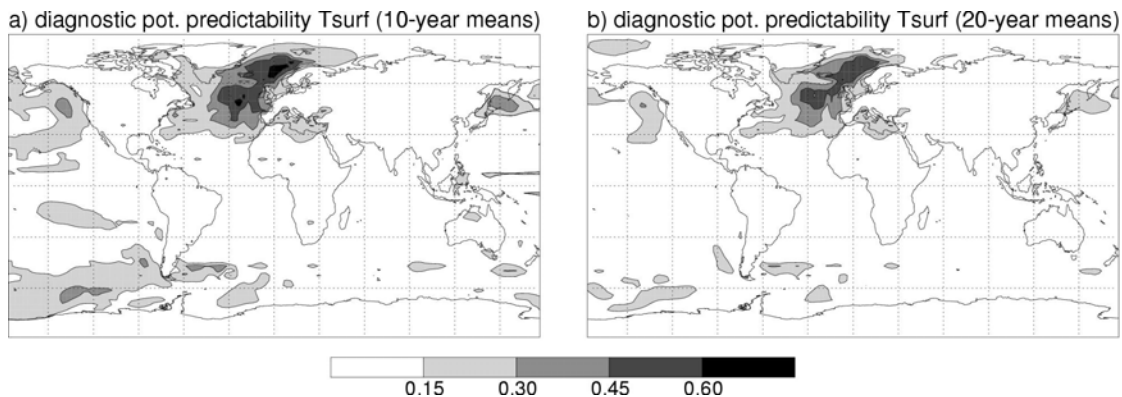


**Figure 5.2** Diagnostic potential predictability of surface temperature ( $T_{surf}$ ) based on (a) 10-yr means and (b) 20-yr means. The shaded values are significant at the 99% significance level according to an  $F$  test.

### 5.4.3 Oceanic prognostic potential predictability

The prognostic potential predictability of surface temperatures are shown as maps averaged over the three ensemble experiments and the first and second prediction decade in Figs. 5.3a and 5.3b, respectively. The result of this method averaged over the first decade is very similar to that of the diagnostic potential predictability method based on 10-yr means. Averaged over the first decade, the most predictable regions are in the North Atlantic, Nordic Seas, and Southern Ocean. The result of the prognostic potential predictability method averaged over the second decade is very similar to that of the diagnostic potential predictability method based on 20-yr means. The prognostic potential predictability of the second decade is everywhere less significant than that of the first decade. In this period, predictability primarily remains significant in the North Atlantic and the Nordic Seas. In these areas, the ocean exhibits multidecadal SST predictability.

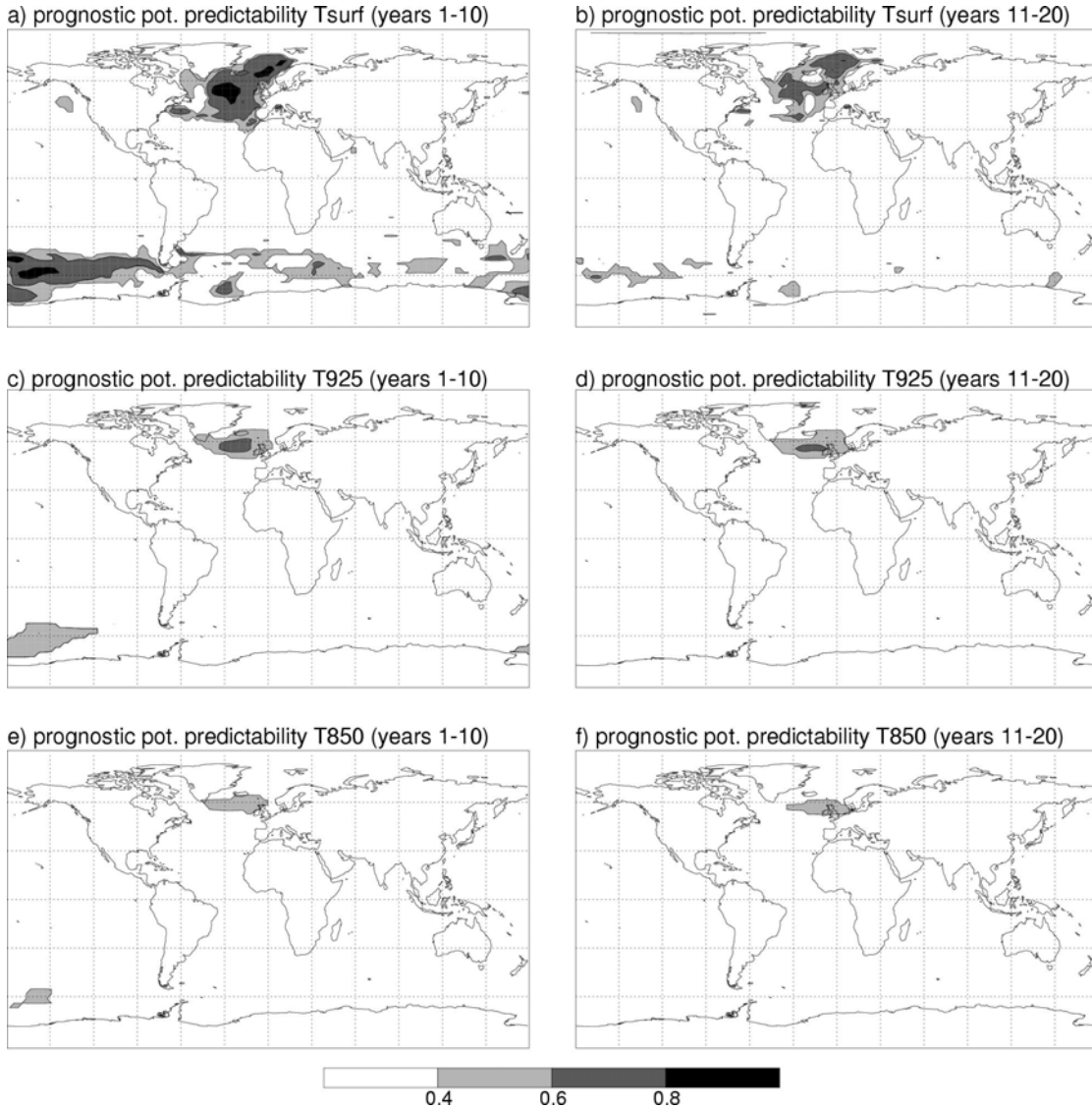


**Figure 5.3** PPP of temperature at (top) the surface ( $T_{surf}$ ), (middle) 925 hPa level ( $T_{925}$ ), and (bottom) 850 hPa level ( $T_{850}$ ) averaged over the three ensemble experiments and the (left column) first and (right column) second prediction decade. The shaded values are significant on the 90% significance level according to an  $F$ -test.

SST indices are defined in regions with high predictabilities to analyze the time dependence of the predictability in more detail. An additional effect of the spatial average is an enhancement of the predictability, since small-scale fluctuations are filtered out. The time series of North Atlantic SST averaged in the region  $40^{\circ}$ – $60^{\circ}$ N,  $50^{\circ}$ – $10^{\circ}$ W of the control integration and the predictability experiments are shown together with the predictability of this SST index in Fig. 5.4a. The skill in predicting the North Atlantic SST index is clearly better than that of the damped persistence forecast and exceeds the 95% significance level over the whole prediction period of 20 yr. Averaged over the first (second) prediction decade, the predictability, PPP, equals 0.86 (0.79). These values are

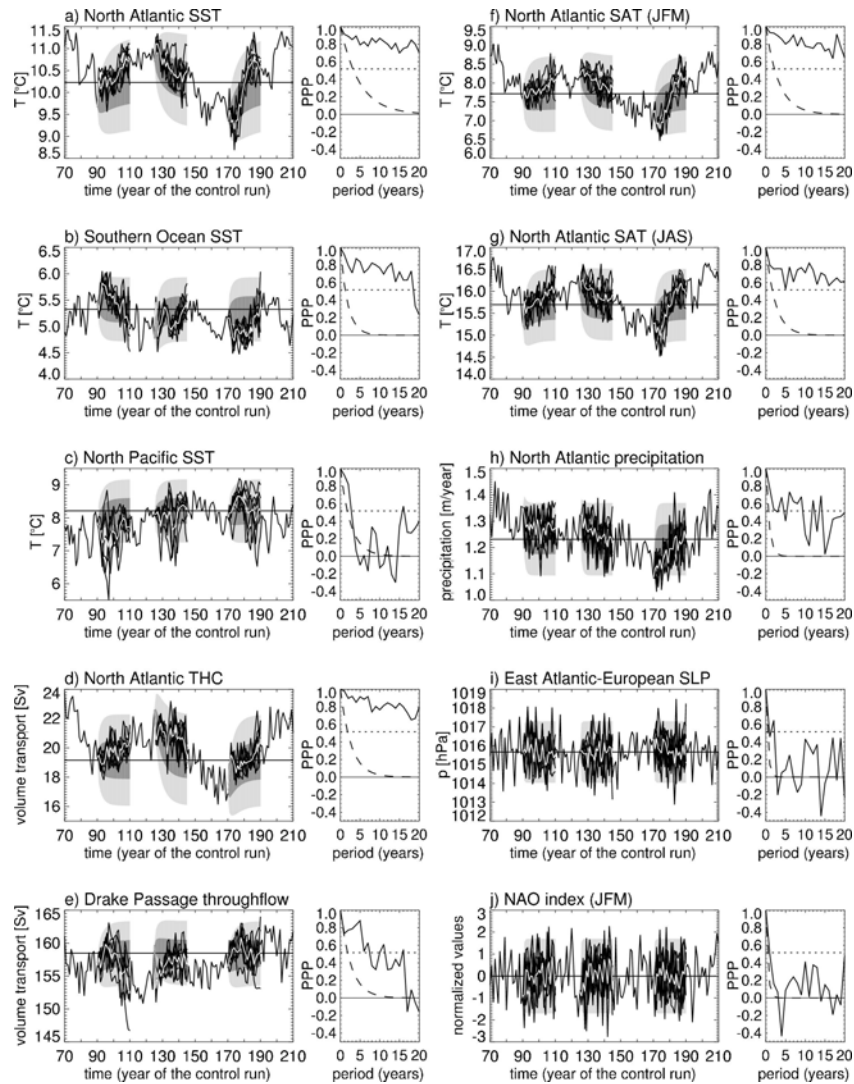


**Figure 5.4** (a) (left) Annual mean North Atlantic SST for years 70 to 210 of the control integration (black); ensemble forecast experiments initialized at the end of the years 90, 125, and 170 (black); and the ensemble means (white). The results of the statistical forecast method of damped persistence are shown as the range expected to contain 90% and 50% of the values from infinite size ensembles of noise driven AR-1 random processes (light and dark gray, respectively). (right) PPP of the North Atlantic SST index averaged over the three ensemble experiments (solid curve), with the damped persistence forecast (dashed) as a function of the prediction period. Additionally, the 95% significance level according to an F test is dotted. (b)–(j) As in (a), but for (b) Southern Ocean SST, (c) North Pacific SST, (d) North Atlantic THC, (e) Drake Passage throughflow, (f) North Atlantic SAT for JFM, (g) North Atlantic SAT for JAS, (h) North Atlantic precipitation, (i) east Atlantic–European SLP, and (j) the NAO index. (a)–(e) and (h)–(i) are based on annual means, (f) and (j) are based on winter (JFM) means, and (g) is based on summer (JAS) means.

considerably higher than the corresponding, spatially averaged predictabilities of individual grid cells as displayed in Fig. 5.3a (5.3b) of 0.61 (0.53). The time series and predictabilities of Southern Ocean SST averaged in the region 50°–60°S, 180°–80°W are shown in Fig. 5.4b. The skill in predicting the Southern Ocean SST index is also good and remains significant at the 95% significance level over the whole prediction period, except for the last two years. Averaged over the first (second) prediction decade, predictability equals 0.82 (0.67). These values are again considerably higher than the spatially averaged predictabilities of individual grid cells as displayed in Fig. 5.3a (5.3b) of 0.62 (0.43). Figure 5.4c shows the North Pacific SST averaged over the region 40°–60°N, 140°E–130°W. This SST index is much less predictable than the North Atlantic and Southern Ocean SST indices. Predictability of North Pacific SST is significant only in the first two years. Thereafter the predictability is of the order of the damped persistence forecast. Latif and Barnett (1994) found in the AOGCM ECHAM3/HOPE a coupled air–sea mode between the subtropical gyre circulation in the North Pacific and the Aleutian low pressure system from which a higher North Pacific SST predictability could be expected. The results of the diagnostic potential predictability confirm this assumption since substantial predictabilities exist in certain regions of the North Pacific (Figs. 5.2a and 5.2b). However, the prognostic potential predictability method suggests almost no significant SST predictability in these regions. A detailed analysis of the predictability in each of the three ensembles shows that the third ensemble exhibits, in contrast to the other ensembles, a significant predictability for the North Pacific SST index of about a decade. This may indicate a dependence of the North Pacific SST predictability on the initial oceanic state.

The result of the North Atlantic THC predictability analysis is shown in Fig. 5.4d. The skill in predicting the North Atlantic THC is significant at the 95% significance level over the whole prediction period of 20 yr and comparable to that of the North Atlantic SST. Latif et al. (2004) show the close relationship between the North Atlantic THC and SST in our AOGCM. The strength of the overturning circulation is related to the convective activity in the deep water formation regions, most notably the Labrador Sea, which is sensitive to freshwater anomalies from the Arctic (Jungclaus et al., 2004, manuscript submitted to *J. Climate*). Another region with a good skill in predicting SST exists in the Southern Ocean. The predictability of the Drake Passage throughflow (Fig. 5.4e) as a measure for the Antarctic Circumpolar Current (ACC) is analyzed. The predictability of the Drake Passage throughflow is clearly significant just over the first five years. This relatively short predictability period and the relatively low correlation values between ACC and Southern Ocean SST in the control integration (not shown) suggest that the strength of the ACC is not the only forcing term determining the predictability of the Southern Ocean SST.

#### **5.4.4 Atmospheric prognostic potential predictability**

The (sea and land) surface temperature and the temperature of the overlying atmosphere are closely related. Therefore the prognostic potential predictability values of SAT (not shown) are very close to the prognostic potential predictability values of the surface temperatures, which are shown in Figs. 5.3a and 5.3b. The highest PPP values of SAT

exist over the North Atlantic, Nordic Seas, and Southern Ocean. Over land there is little evidence of decadal predictability of SAT except for some limited regions of maritime-influenced Europe such as Iceland, Ireland, south Greenland, parts of Great Britain, and Iberia (Figs. 5.3a and 5.3b). The predictability values of air temperature at higher levels are shown for the 925-hPa level (Figs. 5.3c and 5.3d), and the 850-hPa level (Figs. 5.3e and 5.3f). The air temperature is predictable in the lower troposphere over the Southern Ocean in the first prediction decade and over the North Atlantic in both prediction decades. The predictability of decadal mean surface relative humidity is also significant in certain regions of the North Atlantic, Nordic Seas, and Southern Ocean (not shown). However, the predictability of decadal mean SLP is not significant in the North Atlantic–European region (not shown).

Figures 5.4f and 5.4g show the time series and predictabilities for the North Atlantic SAT index defined as the average over sea points in the region  $30^{\circ}$ – $65^{\circ}$ N,  $40^{\circ}$ W– $0^{\circ}$  for winter (JFM) and summer (July–August–September: JAS), respectively. The predictability of this index is significant at the 95% significance level over the whole prediction period in both seasons. The skill of predicting the North Atlantic SAT index is better in winter than in summer, and the variance of North Atlantic SAT is higher in winter than in summer. The atmosphere is dynamically most active in winter. As a result, it is reasonable that the atmosphere over the North Atlantic is strongest coupled to the ocean in this season. The reemergence of persistent oceanic surface anomalies in winter (Timlin et al. 2002) may also contribute to the enhanced signal in this season. Figure 5.4h shows the result for the North Atlantic precipitation index defined as the average over the region  $50^{\circ}$ – $60^{\circ}$ N,  $40^{\circ}$ – $20^{\circ}$ W. The North Atlantic precipitation index is significantly predictable over the first decade. Again, the predictability values of the North Atlantic SAT and precipitation are higher than the corresponding spatial averages of predictabilities at individual grid cells. A detailed analysis shows predictability of humidity to be limited to the lower troposphere. Park and Latif (2004) show that in the ECHAM5/MPI-OM AOGCM the atmospheric response to the North Atlantic decadal SST variability is shallow and that changes in the statistics of transient eddies are not involved. Figure 5.4i shows the result for the east Atlantic–European SLP index and Fig. 5.4j shows the result for the NAO index. The NAO index is defined for the ensemble experiments as the scalar product with the leading EOF mode of the control integration based on SLP averages for the winter season (JFM). The predictabilities of these SLP-based indices are significant just in the first one or two years.

## 5.5 Summary and discussion

In this study, the decadal predictability of the coupled AOGCM ECHAM5/MPI-OM has been systematically investigated, analyzing both the control integration and the perfect model experiments. SSTs are shown to be predictable on decadal to multidecadal time scales in the North Atlantic, Nordic Seas, and Southern Ocean. Ocean dynamics is a candidate in forcing the multidecadal variability and producing the multidecadal predictability of SST. A close relationship between the North Atlantic SST and THC exists. The relation between the ACC and SST in the Southern Ocean is less clear. In addition to the decadal predictability of SST, the AOGCM produces predictable signals

in the temperature of the lower troposphere. Over land there is little evidence of decadal predictability of SAT except for some limited regions of maritime-influenced Europe. Precipitation is predictable up to a decade in advance in a certain region over the North Atlantic. However, no significant decadal SLP predictability in the North Atlantic–European region has been detected, although significant correlation values between the decadal mean North Atlantic SST index and SLP exist in this region. The “noise” (weather) part of the atmospheric circulation overwhelms any decadal climate signal.

The decadal predictability is dependent on the model formulation. In the earlier AOGCM version, ECHAM3/LSG, the North Atlantic THC was predictable on decadal time scales, but the North Atlantic SST was not. (Grötzner et al. 1999). The higher (vertical) resolution of the oceanic component of the ECHAM5/MPI-OM AOGCM and the more realistic oceanic heat transports may be the reason of the higher SST predictability in this AOGCM. Our result of multidecadal SAT predictability is comparable with the results of the GFDL model (Griffies and Bryan 1997a,b), the CCCma model (Boer 2000), and the HadCM3 model (Collins and Sinha 2003). Furthermore, the diagnostic potential predictability in the North Atlantic is higher in ECHAM5/MPIOM than in a superensemble of nine AOGCMs (Boer 2004). An open question is whether our AOGCM is overestimating decadal climate predictability.

In this study, the predictability problem is treated in a highly idealized manner. However, for a “real” climate forecast, the initial state of the three-dimensional ocean must be known. This is a big problem, since only the surface is observable with good spatial coverage by satellites. Latif et al. (2004) suggest that the relationship between variations in THC and SST can be exploited for predictability purposes, as the initial oceanic state may be derived from the history of SST. This may provide a method for determining the initial state of the ocean in order to realize predictions of multidecadal climate variability.

### **Acknowledgments**

We thank Erich Roeckner, Johann Jungclaus, Noel Keenlyside, Ute Merkel, and the reviewers for the discussion of our results and comments on this paper. This work was supported by the European Union project PREDICATE, the German Ministry for Education and Research (BMBF) project DEKLIM, and the Swiss National Center of Competence in Climate Research (NCCR Climate). The climate simulations were conducted at the German Climate Computing Centre (DKRZ) and Swiss Center for Scientific Computing (CSCS).

### **References**

- Boer, G. J., 2000: A study of atmosphere–ocean predictability on long time scales. *Climate Dyn.*, 16, 469–477.
- Boer, G. J., 2001: Decadal potential predictability in coupled models. *CLIVAR Exchanges*, No. 19, International CLIVAR Project Office, 3.

- Boer, G. J. , 2004: Long time-scale potential predictability in an ensemble of coupled climate models. *Climate Dyn.*, 23, 29-44.
- Broecker, W., 1991: The great ocean conveyor. *Oceanography*, 4, 79–89.
- Collins, M., 2002: Climate predictability on interannual to decadal time scales: The initial value problem. *Climate Dyn.*, 19, 671–692.
- Collins, M., and B. Sinha, 2003: Predictability of decadal variations in the thermohaline circulation and climate. *Geophys. Res. Lett.*, 30, 1306, doi:10.1029/2002GL016504.
- Collins, M., A. Carril, H. Drange, H. Pohlmann, R. Sutton, and L. Terray, 2003: North Atlantic decadal predictability. *CLIVAR Exchanges*, No. 28, International CLIVAR Project Office, 6–7.
- Delworth, T. L., and M. E. Mann, 2000: Observed and simulated multidecadal variability in the Northern Hemisphere. *Climate Dyn.*, 16, 661–676.
- Dickson, R., J. Lazier, J. Meinecke, P. Rhines, and J. Swift, 1996: Long-term coordinated changes in the convective activity of the North Atlantic. *Progress in Oceanography*, Vol. 38, Pergamon, 241–295.
- Griffies, S. M., and K. Bryan, 1997a: Predictability of North Atlantic multidecadal climate variability. *Science*, 275, 181–184.
- Griffies, S. M., and K. Bryan, 1997b: A predictability study of simulated North Atlantic multidecadal variability. *Climate Dyn.*, 13, 459–487.
- Grötzner, A., M. Latif, A. Timmermann, and R. Voss, 1999: Interannual to decadal predictability in a coupled ocean–atmosphere general circulation model. *J. Climate*, 12, 2607–2624.
- Hagemann, S., and L. Dümenil Gates, 2001: Validation of the hydrological cycle of ECMWF and NCEP reanalyses using the MPI hydrological discharge model. *J. Geophys. Res.*, 106, 1503–1510.
- Hasselmann, K., 1976: Stochastic climate models, part 1—Theory. *Tellus*, 28, 473–484.
- Latif, M., and T. P. Barnett, 1994: Causes of decadal climate variability over the North Pacific and North America. *Science*, 266, 634–637.
- Latif, M., T. P. Barnett, M. A. Cane, M. Flügel, N. E. Graham, H. von Storch, J.-S. Yu, and S. E. Zebiak, 1994: A review of ENSO prediction studies. *Climate Dyn.*, 9, 167–179.
- Latif, M., and Coauthors, 1998: A review of the predictability and prediction of ENSO. *J. Geophys. Res.*, 103, 14 375–14 393.

Latif, M., and Coauthors, 2004: Reconstructing, monitoring, and predicting multidecadal-scale changes in the North Atlantic thermohaline circulation with sea surface temperature. *J. Climate*, 17, 1605–1614.

Madden, R. A., 1976: Estimates of the natural variability of timeaveraged sea-level pressure. *Mon. Wea. Rev.*, 104, 942–952.

Marsland, S. J., H. Haak, J. H. Jungclaus, M. Latif, and F. Röske, 2003: The Max-Planck-Institute global ocean/sea ice model with orthogonal curvilinear coordinates. *Ocean Modell.*, 5, 91–127.

Park, W., and M. Latif, 2004: Ocean dynamics and the nature of air-sea interactions over the North Atlantic, *J. Climate*, in press.

Rhines, P. B., and S. Häkkinen, 2003: Is the oceanic heat transport in the North Atlantic irrelevant to the climate in Europe? *ASOF Newsletter*, No. 1, 13–17.

Roeckner, E., and Coauthors, 2003: The atmospheric general circulation model ECHAM5: Part I: Model description. MPI Rep. 349, Max-Planck-Institut für Meteorologie, Hamburg, Germany, 127 pp.

Rowell, D. P., 1998: Assessing the potential seasonal predictability with an ensemble of multidecadal GCM simulations. *J. Climate*, 11, 109–120.

Seager, R., D. S. Battisti, J. Yin, N. Gordon, N. Naik, A. C. Clement, and M. A. Cane, 2002: Is the Gulf Stream responsible for Europe's mild winters? *Quart. J. Roy. Meteor. Soc.*, 128, 2563–2586.

Terray, L., S. Valcke, and A. Piacentini, 1998: OASIS 2.2, ocean atmosphere sea ice soil, User's guide and reference manual. Tech. Rep. TR/CMGC/98-05, CERFACS, Toulouse, France, 77 pp.

Timlin, M. S., M. A. Alexander, and C. Deser, 2002: On the reemergence of North Atlantic SST anomalies. *J. Climate*, 15, 2707–2712.

Timmermann, A., M. Latif, R. Voss, and A. Grötzner, 1998: Northern Hemisphere interdecadal variability. *J. Climate*, 11, 1906–1931.

Trenberth, K. E., and J. M. Caron, 2001: Estimates of meridional atmosphere and ocean heat transport. *J. Climate*, 14, 3433–3443.

von Storch, H., and F. W. Zwiers, 1999: *Statistical Analysis in Climate Research*. Cambridge University Press, 484 pp.



## **Influence of the multidecadal Atlantic meridional overturning circulation variability on European climate**

(H. Pohlmann, F. Sienz, and M. Latif)

### **Abstract**

The influence of the natural multidecadal variability of the Atlantic meridional overturning circulation (MOC) on European climate is investigated using a simulation with the coupled atmosphere-ocean general circulation model ECHAM5/MPI-OM. The results show that Atlantic MOC fluctuations, which go along with changes in the northward heat transport, in turn effect European climate. Additionally, ensemble predictability experiments with ECHAM5/MPI-OM show that the probability density functions of surface air temperatures in the North Atlantic/European region are affected by the multidecadal variability of the large-scale oceanic circulation. Thus, some useful decadal predictability may exist in the Atlantic/European sector.

### **6.1 Introduction**

One important role of the large-scale oceanic circulation for climate is the transport of heat. The meridional overturning circulation (MOC) describes the zonally averaged oceanic circulation. The Atlantic MOC consists on a wind driven part and the thermohaline circulation (THC). Although both the Pacific and Atlantic have strong northward-flowing surface currents at their western margins (Kuroshio in the Pacific and Gulf Stream in the Atlantic) only in the Atlantic, which is much saltier than the Pacific, the oceanic water gets dense enough in high latitudes to initiate deep convection. This drives the Atlantic THC, a part of the great conveyor belt (Broecker 1991). Trenberth and Solomon (1994) regard the meridional heat transport of the atmosphere and ocean of unique importance. The recent estimation of Trenberth and Caron (2001) attributes the atmosphere having a much greater dominance. In their study the atmospheric transport accounts at 35°N for 78% of the total meridional heat transport on the Northern Hemisphere. Seager et al. (2002) take the occasion to criticize the responsibility of the Gulf Stream for European's mild winters at all. However, sea surface temperature (SST) in the northern North Atlantic is warmer than in the northern North Pacific at the same latitudes (Manabe and Stouffer 1999a). One way of estimating the effect of the THC on climate is to switch it off in coupled atmosphere-ocean general circulation models (AOGCMs). The results show a cooling over the Nordic Seas (e.g., Schiller et al. 1997, Manabe and Stouffer 1999b, Vellinga and Wood 2002), but the magnitude depends on the AOGCM considered. In most models the temperatures over northern Europe decrease by several degrees. Furthermore, a collapse of the Atlantic THC in response to global warming is discussed (Broecker 1987, Manabe and Stouffer 1993, 1994, Weaver and Hillaire-Marcel 2004). The abrupt climate change associated with the collapse of the Atlantic THC might even be irreversible (Alley et al. 2003). More likely than a

breakdown of the THC seems to be a weakening as simulated by many coupled climate models (e.g., Rahmstorf 1999, Wood et al. 1999, Latif et al. 2000). This study, however, focuses on the influence of the internally generated multidecadal Atlantic MOC variability on European climate. Observational data of the Atlantic MOC are rare. The existing observations give an estimate of the current strength of the MOC (Ganachaud and Wunsch 2000) but not of its past evolution. Climate model simulations provide a measure to estimate the MOC variability, its predictability and influence on climate.

## **6.2 Model and experiments**

The coupled AOGCM used in this study is the European Centre Hamburg version 5 / Max Planck Institute Ocean Model (ECHAM5/MPI-OM) (Latif et al. 2004). The atmospheric component, ECHAM5 (Roeckner et al. 2003), is run at a spectral T42 resolution with 19 vertical layers. The oceanic component, MPI-OM (Marsland et al. 2003), is run on a bipolar orthogonal spherical coordinate system with equatorial refinement and 23 vertical levels. A dynamic/thermodynamic sea ice model and a river runoff scheme are included in this model. The components are coupled without the use of flux adjustments. A 500 year long control integration with greenhouse gases fixed to values of the 1990s is used to investigate the influence of the Atlantic MOC on European climate. Additionally, ensemble experiments are used to estimate the predictability of European climate. Started from the control integration, three different years (90, 125 and 170) corresponding to intermediate, strong, and weak Atlantic MOC conditions, are selected and used as initial conditions for three ensemble predictability experiments. Each ensemble consists on six ensemble members realized with slightly perturbed atmospheric initial conditions. The ensemble predictability experiments are integrated over a period of 20 years.

## **6.3 Results**

The Atlantic MOC is strongest at 30°N in the ECHAM5/MPI-OM control integration. Figure 6.1 shows the anomalies of the maximum of the Atlantic MOC together with the anomalies of the oceanic heat transport (OHT) at this latitude. The first period (80 years) of the integration is characterized by the spin-up of the coupled system and therefore not considered. However, rather strong MOC fluctuations with a period of 70-100 years (Pohlmann et al. 2004) are also apparent in the following centuries. The strength of the overturning circulation is related to the convective activity in the deep-water formation regions, most notable the Labrador Sea, which is sensitive to fresh water anomalies from the Arctic (Jungclauss et al. 2004). MOC fluctuations go along with changes in the northward heat transport and have therefore the potential to influence North Atlantic/European climate. The influence of the Atlantic MOC on European climate cannot be strictly separated from that of the North Atlantic Oscillation on interannual timescales. However, on longer timescales the North Atlantic MOC variability leads European climate variability, which indicates an influence from the ocean to the atmosphere (not shown).

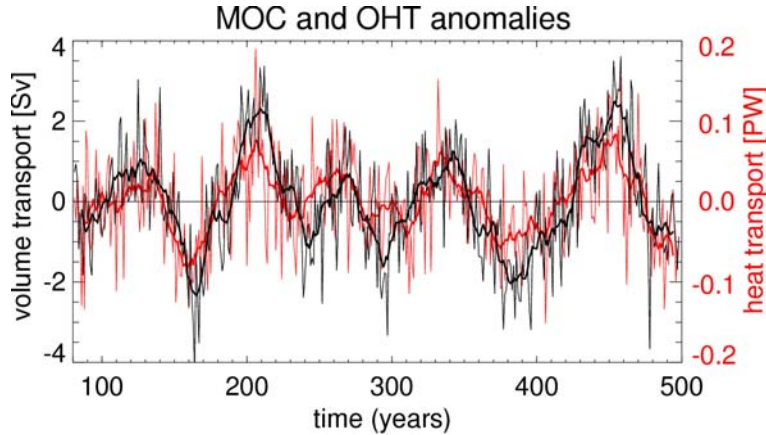


**Figure 6.1** Time series of the Atlantic MOC (black) and OHT (red) anomalies at 30°N of the ECHAM5/MPI-OM control integration starting at year 80. The mean of the Atlantic MOC amounts to 19 Sv ( $1\text{Sv}=10^6\text{ m}^3\text{ s}^{-1}$ ) and that of the Atlantic OHT is 0.8 PW ( $1\text{PW}=10^{15}\text{ W}$ ). The data are detrended prior to the analysis. The thick curves are the corresponding 11-year running means, used to low pass filter the data.

The influence of the Atlantic MOC on European surface air temperature (SAT) is investigated by calculating the probability density functions (PDFs) of European SAT for strong and weak overturning conditions. Figure 6.2 shows the fitted PDFs of European SAT averaged over the region 35°-75°N, 10°W-40°E for years in which the maximum Atlantic MOC anomalies at 30°N exceed  $\pm 0.44$  standard deviations (i.e., a third of the years as the data are Gauss distributed), respectively. In the case of weak MOC conditions the SAT averaged over Europe is colder than in the case of strong MOC conditions, and vice versa. The difference of the mean European SAT for these two cases amounts to 0.5K. The two distributions are significantly different at the 95% level according to a Kolmogorov-Smirnov test.

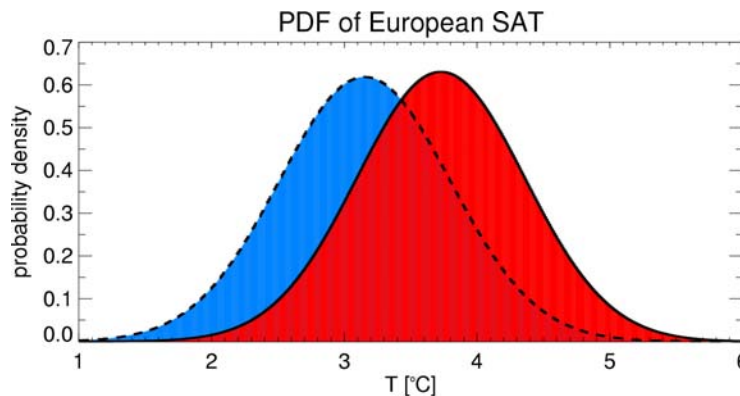


**Figure 6.2** Fitted probability density functions (PDFs) of the European SAT for years with strong (red/solid) and weak (blue/dashed) anomalies of the North Atlantic MOC, defined as exceeding  $\pm 0.44$  standard deviations, respectively.

The regional patterns of the influence of the North Atlantic MOC on European climate are presented in Figure 6.3. Years with anomalously strong and weak Atlantic MOC conditions are defined, as above, as exceeding  $\pm 0.44$  standard deviations, respectively. The differences of the mean SAT and precipitation between high and low phases of the MOC are based on annual means, which are available from the complete control run. The differences of the mean frost and summer days are calculated from daily means, which are processed from daily maximum and minimum SAT for a 100 year segment of the control integration. The difference of the mean SAT between years with strong and weak MOC conditions is strongest in the Baltic region with values up to 1K. Additionally, a separate analysis based on seasonal means shows that the differences are strongest in winter. Strong anomalies of the Atlantic MOC are associated with enhanced northward oceanic heat transports, which generally lead to increased atmospheric temperatures over the North Atlantic/European region. The difference of the mean precipitation between strong and weak MOC conditions displays a north – south orientated dipole with an enhancement over northern Europe and a reduction in southern and eastern Europe. Strongest increases are present in southern Norway and strongest decreases on the Iberian peninsula and around the Adriatic Sea with values up to 4 mm/month. An enhanced MOC leads to a reduced number of frost days over the whole European continent. The

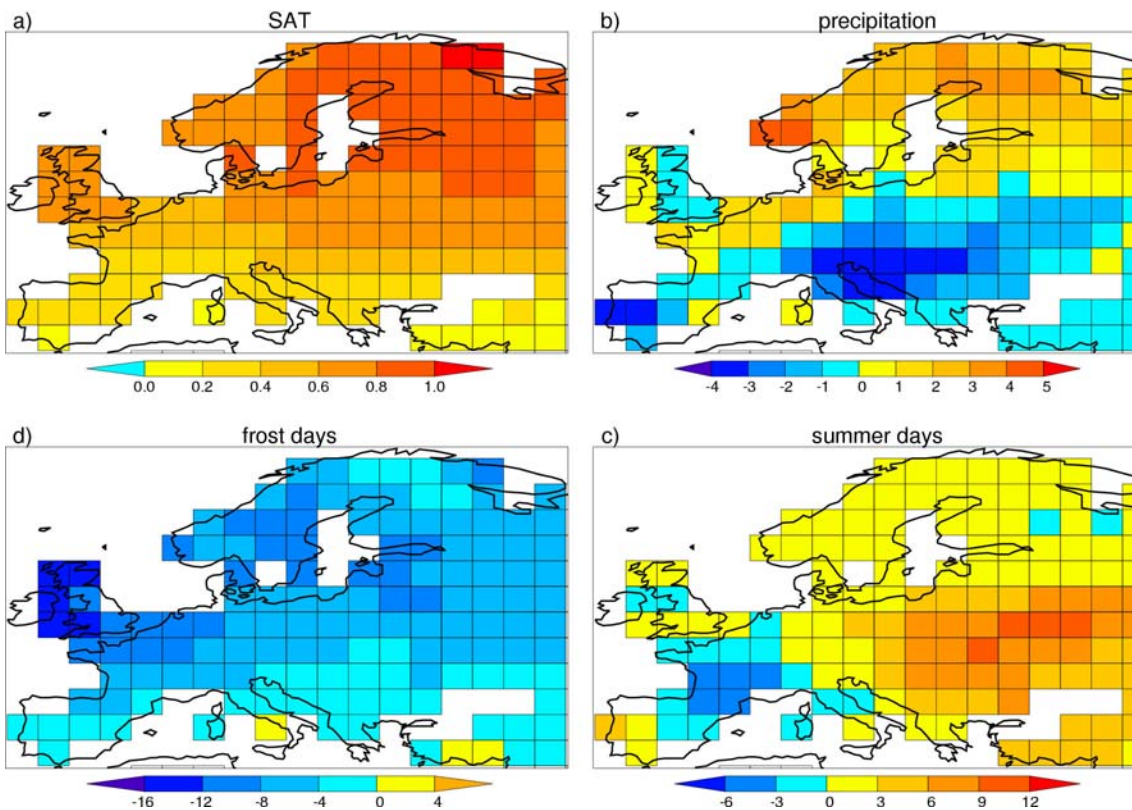


**Figure 6.3** Difference of (a) SAT [°C], (b) precipitation [mm/month], and days per year with temperature (c) below 0°C and (d) over 25°C over Europe between years with strong and weak Atlantic MOC conditions exceeding  $\pm 0.44$  standard deviations.

reduction is strongest in western and northern Europe with a maximum of more than 12 days/year in Great Britain. The difference in summer days, defined as days reaching 25°C, between strong and weak MOC conditions displays a west – east orientated dipole with a reduction over western Europe of more than 3 days/year and an enhancement over eastern Europe up to 9 days/year.

The decadal Atlantic MOC predictability of the AOGCM ECHAM5/MPI-OM is shown in Pohlmann et al. (2004) using ensemble predictability experiments. In contrast to results with the AOGCM ECHAM3/LSG (Grötzner et al. 1999) the MOC variability is affecting North Atlantic SST north of 30°N resulting in SST predictability comparable to the MOC predictability. In this study a different method of predictability is applied to the same ensemble experiments, which estimates predictability in a probabilistic manner. This method is commonly used for seasonal forecasts and also to estimate decadal predictability (Collins and Sinha 2003). The probabilistic method decides, whether the ensemble mean is significantly shifted with respect to climatology. A shift to stronger (e.g., warmer) or weaker (e.g., colder) conditions is defined for the probabilistic forecast commonly by reaching the upper or lower tercile of the climatological PDF, which is equivalent to exceeding 0.44 standard deviations. The probability of this shift in the forecast ensemble gives a measure for predictability, which is by chance 33% for each case.

The probability of the SAT being in the warm tercile of the climatological PDF for the three ensemble experiments averaged over the first and second prediction decade are shown in Figure 6.4. In all experiments and in both prediction decades there exists predictability of SAT over parts of Europe. The experiments are started from intermediate, strong and weak Atlantic MOC conditions, which are associated with intermediate, warm, and cold SAT over the North Atlantic, respectively. The SAT anomalies over the North Atlantic mainly persist during the first, but not the second prediction decade. Additionally, the probability of European SAT anomalies being in the warm tercile of the climatological PDF is in all three experiments higher in the second than in the first prediction decade.

We note one important caveat. The predictability experiments used in this study are idealized, since the initial oceanic conditions were not perturbed. This implies the assumption that the AOGCM could be initialized perfectly by ocean observations. Thus, since this is not possible, we show here only the usefulness of decadal forecasts with respect to European climate.

## **6.4 Summary and discussion**

The experiments with the AOGCM ECHAM5/MPI-OM indicate an influence of the internal multidecadal variability of the Atlantic MOC on European climate. Strong overturning conditions coincide with strong northward heat transports in the Atlantic. During such conditions the European SAT is enhanced, and the number of frost days per year are reduced. The precipitation is enhanced in northern and decreased in southern

Europe. The number of summer days per year is decreased in western and increased in eastern Europe.

Although predictability measured by classical measures is mostly restricted to oceanic regions in ECHAM5/MPI-OM (Pohlmann et al. 2004), the probability density functions of SAT and precipitation are significantly affected by the large-scale oceanic circulation changes also over Europe. Thus some useful decadal predictability of economic value may exist in the Atlantic/European sector. To exploit this decadal predictability, however, a suitable oceanic observing system must be installed, since the memory of the climate system resides in the North Atlantic Ocean. In particular, the North Atlantic MOC should be monitored carefully, since its variations are most interesting in the light of decadal predictability.

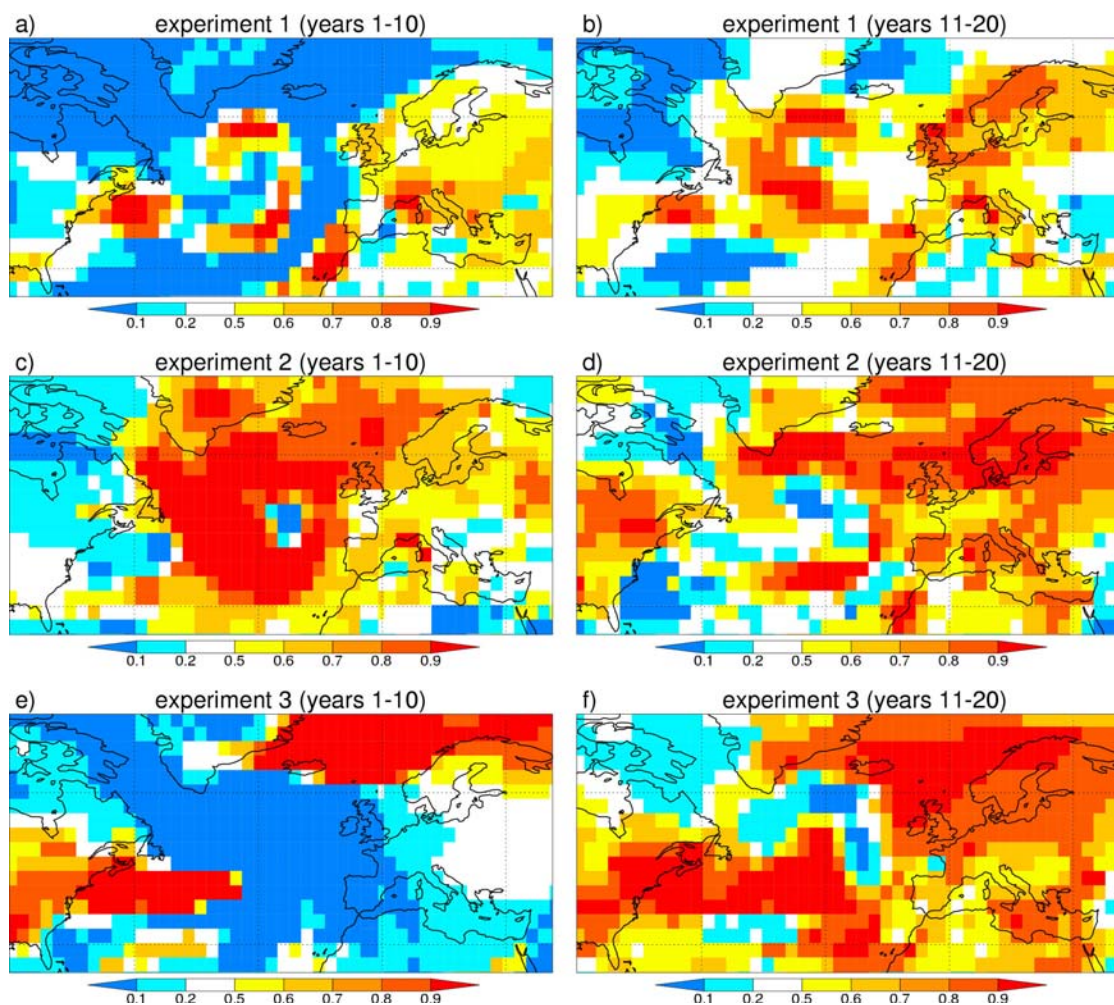


**Figure 6.4** Probability of SAT anomalies being in the warm tercile of the climatological PDF (equivalent to exceeding of 0.44 standard deviations) averaged over the first (left column) and second (right column) prediction decade and the first (top), second (middle), and third (bottom) ensemble experiment.

## Acknowledgments

We thank Jürgen Bader, Johanna Baehr, and Clotilde Dubois for the discussion of our results and comments on this paper. This work was supported by the European Union project PREDICATE, and the German Ministry for Education and Research (BMBF) project DEKLIM. The climate simulations were conducted at the German Climate Computing Centre (DKRZ) and Swiss Center for Scientific Computing (CSCS). We thank Michael Botzet, Andreas Roesch, Martin Wild, and Peter Tschuck for providing the climate simulations.

## References

Alley, R. B., J. Marotzke, W. D. Nordhaus, J. T. Overpeck, D. M. Peteet, R. A. Pielke Jr., R. T. Pierrehumbert, P. B. Rhines, T. F. Stocker, L. D. Talley, and J. M. Wallace, 2003: Abrupt climate change. *Science*, 299, 2005-2010.

Broecker, W., 1987: Unpleasant surprises in the greenhouse? *Nature*, 328, 123.

Broecker, W., 1991: The great ocean conveyor. *Oceanography*, 4, 79-89.

Collins, M., and B. Sinha, 2003: Predictability of decadal variations in the thermohaline circulation and climate. *Geophys. Res. Lett.*, 30, 1306, doi:10.1029/2002GL016504.

Ganachaud, A., and C. Wunsch, 2000: Improved estimates of global ocean circulation, heat transport and mixing from hydrographic data. *Nature*, 408, 453-457.

Grötzner, A., M. Latif, A. Timmermann, and R. Voss, 1999: Interannual to decadal predictability in a coupled ocean atmosphere general circulation model. *J. Climate*, 12, 2607-2624.

Jungclauss, J. H., H. Haak, M. Latif, and U. Mikolajewicz, 2004: Arctic-North Atlantic interactions and multidecadal variability of the meridional overturning circulation. *J. Climate*, submitted.

Latif, M., and Coauthors, 2000: Tropical stabilization of the thermohaline circulation in a greenhouse warming simulation. *J. Climate*, 13, 1809-1813.

Latif, M., and Coauthors, 2004: Reconstructing, monitoring, and predicting multidecadal-scale changes in the North Atlantic thermohaline circulation with sea surface temperature. *J. Climate*, 17, 1605-1613.

Manabe, S., and R. J. Stouffer, 1993: Century-scale effects of increased atmospheric CO<sub>2</sub> on the ocean-atmosphere system. *Nature*, 364, 215-218.

Manabe, S., and R. J. Stouffer, 1994: Multiple-century response of a coupled ocean-atmosphere model to an increase of atmospheric carbon dioxide, *J. Climate*, 7, 5-23.

Manabe, S., and R. J. Stouffer, 1999a: The role of thermohaline circulation in climate. *Tellus*, 51A, 91-109.

Manabe, S., and R. J. Stouffer, 1999b: Are two modes of thermohaline circulation stable? *Tellus*, 51A, 400-411.

Marsland, S. J., H. Haak, J. H. Jungclaus, M. Latif, and F. Röske, 2003: The Max-Planck-Institute global ocean/sea ice model with orthogonal curvilinear coordinates. *Ocean Modelling*, 5, 91-127.

Pohlmann, H., M. Botzet, M. Latif, A. Roesch, M. Wild, and P. Tschuck, 2004: Estimating the decadal predictability of a coupled AOGCM. (**Chapter 5**). *J. Climate*, 17, 4463-4472.

Rahmstorf, S., 1999: Shifting seas in the greenhouse? *Nature*, 399, 523-524.

Roeckner, and Coauthors, 2003: The atmospheric general circulation model ECHAM5: Model description. MPI-Report, 349, Max-Planck-Institut für Meteorologie, Hamburg, Germany.

Seager, R., D. S. Battisti, J. Yin, N. Gordon, N. Naik, A. C. Clement, and M. A. Cane, 2002: Is the Gulf Stream responsible for Europe's mild winters? *Q. J. R. Meteorol. Soc.*, 128, 2563-2586.

Schiller, A., U. Mikolajewicz, and R. Voss, 1997: The stability of the thermohaline circulation in a coupled ocean-atmosphere general circulation model. *Climate Dyn.*, 13, 325-347.

Trenberth, K. E., and J. M. Caron, 2001: Estimates of meridional atmosphere and ocean heat transports. *J. Climate*, 14, 3433-3443.

Trenberth, K. E., and A. Solomon, 1994: The global heat balance: Heat transports in the atmosphere and ocean. *Climate Dyn.*, 10, 107-134.

Vellinga, M., and R. A. Wood, 2002: Global climatic impacts of a collapse of the Atlantic thermohaline circulation. *Climatic Change*, 54, 251-267.

Weaver, A. J., and C. Hillaire-Marcel, 2004: Global warming and the next ice age. *Science*, 304, 400-402.

Wood, R. A., and Coauthors, 1999: Changing spatial structure of the thermohaline circulation in response to atmospheric CO<sub>2</sub> forcing in a climate model. *Nature*, 399, 572-575.

## **Interannual to decadal climate predictability: A multi-perfect-model-ensemble study**

(M. Collins, M. Botzet, A. Carril, H. Drange, A. Jouzeau, M. Latif, O. H. Otterå, H. Pohlmann, A. Sorteberg, R. Sutton, L. Terray)

### **Abstract**

Perfect model ensemble experiments are performed with five coupled atmosphere-ocean models to investigate the potential for initial-value climate forecasts on interannual to decadal time scales. Experiments are started from similar initial states and common diagnostics of predictability are used. We find that; variations in the ocean Meridional Overturning Circulation are potentially predictable on interannual to decadal time scales, a more consistent picture of the surface temperature impact of decadal variations in the MOC is now apparent, and variations of surface air temperatures in the N. Atlantic are also potentially predictable on interannual to decadal time scales, albeit with potential skill levels which are less than those seen for MOC variations. This inter-comparison represents a step forward in assessing the robustness of model estimates of potential skill and is a pre-requisite for the development of any operational forecasting system.

### **7.1 Introduction**

Predictions of the future state of the climate system are of potential benefit to society. The ability to predict (here we consider the *potential* ability to predict) can also give insight into the physical aspects of the climate system which are not simply the averaged or integrated effects of chaotic, unpredictable weather “noise”. Restricting attention to variations in climate which are purely internally generated, predictability in the system hints at processes which have long time scales or which possibly have periodic behaviour. Quantifying the predictability associated with such processes can lead to a greater understanding of the climate system.

Operational predictions of climate on seasonal to interannual time scales associated with the El Niño Southern Oscillation (ENSO) are now commonplace (e.g., Goddard et al. 2001). Prediction systems for other seasonal-interannual “modes” of climate are also emerging (e.g., Rodwell and Folland 2004). Here we consider the predictability of interannual to decadal variations in climate. On these time scales, both the initial conditions (principally the initial state of the ocean) and the boundary conditions (associated with both natural and anthropogenic forcing of the system) are important (Collins and Allen 2002, Collins 2002) but here we focus solely on the initial value problem of the predictability of internally generated interannual to decadal climate variability.

The Atlantic Meridional Overturning Circulation (MOC) is the main northward heat carrying component of the ocean part of the climate system (e.g., Trenberth and Caron 2001). Coupled atmosphere-ocean models (AOGCMs) exhibit internally generated variations the strength of the MOC and associated heat transport (e.g., Dong and Sutton 2001) and the surface climate impact of those variations have also been seen in historical (Latif et al. 2004) and palaeo-climate records (Delworth and Mann 2000). Shorter records of ocean observations (Dickson et al. 1996, Curry et al. 2003, Marsh 2000), also exhibit variations which have been linked with the MOC. Variations in the MOC thus represent an ideal candidate for the study of interannual to decadal climate predictability.

Predictability studies with AOGCMs in which ensembles of simulations with small perturbations to the initial conditions are performed have revealed the potential predictability in these MOC variations and in related surface and atmosphere variables (Griffies and Bryan 1997, Grötzner et al. 1999, Boer 2000, Collins and Sinha 2003, Pohlmann et al. 2004). While all studies show some level of potential predictability, it is difficult to form robust conclusions because of the range of complexity (and hence realism) of the different models used, because of the range of different initial states considered and because of subtle differences in the measures of predictability employed. For example, it is well known in weather forecasting that predictive skill can vary considerably with different initial conditions. Clearly it is important to quantify the potential skill-level of interannual-decadal climate forecasts prior to the expensive development of operational prediction schemes and the deployment of operational observing systems.

Here we present a step-forward in making a robust estimate of the potential predictive skill of interannual to decadal climate predictions associated with internally generated variations in the MOC. A coordinated set of potential predictability experiments have been performed with five recently developed complex AOGCMs. An attempt is made to initiate the experiments from similar ocean states and a common set of measures of potential skill are used. This “multi-model” approach has proved useful in other areas of weather and climate prediction. Here the emphasis is on a comparison of the levels of potential predictability seen in the different models. Other publications discuss the individual model results (e.g., Collins and Sinha 2003, Pohlmann et al. 2004a, Pohlmann et al. 2004b) in more detail.

## **7.2 The ensemble experiments**

Five coupled atmosphere-ocean models are used (see Table 7.1):

The ARPEGE3-ORCALIM has an atmosphere component (Déqué et al. 1994) with a horizontal resolution of T63 with 31 levels in the vertical (20 in the troposphere). The ocean component, ORCA2, is the global configuration of the OPA8 Ocean model (Madec et al. 1998) with a horizontal resolution of  $2^\circ$  in longitude and  $0.5^\circ$  to  $2^\circ$  in latitude. It includes a dynamic-thermodynamic sea-ice model (Fichefet and Morales Maqueda 1997). The components are coupled through OASIS 2.5 (Valcke et al. 2000), which ensures the time synchronization and performs spatial interpolation from one grid to another.

The Bergen Climate Model (BCM) (Furevik et al. 2003, Bentsen et al. 2004) uses the Miami Isopycnic Coordinate Ocean Model (Bleck et al. 1992) coupled to a dynamic-thermodynamic sea ice module. The ocean mesh is formulated on a Mercator projection with a nominal resolution of 2.4 degrees, and 24 vertical layers. The atmospheric component is version three of the ARPEGE model with a horizontal resolution of T63 and 31 layers in the vertical – essentially the same atmosphere that is used in ARPEGE3-ORCALIM. Fresh water and heat flux adjustments are applied.

ECHAM5/MPI-OM (Latif et al. 2004) uses version 5 of the European Centre-Hamburg atmosphere model (ECHAM5, Roeckner et al. 2003) at T42 resolution with 19 vertical layers. The oceanic component, the Max Planck Institute Ocean Model (MPI-OM, Marsland et al. 2003) is run on a curvilinear grid with equatorial refinement and 23 vertical levels. A dynamic-thermodynamic sea ice model and a river runoff scheme are included.

Version 3 of the Hadley Centre Climate Model (HadCM3 – Gordon et al. 2000, Collins et al. 2001) uses an ocean component with a horizontal resolution of 1.25° longitude by 1.25° latitude and 20 levels in the vertical. The atmospheric component uses a grid-point formulation with a horizontal resolution of 3.75° x 2.5° in longitude and latitude with 19 unequally spaced vertical levels (Pope et al. 2000). A simple thermodynamic sea-ice scheme is used.

The INGV model uses the ECHAM4 model (Roeckner 1996) at T42 resolution with 19 vertical levels. The ocean component is essentially the same as that used in the ARPEGE3-ORCALIM model. More details can be found in Gualdi (2003).

Model	Number of ensemble experiments	Number of ensemble members in each experiment	Length of ensemble experiments (years)	Length of control run (years)
ARPEGE3-ORCALIM	2	6(+1)	25	200
BCM	2	3(+1)	20	300
ECHAM5/MPI-OM	3	6(+1)	20	500
HadCM3	3	8(+1)	20	2000
INGV	2	2(+1)	20	100

**Table 7.1** A summary of the AOGCMs used in the perfect model potential predictability experiments. The numbers in column 3 of the form 6(+1) indicate that 6 ensemble members were performed from a state taken from the control run but that the section of the control run may also be viewed as an additional ensemble member.

Ensemble experiments are performed from initial states of anomalously high and anomalously low MOC taken from a control (i.e. unforced) run of each model (Figure 7.1). In addition, some models were used to perform experiments with initial states near the time-mean value of overturning. Perturbations to the initial conditions were made using the common method of taking different atmospheric start conditions with the same

ocean start condition (the “perfect model” approach e.g., Collins and Sinha 2003). While this perturbation methodology is in no way optimal in terms of, for example, sampling the likely range of atmosphere-ocean analysis error, it is sufficient to generate ensemble spread on the time scales of interest.

The availability of computer resources limited the number of ensemble members and experiments that could be performed: nevertheless all experiments were integrated out to at least 20 years. The experiments correspond to a total 1340 simulated years for the predictability experiments combined with a total of 3100 simulated years for the control experiments used to assess background variability. Annual mean diagnostics are examined because of the focus on interannual to decadal time scales.

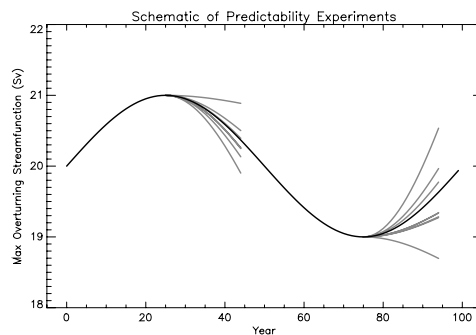


**Figure 7.1** *A schematic figure of the experimental design used in this study. The thick black line represents decadal-time scale internally generated variations in the strength of the Meridional Overturning Circulation (MOC) from a control run of a coupled atmosphere-ocean model. The grey lines represent “perfect model” ensemble experiments in which small perturbations to the initial conditions are made. For each of the models used in the study, we endeavoured to initiate the ensemble experiments from a state of relatively strong and relatively weak overturning. In addition, some models we use to initiate experiments from a state of relatively normal overturning.*

### 7.3 Potential predictability of MOC variations

The first point to note is the wide range of time scales and magnitudes of MOC variability in the different models (Figure 7.2). The ECHAM5/MPI-OM model shows the largest variations in MOC strength with clear interdecadal variability present. HadCM3 and BCM also show interdecadal variations but at a reduced level in comparison. The ARPEGE3-ORCALIM model has the lowest level of variability but decadal-interdecadal time scales are still clearly present in the time series. The large trend seen in the INGV model is almost certainly due to a drift seen in this particular control experiment - the model has yet to reach equilibrium and we do not attempt to extract quantitative measures of predictability. Although not calculated, diagnostic measures of predictability/variability (e.g., Boer 2000) would clearly show a range of different levels of MOC potential predictability in these models. However, the only reliable way to assess predictability is to perform ensemble experiments.

The perfect model ensemble experiments are also shown in Figure 7.2. Potential predictability is evident when the ensemble spread is small in comparison with the total level of variability in the control time series, or even if the ensemble spread is relatively large but the centre of gravity of the ensemble is displaced significantly with respect mean of the control (e.g., Collins 2001). We may imagine a background or climatological distribution which, in the absence of a forecast, would be all the information we would have to form an assessment of the future strength of the MOC. A forecasts may allow us to reduce the potential range (low ensemble spread) or shift the mean of the distribution (displaced ensemble), or both. Both types of (potential) predictability are seen on interannual to decadal time scales in the experiments shown in Figure 7.2. For example, the first HadCM3 ensemble (anomalously strong MOC initial conditions) has relatively small ensemble spread in the first decade of the experiment and the ensemble is significantly shifted to stronger values with respect to the mean with no ensemble members indicating weaker than average overturning (see Collins and Sinha (2001) for more details). Other examples are clear.

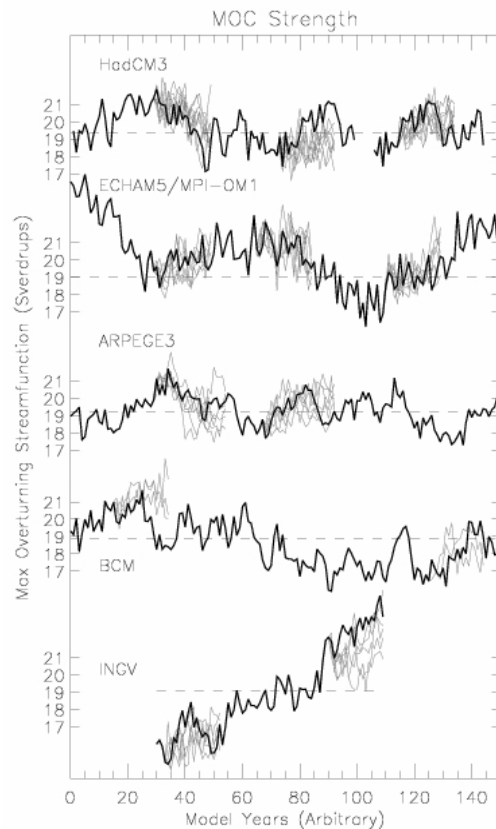


**Figure 7.2** Time series of the strength of the MOC taken from the unforced control runs of five coupled atmosphere-ocean models (black lines - names indicate on the figure) and from the perfect model ensemble experiments (grey lines). MOC variations arise purely because of the internal dynamics of the coupled system and model years are arbitrary. The drift seen in the INGV model is a spin-up effect and the experiments are excluded from any quantitative analysis.

There are a wide range of measures which may be used for forecast verification (here we measure the potential skill of a perfect model forecast – an upper limit). We examine two of the most-simple measures of forecast skill to quantify levels of potential predictability; the anomaly correlation (ACC) and normalised root mean squared error (RMSE). Formulas are given in Collins (2001) for the perfect model case.

Figure 7.3 shows both measures for the MOC in the ensemble experiments discussed above. For the strong MOC initial states, the ACC is “high” for approximately the first decade in all the model experiments, with “high” being above 0.6 – a commonly used cut-off value in weather forecasting. The RMSE is correspondingly low. After the first decade, the ARPEGE3 model predictability drops off rapidly whereas for the other models the ACC drops off slowly to low values by the end of the 20 year experiments. The RMSE similarly saturates in 20 years. For the weak MOC initial states, error growth and loss of predictability seems to happen sooner in the ensemble experiments, although there is some noise in these measures because of small ensemble sizes. ACC and RMSE are not shown for the normal initial states because of the small sample size.

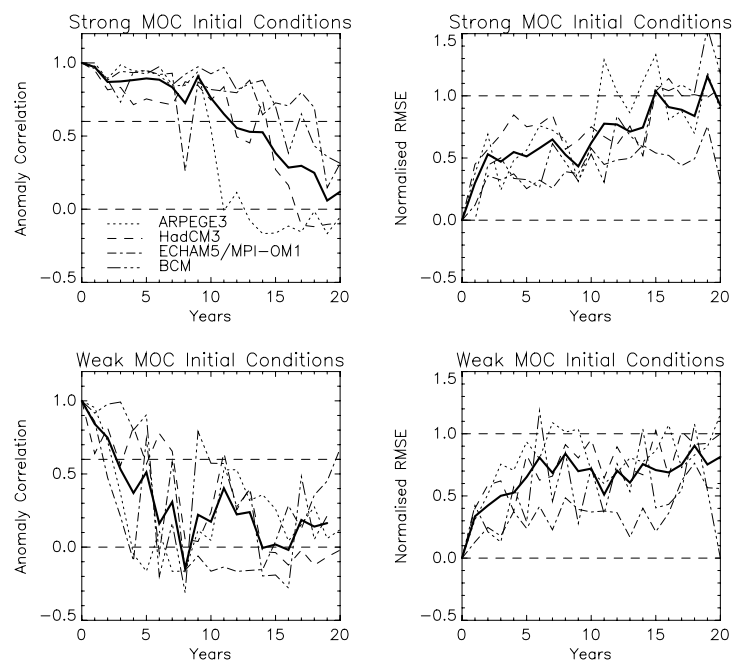


**Figure 7.3** Measures of the potential predictability of variations in the strength of the MOC from four of the five coupled models (see legend). The left panels show the anomaly correlation coefficient (ACC - unity for perfect potential predictability, zero for no potential predictability) for strong MOC initial conditions (top panel), weak MOC initial conditions (middle panel) and normal MOC initial conditions (bottom panel). The right panels show the normalised root mean squared error (RMSE - zero for perfect potential predictability, unity for no potential predictability) in the same order. Also shown in the figures are the multi-model average ACC and RMSE (thick black line).

While the number of ensemble experiments is small, we may attempt to draw some conclusions about the multi-model estimate of potential predictability of MOC variability in these experiments (Figure 7.3 – thick solid line). The multi-model ensemble indicates potential predictability of interannual-decadal MOC variations for 1-2 decades into the future. It also indicates that initial states which have anomalously strong overturning are more predictable than those with anomalously weak overturning. This latter result is intriguing, but is subject to some uncertainty because of the relative small number of models and ensemble experiments included in the multi-model analysis. Nevertheless, some consensus is emerging in contrast to the previous situation in which a large range of predictability is seen in the literature. It would be safe to conclude that there is a robust signal of potential predictability of variations in the MOC on interannual to decadal time scales.

#### 7.4 Potential predictability of surface climate variations

Predictions of MOC variability may be of interest to scientists, but they would be of little relevance to society unless they are accompanied by predictions of surface climate variables. A simple measure of the impact of MOC variations can be obtained by performing a regression between decadal-averaged MOC strength and decadal-averaged surface air temperature (SAT) in the different models (Figure 7.4). The general

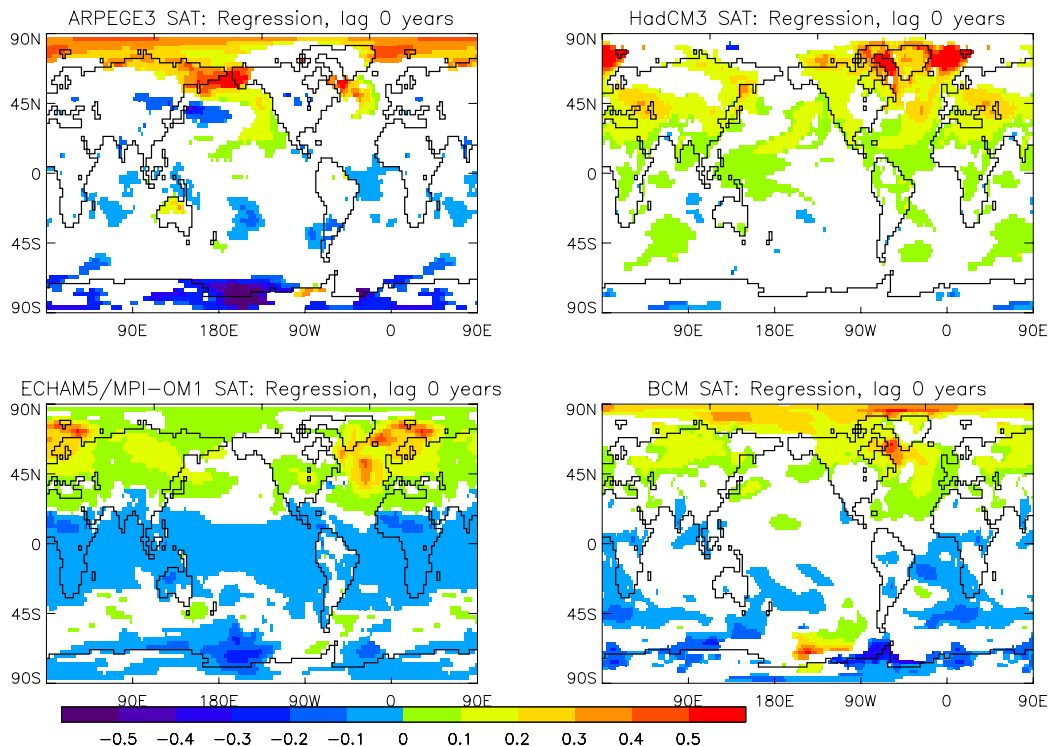


**Figure 7.4** The coefficient of regression (degrees K per Sverdrup) of decadal mean surface air temperature against decadal mean MOC strength from four of the five coupled atmosphere-ocean models. Regions are shaded only where the coefficient is significantly different from zero at the 5% confidence level (based on an F-test).

impression in all the models is of a warmer Northern Hemisphere when the MOC is stronger and is transporting more heat polewards. Differing levels of statistical significance seen in Figure 7.4 may be interpreted as resulting from different levels of signal to noise in the sense that in models with larger variations in MOC, the surface signal has a better chance of overwhelming the noise of unrelated random climate variations. What is interesting is that the magnitude of the surface response (in K/Sv) is similar across all models.

The North Atlantic ocean is a region in all the models in which there is a significant relationship between decadal variations in SAT (and underlying SST) and the MOC. Time series of annual mean SAT from the control and ensemble experiments averaged over a region of the North Atlantic (used in Collins and Sinha 2001 and Pohlmann et al. 2004a) are shown in Figure 7.5. Strong similarities between these time series and those shown in Figure 7.2 for the MOC are evident, although there is clearly more noise in this variable as a result of unrelated random variability.

ACC and RMSE measures of ensemble spread (Figure 7.6) for N. Atlantic SAT are similar to those computed for MOC variations (Figure 7.3) but the levels of potential

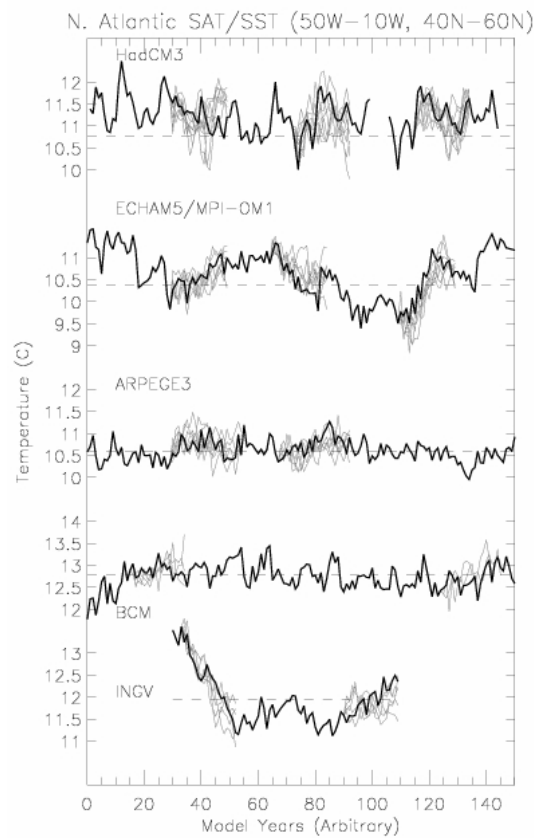


**Figure 7.5** As in Figure 7.2 but for surface air temperature averaged in the region 50°W-10°W, 40°N-60°N.

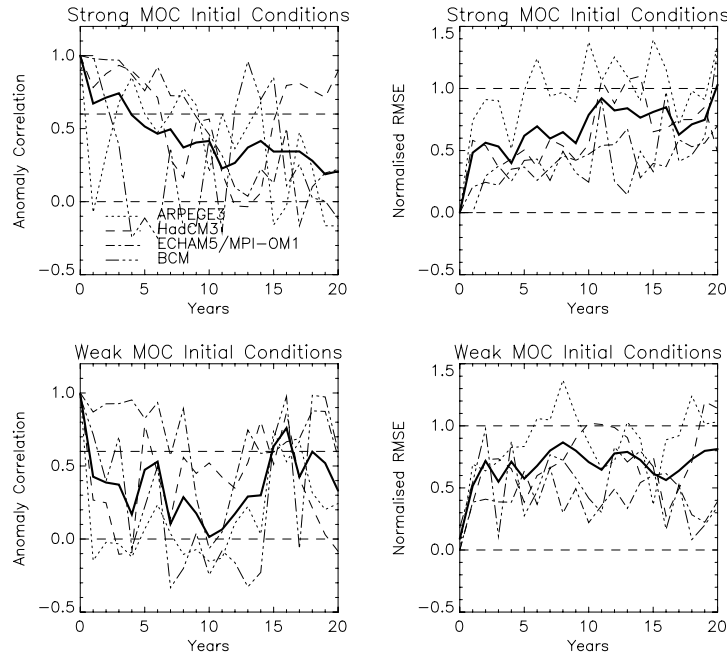


**Figure 7.6** As in Figure 7.3 but for surface air temperature averaged in the region  $50^{\circ}\text{W}-10^{\circ}\text{W}$ ,  $40^{\circ}\text{N}-60^{\circ}\text{N}$ .

predictability are clearly less and the differences between ensemble members greater. It may be possible to find greater levels of potential predictability for each individual model by adjusting the boundaries of the region chosen but here we compare the models on an equal footing. Also, the effects of interannual noise which are more prominent in this variable may be reduced by taking averages over a greater number of years. Nevertheless, the picture of potentially predictable surface climate variations associated with variations in the MOC appears consistent.

## 7.5 Discussion

Whereas previously it has been difficult to assess the potential for making interannual to decadal forecasts of climate due to different studies indicating different levels of predictability, a more complete picture of the predictability is emerging. This intercomparison study shows that;

1. variations in the ocean Meridional Overturning Circulation are potentially predictable on interannual to decadal time scales,
2. a more consistent picture of the surface temperature impact of decadal variations in the MOC is now apparent, and
3. variations of surface air temperatures in the N. Atlantic are also potentially predictable on interannual to decadal time scales, albeit with potential skill levels which are less than those seen for MOC variations.

Perhaps the biggest difference between the models is in the wide range of strengths of decadal variability evident in Figure 7.2. In general, models with greater decadal MOC

variability have greater levels of potential predictability – despite the fact that the ACC and RMSE are signal-to-noise measures and thus allow for a differences in background natural variability. Investigation into the mechanisms responsible for the different levels of variability would seem a priority.

The far more pertinent question is, of course, that of the (potential) prediction of surface climate variations over land. The simple measures used in this study do not reveal robustly predictable land signals. Collins and Sinha (2001) and Pohlmann et al. (2004b) investigate probabilistic techniques more commonly used in medium-range and seasonal forecasting in the context of the interannual-decadal problem with some limited success. However, the application and verification of such measures (here the assessment of potential skill) requires much larger ensemble sizes and many more ensemble simulations than used here. Hopefully such ensembles will be performed in future. In addition, the number of modelling, initialisation and observational issues that need to be addressed before we routinely produce interannual-decadal climate forecasts are numerous.

## References

Bentsen, M., H. Drange, T. Furevik, and T. Zhou, 2004: Simulated variability of the Atlantic meridional overturning circulation. *Climate Dyn.*, doi: 10.1007/s00382-004-0397-x

Bleck, R., C. Rooth, D. Hu, L. T. Smith, 1992: Salinity-driven thermohaline transients in a wind- and thermohaline-forced isopycnic coordinate model of the North Atlantic. *J. Phys. Oceanogr.*, 22, 1486–1515.

Boer, G. J., 2000: A study of atmosphere-ocean predictability on long timescales. *Climate Dyn.*, 16, 469-477.

Collins, M., 2002: Climate predictability on interannual to decadal time scales: The initial value problem. *Climate Dyn.*, 19, 671-692.

Collins, M, and M. R. Allen, 2002: On assessing the relative roles of initial and boundary conditions in interannual to decadal climate predictability. *J. Climate*, 21, 3104-3109.

Collins, M. and B. Sinha, 2003: Predictability of decadal variations in the thermohaline circulation and climate. *Geophys. Res. Lett.*, 30, 1306, doi:10.1029/2002GL016504.

Collins, M., S. F. B. Tett, and C. Cooper, 2002: The internal climate variability of HadCM3, a version of the Hadley Centre coupled model without flux adjustments. *Climate Dyn.*, 17, 61-81.

Curry, R., R. Dickson, I. Yashayaev, 2003: A change in the freshwater balance of the Atlantic Ocean over the past four decades. *Nature*, 426, 826–829, doi:10.1038/nature02206.

Delworth, T. L., and M. E. Mann, 2002: Observed and simulated multidecadal variability in the Northern Hemisphere. *Climate Dyn.* 16, 661-676.

Déqué, M., C. Drevet, A. Braun and D. Cariolle, 1994: The climate version of ARPEGE/IFS: a contribution to the French community climate modelling. *Climate Dyn.*, 10, 249-266.

Dickson, R., J. Lazier, J. Meincke, P. Rhines, J. Swift, 1996: Long term coordinated changes in the convective activity of the North Atlantic. *Progress in Oceanography*, 38, 241-295.

Dong, B., and R. T. Sutton, 2001: The dominant mechanisms of variability in Atlantic ocean heat transport in a coupled ocean-atmosphere GCM. *Geophys. Res. Lett.* 28, 2445-2448.

Fichefet T. and M. A. Morales Maqueda, 1997: Sensitivity of a global sea ice model to the treatment of ice thermodynamics and dynamics. *J. Geophys. Res.*, 102, 12609-12646.

Furevik, T., M. Bentsen, H. Drange, I. K. T. Kindem, N. G. Kvamstø, and A. Sorteberg, 2003: Description and validation of the Bergen Climate Model: ARPEGE coupled with MICOM, *Climate Dyn.*, 21, 27-51, doi:10.1007/s00382-003-0317-5.

Goddard, L., S. Mason, S. Zebiak, C. Ropelewski, R. Basher, and M. Cane, 2001: Current approaches to seasonal to interannual climate predictions. *Int. J. Climatol.*, 21, 1111-1152.

Gordon, C., C. Cooper, C. A. Senior, H. Banks, J. M. Gregory, T. C. Johns, J. F. B. Mitchell, R. A. Wood, 2000: The simulation of SST, sea ice extents and ocean heat transport in a version of the Hadley Centre coupled model without flux adjustments. *Climate Dyn.* 16, 147-168.

Grötzner, A., M. Latif, A. Timmermann, and R. Voss, 1999: Interannual to decadal predictability in a coupled ocean atmosphere general circulation model. *J. Climate*, 12, 2607-2624.

Griffies, S. M., and K. Bryan, 1997: Predictability of North Atlantic multidecadal climate variability. *Science*, 275, 181-184.

Gualdi S., E. Guilyardi, A. Navarra, S. Masina, and P. Delecluse, 2003: The Interannual Variability in the Tropical Indian Ocean as Simulated by a CGCM. *Climate Dyn.*, 20, 567-582.

Latif, M., E. Roeckner, M. Botzet, M. Esch, H. Haak, S. Hagemann, J. Jungclaus, S. Legutke, S. Marsland, U. Mikolajewicz, and J. Mitchell, 2004: Reconstructing, monitoring, and predicting decadal-scale changes in the North Atlantic thermohaline circulation with sea surface temperature. *J. Climate*, 17, 1605-1614.

- Madec, G., P. Delecluse, M. Imbard and C. Lévy, 1998: OPA 8.1 Ocean general circulation model reference manual. Note du Pôle de modélisation, Institut Pierre-Simon Laplace, N°11, pp 91.
- Marsh, R., 2000: Recent variability of the North Atlantic Thermohaline Circulation inferred from surface heat and freshwater fluxes, *J. Climate*, 13, 3239-3260.
- Marsland, S., H. Haak, J. Jungclaus, M. Latif and F. Röske, 2003: The Max-Planck-Institute global ocean/sea ice model with orthogonal curvilinear coordinates. *Ocean Modelling*, 5, 91-127.
- Pohlmann, H., M. Botzet, M. Latif, A. Roesch, M. Wild, and P. Tschuck, 2004a: Estimating the decadal predictability of a coupled AOGCM. (**Chapter 5**). *J. Climate*, 17, 4463-4472.
- Pohlmann, H., F. Sienz, and M. Latif, 2004b: Influence of the multidecadal Atlantic meridional circulation variability on European climate. (**Chapter 6**). *J. Climate*, submitted.
- Pope, V. D., M. L. Gallani, P. R. Rowntree, and R. A. Stratton, 2000: The impact of new physical parametrizations in the Hadley Centre climate model – HadAM3. *Climate Dyn.* 16, 123-146.
- Roeckner, E., G. Bäuml, L. Bonaventura, R. Brokopf, M. Esch, M. Giorgetta, S. Hagemann, I. Kirchner, L. Kornbluh, E. Manzini, A. Rhodin, U. Schlese, U. Schulzweida, and A. Tompkins, 2003: The atmospheric general circulation model ECHAM5. PART I: Model description. MPI Rep. 349, Max-Planck-Institut für Meteorologie, Hamburg, Germany, 127 pp.
- Rodwell, M. J., and C.-K. Folland, 2002: Atlantic air-sea interaction and seasonal predictability. *Quart. J. R. Met. Soc.*, 128, 1413-1444.
- Roullet, G., and G. Madec, 2000: Salt conservation, free surface and varying volume: a new formulation for ocean GCMs. *J. Geophys. Res.*, 105, 23927-23942.
- Trenberth, K. E., and J. M. Caron, 2001: Estimates of meridional atmosphere and ocean heat transports. *J. Climate*, 14, 3433-3443.
- Valcke, S., L. Terray, and A. Piacentini, 2000: The OASIS coupled user guide version 2.4. Tech. Rep. TR/CMGC/00-10, CERFACS, 85 pp.

## Summary and outlook

### 8.1 Summary of results

In the first part of this thesis (Chapters 2-7) the focus has been the investigation of the mechanisms and predictability of North Atlantic-European climate. In addition to the conclusions given at the end of Chapters 2-7, the results are now summarized in order to answer the questions raised in the introduction (Section 1.2):

- I. Has the ocean an influence on North Atlantic-European climate and - if this is the case - which part of the world's ocean is most important?

The results of Chapters 2-4 support the conclusion that variability in SST/SI has a significant influence on the North Atlantic-European climate.

Experiments with the AGCM ECHAM4, in which the SST/SI forcing is restricted to either the Atlantic or the Indo-Pacific oceans, show that both oceanic regions are important for the generation of the atmospheric variability in the Atlantic-European region in winter. In the experiment with SST/SI forcing restricted to the Indo-Pacific oceans the atmospheric response projects on the NAO, while in the experiment with SST/SI forcing restricted to the Atlantic Ocean the atmospheric response projects on the EAP.

However, a multi-model intercomparison study shows that the region with the dominant influence on North Atlantic-European climate varies between different AGCMs. The principal forcing of the dominant winter time mode of SST-forced atmospheric variability in the North Atlantic region, an NAO-like dipole, is in ECHAM4 from the tropical eastern Pacific. But in three other AGCMs the dominant forcing of this mode is from the tropical North Atlantic region.

Another multi-model intercomparison study shows the importance of North Atlantic SST for North Atlantic-European climate. Between the responses of the individual AGCMs to idealized North Atlantic SST/SI anomalies an unexpected global agreement is found. This concerns the NAO, Eurasian temperatures, rainfall over America and Africa, and Asian monsoon. The extratropical North Atlantic region response appears to be associated with remote Caribbean and tropical Atlantic SST anomalies, and with local forcing.

- II. To which extent is North Atlantic-European climate predictable?

The results of Chapters 5-7 show that North Atlantic SST is potentially predictable on decadal timescales, albeit the potential skill levels dependent on the considered AOGCM.

Although the mechanisms behind the decadal to multidecadal variability in the Atlantic sector are still controversial, there is some consensus that the long-term multidecadal variability is driven by variations in the THC. In general, models with greater decadal THC variability have higher levels of potential predictability. The far more pertinent question is, of course, that of the predictability of surface climate variations over land. The simple measures used in Chapters 5 and 7 do not reveal robustly predictable land signals. However, the probabilistic technique introduced in Chapter 6 - more commonly used in medium-range and seasonal forecasting - prevails in the context of the decadal problem some limited success.

## 8.2 Outlook

This study has explained some aspects of the mechanisms behind interannual to multidecadal climate variability in the North Atlantic-European region. However, the understanding of these climate fluctuations is still limited. This is due to a lack in long-term observations and accuracy of GCMs. To determine the mechanisms of climate variability it would be desirable to have longer observational timeseries with a higher spatial coverage. With a coarse grid spacing in GCMs, some small-scale climate features like oceanic eddies cannot be represented. Hence, an enhanced resolution of the GCM grid may result in more realistic climate simulations.

The results of the potential decadal predictability are encouraging. The practicability of decadal climate prediction has now to be demonstrated by hindcast experiments with AOGCMs. The initialization of the AOGCM with oceanic data seems to be the biggest problem for decadal climate predictions. The following solutions are conceivable:

- a) A suitable long-term ocean observing system must be installed, since the memory of the climate system resides in the ocean. In particular, the North Atlantic THC should be monitored carefully, since its variations are most interesting in the light of decadal predictability.
- b) The relationship between variations in THC and SST may be exploited for predictability purposes, as the initial oceanic state may be derived from the history of SST. This may provide a method for determining the initial state of the ocean in order to realize predictions of multidecadal climate variability.
- c) The estimation of the global state of the ocean in near-real time programs provides a new data source for the initialization of ensemble predictability experiments with coupled AOGCMs. These 'ocean reanalyses' bring together a global ocean general circulation model with existing global data streams - including altimeter observations and in situ hydrographic and flow measurements - to obtain the best possible estimate of the time evolving ocean circulation and related uncertainties.
- d) Remote sensing of the ocean plays a crucial role in seasonal forecasts. The main oceanic observations from space are measurements of brightness temperatures of

the earth's surface and altimetry. Brightness temperatures can be converted into SSTs and sea ice concentrations which may be useful to estimate the THC as noted in b). Satellite altimetry measures the height of the satellite above the earth's surface. Combined with precise satellite location data, altimetry measurements yield sea surface heights, which may be useful to estimate the oceanic circulation as noted in c).

The European Union's 'Development of a European Multimodel Ensemble System for Seasonal to Interannual Prediction' (DEMETER) project addressed the issue of sampling model uncertainty in making predictions. In this project a multi-model ensemble for seasonal forecasting was constructed and tested: Seven comprehensive coupled AOGCMs from research centers around Europe were used to make six-month long hindcasts over an extended period (of at least 29 years). An important outcome from DEMETER is the demonstration that a multi-model ensemble is an effective method for sampling model uncertainties and for making more reliable forecasts, a result that should carry over to decadal-to-multidecadal climate predictions.

Further research on these aspects of predictability will be carried out in the European Union's ENSEMBLES project. The project aims to develop an ensemble prediction system for climate change based on the principal state-of-the-art, high resolution, global and regional Earth System models developed in Europe. The Earth System models will be validated against quality controlled, high resolution gridded datasets for Europe, to produce for the first time, an objective probabilistic estimate of uncertainty in future climate at the seasonal to decadal and longer timescales.

## **Acknowledgments**

I would like to thank Prof. Dr. Lennart Bengtsson and Prof. Dr. Guy Brasseur for making it possible to write this thesis at the Max Planck Institute for Meteorology in Hamburg. I thank Prof. Dr. Mojib Latif for his supervision and steady and patient support of my work. I have been involved in the European Union's 'Mechanisms and Predictability of Decadal Fluctuations in Atlantic-European Climate' (PREDICATE) project under the leadership of Dr. Rowan T. Sutton and the 'German Ministry for Education and Research' (BMBF) 'Deutsches Klimaforschungsprogramm' (DEKLIM) in the subproject 'Dynamics of the Low-Frequency Changes in the NAO' under the leadership of Prof. Dr. Mojib Latif. My special thanks to these research teams, the many coauthors of the papers presented in this study, and my colleagues at the Max Planck Institute for Meteorology for a fruitful collaboration. Thanks to Jürgen Bader, Helmuth Haak, Noel Keenlyside, and Katja Lohmann for proof-reading this manuscript.



## APPENDIX

### Methodologies

Here are introduced two methodologies to separate the oceanic forced signal from the internal noise component in an ensemble of AGCM simulations. Each member of the ensemble is forced by the same varying SST/SI and each one is differing from the others only by its initial atmospheric conditions. Seasonal means of a certain climate variable from the ensemble are considered ( $x_{ij}$ ), where  $i$  is the particular year ( $i = 1, \dots, m$ ) and  $j$  is the particular ensemble member ( $j = 1, \dots, n$ ). The ensemble members are assumed to be independent and normally distributed. The variable can be decomposed into the ensemble mean ( $\mu_i$ ) and the departure from that mean ( $\varepsilon_{ij}$ )

$$x_{ij} = \mu_i + \varepsilon_{ij} \quad (\text{A1})$$

For an infinite ensemble size the forced response would simply be the time-varying part of the ensemble mean. For small ensembles, however, internal variability makes an important contribution to the temporal variability of the ensemble mean. As a consequence any nonlinear function of the ensemble mean (e.g., variance, empirical orthogonal function (EOF), etc.) is a biased estimate of the corresponding true forced response.

#### A.1 Analysis of variances

This Section gives an introduction to the analysis of variances (ANOVA). The reader is referred to Rowell et al. (1995) and Rowell (1998) for a detailed description of the ANOVA. Applications of the ANOVA can be found e.g. in Davies et al. (1997) or Rowell and Zwiers (1999).

For this method the internal variability is estimated by computing the variance of each datum's deviation from its ensemble mean

$$\sigma_{INT}^2 = \frac{1}{m(n-1)} \sum_{i=1}^m \sum_{j=1}^n (x_{ij} - \bar{x}_i)^2 \quad (\text{A2})$$

where  $\bar{x}_i = \frac{1}{n} \sum_{j=1}^n x_{ij}$  is the ensemble mean for the  $i$ th year.

The variance of the ensemble mean is

$$\sigma_{EM}^2 = \frac{1}{m-1} \sum_{i=1}^m (\bar{x}_i - \bar{x})^2 \quad (\text{A3})$$

where  $\bar{x} = \frac{1}{nm} \sum_{i=1}^m \sum_{j=1}^n x_{ij}$  is the total mean.

The oceanic forced variance is expressed in terms of the variance of the ensemble mean and the internal variance (e.g. Scheffe 1959, p. 226)

$$\sigma_{SST}^2 = \sigma_{EM}^2 - \frac{1}{n} \sigma_{INT}^2 \quad (A4)$$

The ratio ( $\rho$ ) of the SST forced variance to the total variance ( $\sigma_{TOT}^2$ ) is then

$$\rho = \frac{\sigma_{SST}^2}{\sigma_{TOT}^2} = \frac{\sigma_{EM}^2 - \frac{1}{n} \sigma_{INT}^2}{\sigma_{TOT}^2} \quad (A5)$$

where  $\sigma_{TOT}^2 = \sigma_{SST}^2 + \sigma_{INT}^2$ .

## A.2 Optimal detection analysis

This Section gives an introduction of the optimal detection analysis (ODA). The reader is referred to Venzke et al. (1999) for a detailed description of the ODA. The ODA is also called signal-to-noise maximizing EOF analysis (Terray and Cassou 2002). An additional application of the ODA can be found in Sutton and Hodson (2003). Similar to the ANOVA, the ODA aims to separate the oceanic forced signal from the internal noise component in an ensemble of simulations. The advantage of the ODA over the ANOVA is that it derives the spatio-temporal characteristics of the dominant forced response, in addition to identify the regions where such a response may exist.

The aim of the ODA is to derive EOFs, which represent the oceanic forced response from an ensemble of AGCM simulations. These EOFs are derived as follows. Equation (A1) is rewritten with the data in the  $j$ th ensemble member represented as the matrix  $\mathbf{X}_j$

$$\mathbf{X}_j = \mathbf{X}_M + \mathbf{X}_{Nj} \quad (A6)$$

where  $\mathbf{X}_M$  and  $\mathbf{X}_{Nj}$  represents the ensemble mean and the departure from that mean, respectively. The noise terms  $\mathbf{X}_{Nj}$  are append to one set  $\mathbf{X}_N$ . EOFs are the eigenvectors of the covariance matrix,

$$\hat{\mathbf{C}}_M = \frac{1}{m-1} \mathbf{X}_M \mathbf{X}_M^T \quad (A7)$$

where  $\mathbf{X}_M^T$  is the transposed of  $\mathbf{X}_M$ .

The expectation value of the covariance matrix of the ensemble mean is

$$E(\hat{\mathbf{C}}_M) = \mathbf{C}_F + \frac{1}{n} \mathbf{C}_N \quad (\text{A8})$$

where  $\mathbf{C}_F$  and  $\mathbf{C}_N$  are the true (unknown) spatial covariances of the forced response and internal variability, respectively. The true covariance of the internal variability,  $\mathbf{C}_N$ , is unknown, but an unbiased estimate can be obtained from the deviations from the ensemble mean

$$\hat{\mathbf{C}}_N = \frac{1}{m(n-1)} \sum_{j=1}^n \mathbf{X}_{Nj} \mathbf{X}_{Nj}^T. \quad (\text{A9})$$

The eigenvectors of  $\hat{\mathbf{C}}_M$ , or EOFs, provide an estimate of the eigenvectors of  $\mathbf{C}_F$  if and only if the internal variability is uncorrelated in space, or  $\mathbf{C}_N = s \mathbf{I}$ , since adding  $s \mathbf{I}$  (i.e. a scalar  $s$  and the identity matrix  $\mathbf{I}$ ) to any matrix simply raises its eigenvalues by  $s$  and does not change its eigenvectors. But the internal variability is not uncorrelated in space. Allen and Smith (1997) resolved this problem by introducing a prewhitening transformation,  $\mathbf{F}$ , such that

$$\mathbf{F}^T \hat{\mathbf{C}}_M \mathbf{F} = \mathbf{F}^T \mathbf{C}_F \mathbf{F} + s \mathbf{I} \quad (\text{A10})$$

or in other words

$$\mathbf{F}^T \mathbf{C}_N \mathbf{F} = s \mathbf{I} \quad (\text{A11})$$

i.e.  $\mathbf{F}$  removes any spatial correlation. It is already white in time. If the columns of  $\mathbf{E}_N^{(j)}$  are defined to be the  $j$  highest-ranked normalized eigenvectors (EOFs) of  $\hat{\mathbf{C}}_N$ , and  $\Lambda_N^{(j)}$  the corresponding eigenvalues, the prewhitening transformation can be defined as

$$\mathbf{F} = n^{\frac{1}{2}} \mathbf{E}_N^{(j)} (\Lambda_N^{(j)})^{-1} \quad (\text{A12})$$

and its transposed pseudo-inverse as

$$\mathbf{F}^{(-1)} = n^{-\frac{1}{2}} \mathbf{E}_N^{(j)} \Lambda_N^{(j)} \quad (\text{A13})$$

One is obliged to truncate because variance will generally be underestimated in the low-ranked EOFs of internal variability.

The prewhitening transformation is applied to  $\hat{\mathbf{C}}_M$  such that

$$\mathbf{C}'_M = \mathbf{F}^T \hat{\mathbf{C}}_M \mathbf{F} = \mathbf{C}'_F + \mathbf{I} \quad (\text{A14})$$

Since the transformed internal variability has equal variance in all state-space directions, the highest-ranked eigenvectors  $\mathbf{e}'_1$  of  $\mathbf{C}'_M$  provides an estimate of the highest-ranked eigenvectors of  $\mathbf{C}'_F$ . The elements of  $\mathbf{e}'_1$ , however, correspond to EOF indices rather than spatial locations, so it aids interpretation to convolve it with the prewhitening transformation,  $\mathbf{F}$ , giving  $\tilde{\mathbf{E}} = \mathbf{F} \mathbf{E}'$ . The vector  $\tilde{\mathbf{e}}_1$  is the pattern that for a given truncation maximizes the ratio of ensemble-mean variance to within-ensemble variance. This vector  $\tilde{\mathbf{e}}_1$  is the optimal filter for characterizing the forced response.

Equivalently to conventional EOF analysis, the optimized principal component (OPC) of  $\tilde{\mathbf{e}}_1$  in the ensemble mean  $\mathbf{X}_M$  is given by

$$\mathbf{p}_1 = \lambda_1'^{-1} \mathbf{X}_M^T \tilde{\mathbf{e}}_1 \quad (\text{A15})$$

The spatial pattern associated with the dominant forced response is derived by projecting  $\mathbf{X}_M$  onto the OPC

$$\hat{\mathbf{e}}_1 = \lambda_1'^{-1} \mathbf{X}_M \mathbf{p}_1 \quad (\text{A16})$$

The procedure can be summarized as follows. The noise covariance matrix  $\hat{\mathbf{C}}_N$  is constructed from the noise ensemble.  $\hat{\mathbf{C}}_N$  is used to perform a prewhitening filter  $\mathbf{F}$ . This filter is used to remove any spatial correlation in the noise, which makes the noise spatially white. An EOF analysis of the prewhitened data is performed. This yields a set of optimal spatial filters and timeseries (OPCs). The highest ranked filter is the spatial pattern that maximizes the ratio of the ensemble-mean to the within-ensemble variance. The spatial pattern associated with the dominant forced response is derived by projecting the ensemble mean onto the OPC.

## References

- Allen M. R., and L. A. Smith, 1997: Optimal filtering in singular spectrum analysis. *Phys. Lett.*, 234, 419-428.
- Davies, J. R., D. P. Rowell, and C. K. Folland, 1997: North Atlantic and European seasonal predictability using an ensemble of multidecadal atmospheric GCM simulations. *Int. J. Climatol.*, 17, 1263-1284.
- Rowell, D. P., C. K. Folland, K. Maskell, and M. N. Ward, 1995: Variability of summer rainfall over tropical north Africa (1906-92): Observations and modeling. *Q. J. Roy. Meteor. Soc.*, 121, 669-704.

Rowell, D. P., 1998: Assessing the potential seasonal predictability with an ensemble of multidecadal GCM simulations. *J. Climate*, 11, 109-120.

Rowell, D. P., and F. W. Zwiers, 1999: The global distribution of sources of atmospheric decadal variability and mechanisms over the tropical Pacific and southern North America. *Climate Dyn.*, 15, 751-772.

Scheffe, H., 1959: *The analysis of variance*. John Wiley and Sons, New York.

Sutton, R. T., and D. I. R. Hodson, 2003: Influence of the ocean on North Atlantic climate variability 1971-1999. *J. Climate*, 16, 3296-3313.

Terray, L., and C. Cassou, 2002: Tropical Atlantic sea surface temperature forcing of quasi-decadal climate variability over the North Atlantic-European region. *J. Climate*, 15, 3170-3187.

Venzke, S., M. R. Allen, R. T. Sutton, and D. P. Rowell, 1999: The atmospheric response over the North Atlantic to decadal changes in sea surface temperature. *J. Climate*, 12, 2562-2584.



**MPI-Examensarbeit-Referenz:**

Examensarbeit Nr. 1-79 bei Bedarf bitte Anfragen:  
MPI für Meteorologie, Abtlg.: PR, Bundesstr. 53, 20146 Hamburg

<b>Examensarbeit Nr. 80</b> November 2000	<b>Vertikalmessungen der Aerosolextinktion und des Ozons mit einem UV-Raman-Lidar</b> Volker Matthias
<b>Examensarbeit Nr. 81</b> Dezember 2000	<b>Photochemical Smog in Berlin-Brandenburg: An Investigation with the Atmosphere-Chemistry Model GESIMA</b> Susanne E. Bauer
<b>Examensarbeit Nr. 82</b> Juli 2001	<b>Komponenten des Wasserkreislaufs in Zyklonen aus Satellitendaten – Niederschlagsfallstudien-</b> Klepp Christian-Philipp
<b>Examensarbeit Nr. 83</b> Juli 2001	<b>Aggregate models of climate change: development and applications</b> Kurt Georg Hooss
<b>Examensarbeit Nr. 84</b> Februar 2002	<b>Ein Heterodyn-DIAL System für die simultane Messung von Wasserdampf und Vertikalwind: Aufbau und Erprobung</b> Stefan Lehmann
<b>Examensarbeit Nr. 85</b> April 2002	<b>Der Wasser- und Energiehaushalt der arktischen Atmosphäre</b> Tido Semmler
<b>Examensarbeit Nr. 86</b> April 2002	<b>Auswirkungen der Assimilation von Meereshöhen-Daten auf Analysen und Vorhersagen von El Niño</b> Sigrid Schöttle
<b>Examensarbeit Nr. 87</b> Juni 2002	<b>Atmospheric Processes in a young Biomass Burning Plume - Radiation and Chemistry</b> Jörg Trentmann
<b>Examensarbeit Nr. 88</b> August 2002	<b>Model Studies of the Tropical 30 to 60 Days Oscillation</b> Stefan Liess
<b>Examensarbeit Nr. 89</b> Dezember 2002	<b>Influence of Sub-Grid Scale Variability of Clouds on the Solar Radiative Transfer Computations in the ECHAM5 Climate Model</b> Georg Bäuml
<b>Examensarbeit Nr.90</b> Mai 2003	<b>Model studies on the response of the terrestrial carbon cycle to climate change and variability</b> Marko Scholze
<b>Examensarbeit Nr.91</b> Juni 2003	<b>Integrated Assessment of Climate Change Using Structural Dynamic Models</b> Volker Barth

**MPI-Examensarbeit-Referenz:**

Examensarbeit Nr. 1-79 bei Bedarf bitte Anfragen:  
MPI für Meteorologie, Abtlg.: PR, Bundesstr. 53, 20146 Hamburg

<b>Examensarbeit Nr.92</b> Juli 2003	<b>Simulations of Indonesian Rainfall with a Hierarchy of Climate Models</b> Edvin Aldrian
<b>Examensarbeit Nr.93</b> Juli 2003	<b>ENSO Teleconnections in High Resolution AGCM Experiments</b> Ute Merkel
<b>Examensarbeit Nr.94</b> Juli 2003	<b>Application and Development of Water Vapor DIAL Systems</b> Klaus Ertel

---

**Beginn einer neuen Veröffentlichungsreihe des MPIM, welche die vorherigen Reihen "Reports" und "Examensarbeiten" weiterführt:**

**„Berichte zur Erdsystemforschung“ , „Reports on Earth System Science“, ISSN 1614-1199  
Sie enthält wissenschaftliche und technische Beiträge, inklusive Dissertationen.**

---

<b>Berichte zur Erdsystemforschung Nr.1</b> Juli 2004	<b>Simulation of Low-Frequency Climate Variability in the North Atlantic Ocean and the Arctic</b> Helmuth Haak
<b>Berichte zur Erdsystemforschung Nr.2</b> Juli 2004	<b>Satellitenfernerkundung des Emissionsvermögens von Landoberflächen im Mikrowellenbereich</b> Claudia Wunram
<b>Berichte zur Erdsystemforschung Nr.3</b> Juli 2004	<b>A Multi-Actor Dynamic Integrated Assessment Model (MADIAM)</b> Michael Weber
<b>Berichte zur Erdsystemforschung Nr.4</b> November 2004	<b>The Impact of International Greenhouse Gas Emissions Reduction on Indonesia</b> Armi Susandi
<b>Berichte zur Erdsystemforschung Nr.5</b> Januar 2005	<b>Proceedings of the first HyCARE meeting, Hamburg, 16-17 December 2004</b> Edited by Martin G. Schultz

